1972

Ultimate strength analysis of plate grillages under combined loads, September 1972

Siamak Parsanejad

Alexis Ostapenko

ULTIMATE STRENGTH ANALYSIS OF PLATE GRILLAGES UNDER COMBINED LOADS

by

Siamak Parsanejad

and

Alexis Ostapenko

Department of Civil Engineering
Fritz Engineering Laboratory
Lehigh University
Bethlehem, Pennsylvania

September 1972

Fritz Engineering Laboratory Report No. 323.11

TABLE OF CONTENTS

LIST OF FIGURES

L I S T O F T A B L E S

323.11

ULTIMATE STRENGTH ANALYSIS OF PLATE GRILLAGES UNDER COMBINED LOADS

by

Siamak Parsanejad

and

Alexis Ostapenko

ABSTRACT

A method for analyzing plate grillages subjected to lateral and axial loads is described. A grillage consists of a flat plate reinforced on one side by a set of orthogonal tee stiffeners. It is treated as a longitudinally stiffened panel continuous over the transverses. The post-buckling behavior of the plate and large deformation elasto-plastic behavior of the longitudinals are considered. Each transverse stiffener together with an assumed effective width of the plate is treated according to the small deflection elasto-plastic beam theory. The generalized Newton-Raphson technique in conjunction with incremental loading is used to establish the complete load-deflection relationship. The feasibility of the method is demonstrated by analyzing some sample grillages. The accuracy of the method is shown by comparison with some available test results. The effect of some of the grillage parameters (such as the effective width of the plate for transverse stiffeners, residual stresses, and initial lateral deflections) and of the boundary conditions on the ultimate strength is studied for the sample grillages.

1. INTRODUCTION

1.1 INTRODUCTORY REMARKS

A plate grillage consists of a flat plate reinforced with a set of stiffeners. Examples of these are grillages used in hulls and decks of ships, orthotropic decks of bridges, and walls of storage bins. In general, the stiffeners can be arranged at any arbitrary angle. However, in grillages commonly used, the stiffeners form an orthogonal system (Fig. 1).

Grillages are usually subjected to combined in-plane and lateral loads. A grillage in a ship bottom, for example, is subjected to lateral loading due to water pressure, to a high axial force in the longitudinal direction due to hull bending, to a small axial force in the transverse direction, and to shear forces (Fig. 2).

A grillage, like any other structure, must be designed so that it fulfills its function under working loads and has sufficient strength to withstand an overload. Thus, a rational method of analysis should enable one to predict the behavior of the grillage under the working as well as under the ultimate loads.

1.2 AVAILABLE METHODS

Up to the present time, the most common approach to the design of grillages has been treating the grillage as a grid system or as an orthotropic plate. The grid model has been used in the small deflection elastic analysis of grillages under lateral loading alone[1 to 7]

or in combination with in-plane loads,[8,9] in the elastic buckling analysis,[9,10] and in the ultimate strength analysis of grillages under lateral loading.[11,12,13] Orthotropic plate theory has also been applied to small deflection elastic analysis of grillages under lateral loading[14,15] or combined lateral and in-plane loads[16,17,18] and to buckling analysis.[19,20] A large deflection orthotropic plate theory, in which yielding of the rectangular stiffeners was accounted for but the plate was assumed to remain elastic and not to buckle, has been applied to the analysis of grillages under lateral loads.[21] Comparison of this method with one test result gave a good correlation at the elastic limit, but the deviation was large, up to about 20% overestimate, in the plastic range.

In a few instances, a direct application of the plate and beam theories has been used in analysis of grillages. One such formulation based on the assumptions of small deflections and elastic behavior is described in Ref. 1. Reference 22 describes a method of analysis for box beam bridges based on the folded plate theory of Goldberg and Leve.[23] The structure considered is a doubly plated grillage with longitudinals and transverses (diaphragms) of equal depth, and it is assumed that the transverses are perfectly rigid in their principal plane of bending and perfectly flexible in the direction normal to this plane.

Kerfoot and Ostapenko[24] reported a large-deflection elasto-plastic analysis of grillages with tee stiffeners in terms of the plate and beam theories. They extended the general large deflection

differential equations of plates and beams to include the inelastic effects. Due to the geometrical and material nonlinearities, these equations were of a highly complex nature. Using a variant of the method of collocation, they succeeded in numerically generating a set of nonlinear equations. However, because the resultant system of equations was very ill-conditioned, they failed to obtain an acceptable solution.

In recent years the finite element method has gained a widespread acceptance, especially for solving complex problems. Bergan et al.[25] have described a small deflection elastic finite element analysis of grillages (with tee stiffeners) subjected to normal loads. Kavlie and Clough[26] have reported an elastic finite element analysis of grillages subjected to combined loads; they have assumed that the stiffeners are symmetric about the mid-plane of the plate, and thus, the plane stress and plate bending problems could be uncoupled. Geometrical and/or material nonlinearities have also been considered in finite element methods for analyzing plates, shells, and rectangular beams under various loading conditions.[27 to 39] However, it seems that no method capable of determining the ultimate strength of plate grillages under combined loads is as yet available.

If the transverse stiffeners of a grillage have sufficiently large bending rigidity, they may be assumed undeformable. Then, a portion between two adjacent transverses can be analyzed as a longitudinally stiffened panel (plate with stiffeners in the direction of the axial load). Kondo,[40] Tsuiji,[41] Voita and Ostapenko,[42]

and Rutledge and Ostapenko[43] have reported an ultimate strength analysis for such panels subjected to combined lateral and axial loads. The post-buckling behavior of the plate and the large deflection and inelastic behavior of the stiffeners were considered*. The method, however, could not be applied to grillages with flexible transverses.

1.3 OBJECTIVE AND SCOPE

A method for the ultimate strength analysis of plate grillages subjected to combined lateral and axial loads is described here. It is based on treating the grillage as a longitudinally stiffened plate panel continuous over a series of transverses. The longitudinals with the adjoining plate are analyzed according to the method reported in Ref. 43 in which the post-buckling plate behavior and the large deformation elasto-plastic behavior of the longitudinals were considered. The transverse stiffeners, each with an assumed effective plate portion, are treated according to the small deflection elasto-plastic beam theory.

A computer program based on the method was used to compare its accuracy with some available test results (Chapter 3). The effects of some parameters such as residual stresses, initial lateral deflections, the assumed effective width for the transverses, and of the boundary conditions at the loaded edges on the ultimate strength of grillages was briefly investigated using this method (Chapter 4).

---

*This method is discussed further in Section 2.2.

2. METHOD OF ANALYSIS

2.1 PROPOSED MODEL

In general, a grillage is subjected to lateral load normal to the plate surface, to in-plane loads in longitudinal as well as transverse directions, and to shear (Fig. 2). However, in grillages commonly encountered in practice, such as ship grillages, in-plane loads in the transverse direction are of much lower intensity than in the longitudinal direction,and, therefore, of much less significance. Shear forces could be significant in some cases such as in the side grillages of ship bottom structures, but in grillages located toward the center of a ship, the magnitude of shear forces is small and can be neglected. In this study, a grillage is assumed to be subjected only to a uniformly distributed lateral loading and a uniformly distributed axial compression in the longitudinal direction (Fig. 3).

The model, on which the proposed method of analysis is based, treats the grillage of Fig. 3 as a longitudinally stiffened panel continuous over a series of transverses; each transverse stiffener together with an assumed effective portion of the plate* is assumed to provide only knife edge support for the longitudinals. Thus, the grillage can be divided into two separate systems: 1) a longitudinally stiffened panel subjected to externally applied lateral and axial loads and to unknown redundants V_{ij} acting at the junctions with the transverses

*In a later discussion, the term "transverse beam" or, loosely, "transverse" will denote a beam composed of a transverse stiffener and an effective portion of the plate. Wherever the transverse stiffener alone is meant, the phrase "transverse stiffener" will be used.

(Fig. 4a), and 2) a series of transverse beams subjected to the same but opposite redundants V_{ij} (Fig. 4b).

The longitudinally stiffened panel of Fig. 4a is treated as a series of beam-columns each consisting of a plate of width b (spacing of the longitudinal stiffeners) and a longitudinal stiffener* (Fig. 5). Each longitudinal beam is then assumed to act as if it were a part of a longitudinally stiffened panel with an infinite number of identical stiffeners. This assumption ignors the deflectional and shear interaction of longitudinal stiffeners through the plate.

The behavior of the plate before and after buckling is described by an effective average stress, which is the average of the imposed stresses caused by the loading, versus the edge strain (strain at the plate-stiffener junction) relationship. This approach is equivalent to the consideration of a variable effective width of the plate along the longitudinals. Thus, the grillage is modeled as a grid system composed of a series of transverse beams, treated according to the small deflection elasto-plastic beam theory, and a series of longitudinal beams whose large deflection elasto-plastic behavior is considered. The steps involved in analyzing this grillage model are as follows:

1. Establishment of the effective average stress-edge strain relationship for the plate.

---

*In later discussions, the phrase "longitudinal beam" or, loosely, "longitudinal" will denote such a beam-column. Wherever the longitudinal stiffener alone is meant, the phrase "longitudinal stiffener" will be used.

2. Computation of the moment-curvature-axial force relationship for the beam-column of Fig. 5.

3. Stepwise integration of the beam-column differential equations along the length of the longitudinal beams.

4. Establishment of the incremental force-displacement relationship for the transverse beams based on small deflection elasto-plastic beam theory.

5. Enforcement of the compatibility of deformations at the intersection points of transverses with longitudinals, and of the boundary conditions to obtain a set of nonlinear simultaneous equations. (These equations are generated numerically.)

6. Numerical solution of the resulting nonlinear simultaneous equations.

7. Determination of the ultimate capacity by incrementing the loads.

2.2 LONGITUDINAL BEAMS

Since the treatment of the longitudinal beams to a large extent follows the principles of the method developed for analyzing longitudinally stiffened panels under combined loads, a brief review of the development of that method is presented here.

Kondo[40] described an ultimate strength analysis for longitudinally stiffened panels using a beam-column model. This analysis was restricted to plates with small b/t (a plate whose buckling stress is greater than its yield stress). Considered were the variation of strain through the plate thickness and residual stresses in the plate and in the stiffener flange. The materials were assumed to be ideally elastic-plastic.

Davidson[44] surveyed the existing theoretical solutions of the post-buckling behavior of long rectangular plates subjected to edge compression and compared them with some available test results.[45,46,47] He concluded that the behavior of simply supported plates in the elastic post-buckling range can be adequately described by an average stress-edge strain relationship proposed by Koiter.[48] The ultimate average stress equal to the average stress computed at the onset of membrane yielding was assumed to remain constant in the post-yield (post-ultimate) range.

Concurrently with Davidson's work, Tsuiji[41] extended Kondo's approach to longitudinally stiffened panels with large b/t (a plate whose buckling stress is less than its yield stress) by using the average stress-edge strain concept proposed by Davidson. In this analysis, the residual stresses of the stiffener flange were ignored because Kondo found their effect to be negligible on the ultimate strength. Also, the variation of strain through the plate thickness could not be considered concurrently with the average stress-edge strain relationship.

Using Tsuiji's approach, Vojta and Ostapenko[42,49] developed a set of design nomographs for steel panels with a yield stress of 47 ksi.

There was still some doubt on the validity of the assumption of a constant stress in the post-ultimate region. To check this, Rutledge and Ostapenko[43] extended the methods of Kondo and Tsuiji to materials with a general nonlinear stress-strain relationship. Then, by assuming various average stress-edge strain relationships for the plate and studying their effect on the ultimate strength of panels, it was concluded that the post-ultimate plate behavior has little effect on the strength of panels with proportions and loadings common to ship structures.

The method of Ref. 43 was modified to incorporate the concentrated redundants from the transverses (Fig. 5) and is used in Steps 1 to 3 (Section 2.1) of the method proposed here.

2.2.1 Assumptions

The following assumptions are employed in the analysis of the longitudinal beams:

1. Strain variation through the plate thickness is ignored.
2. The residual stress distribution is as shown in Fig. 6 and does not vary along the length.
3. The narrow band of the tensile residual stresses has negligible effect on the buckling stress of the plate.

4. The average stress of plates with small b/t remains constant, in the post-buckling range, and equal to the buckling stress.

5. The behavior of the plate with large b/t is described by its average stress-edge strain relationship proposed in Ref. 44. (For the effect of residual stresses see Section 2.2.2.)

6. The 0.2% offset rule is used in defining the yield stress and strain of materials with nonlinear stress-strain relationships.

7. Stresses produced by the bending of the plate spanning between stiffeners are assumed to have negligible effect on the in-plane plate behavior. In design, they should be considered separately.

8. A strain uniquely defines a corresponding stress (no strain reversal).

9. The cross-sectional plane remains plane and normal to the centroidal axis after deformation (shearing deformations are ignored).

10. Plate components of stiffeners are so proportioned that the ultimate strength of the grillage is reached before local buckling takes place.

Assumptions 1 through 7 are used in obtaining the average stress-edge strain relationship for plates. Assumptions 1 and 8 through 10 influence the development of the moment-curvature-axial force relationship.

2.2.2 Effective Average Stress-Edge Strain Relationship

Depending on whether the critical buckling stress of the plate, given by Eq. 2.1, is greater than or less than its yield stress, the plate is defined here to be of small b/t or of large b/t, respectively.

$$\sigma_{cr} = K \frac{\pi^2 E_t}{12(1-\nu^2)\ (b/t)^2} \qquad (2.1)$$

where K = buckling coefficient, conservatively assumed to be equal to 4.0, thus, neglecting the torsional restraint provided by the longitudinal stiffeners

E_t = tangent modulus of elasticity

ν = Poisson's ratio

b = plate width

t = plate thickness

For plates with small b/t, it is assumed that the plate buckles when the sum of the compressive residual stress and the imposed stress is equal to the critical buckling stress σ_{cr}. The effective average stress-edge strain relationship for the pre-buckling range is then established by computing the average of the imposed stresses for any given plate edge strain (for detailed discussion see Ref. 43). For the post-buckling range, the effective average stress remains constant. Figure 7 shows a

typical effective average stress-edge strain plot for plates with small b/t.

For plates with large b/t, the effective average stress-edge strain curve consists of three parts: a pre-buckling part, an elastic post-buckling part, and a post-ultimate part. The pre-buckling part is established in the same manner as for plates with small b/t.

For the elastic post-buckling part, an equation recommended by Koiter is used.[48]

$$\left(\frac{\sigma_p}{\sigma_{cr}}\right) = 1.2 \left(\frac{\varepsilon_p}{\varepsilon_{cr}}\right)^{0.6} - 0.65 \left(\frac{\varepsilon_p}{\varepsilon_{cr}}\right)^{0.2} + 0.45 \left(\frac{\varepsilon_p}{\varepsilon_{cr}}\right)^{-0.2} \qquad (2.2)$$

where σ_p = average stress in the plate

ε_p = edge strain

Equation 2.2 expresses the average stress in terms of the edge strain. For a plate with no residual stresses, the ultimate average stress is given when the edge strain ε_p is equal to the yield strain ε_y. However, for plates with the residual stress pattern of Fig. 6, the ultimate average stress is not only influenced by the reduction in effective buckling stress, but also by the change of the location of the first yield from point A to point B. By assuming a parabolic stress distribution, the strain at the stiffener is expressed in terms of the ultimat average stress $(\sigma_p)_u$ and can be given in a non-dimensional form.[41,44]

$$\left(\frac{\varepsilon_p}{\varepsilon_{cr}}\right)_u = \frac{2\left(\frac{\varepsilon_{yp}}{\varepsilon_{cr}}\right) + 3\left[\left(1 - \frac{c}{b}\right)^2 - 1\right]\left(\frac{\sigma_p}{\sigma_{cr}}\right)_u}{3\left(1 - \frac{c}{b}\right)^2 - 1} \qquad (2.3)$$

where ϵ_{cr} = strain corresponding to plate critical stress σ_{cr}

ϵ_{yp} = yield strain of the plate

and c and b are as indicated in Fig. 6. Simultaneous solution of Eqs. 2.2 and 2.3 will give the ultimate average stress and its corresponding edge strain.

For the post-ultimate part of average stress-edge strain curve, the plate was assumed to continue carrying the ultimate average stress $(\sigma_p)_u$. A typical plot of the average effective stress-edge strain relationship for a plate with large b/t is shown in Fig. 8.

Since longitudinal stiffeners are assumed to be free of residual stresses and do not buckle prematurely (according to assumption 10), their stress-strain curve is given by their material stress-strain curve.

2.2.3 Moment-Curvature-Axial Load Relationship

The strain and stress distributions for a typical cross section are shown in Fig. 9. The forces and the curvature are shown in the positive direction according to the following sign convention:

1. Bending moment M and curvature ϕ causing compression in the plate are positive.

2. Compressive stress and strain are positive.

3. Compressive axial force N is positive.

The axial force and moment are obtained by integration over the cross section.

$$N = \sigma_p A_p + \sigma_f A_f + \int_o^d \sigma_h t_w \, dh \tag{2.4}$$

$$M = -\sigma_f A_f d - \int_o^d \sigma_h h \, t_w \, dh + N (\alpha d) \tag{2.5}$$

where σ_p = effective average stress in the plate

σ_f = stress in the stiffener flange

A_p = area of the plate = bt

A_f = area of the stiffener flange

t_w = thickness of the stiffener web

h = distance of a point from the mid-plane of the plate

σ_h = stiffener stress at location h

d = distance from the mid-plane of the plate to the mid-plane of the stiffener flange

αd = distance from the centroid to the mid-plane of the plate

Curvature ϕ is given by

$$\phi = \frac{\epsilon_p - \epsilon_f}{d} \tag{2.6}$$

where ϵ_p = plate edge strain

ϵ_f = stiffener flange strain

Equations 2.4, 2.5, and 2.6 can be non-dimensionalized to

$$\bar{N} = k_1 \bar{\sigma}_p + k_2 \bar{\sigma}_f + k_3 \int_o^1 \bar{\sigma}_h \, d\bar{h} \tag{2.7}$$

$$\bar{M} = -k_2 \bar{\sigma}_f - k_3 \int_o^1 \bar{\sigma}_h \, \bar{h} \, d\bar{h} + \alpha \bar{N} \tag{2.8}$$

$$\bar{\phi} = \bar{\varepsilon}_p - \bar{\varepsilon}_f \tag{2.9}$$

where $k_1 = \dfrac{A_p}{A_p + A_s} = \dfrac{1}{1 + A_s/A_p}$

$$k_2 = \frac{A_f}{A_p + A_s} = \frac{A_f}{A_p}\, k_1$$

$$k_3 = \left(1 - \frac{A_f}{A_s}\right)\left(\frac{A_s}{A_p}\right) k_1$$

$$\alpha = \frac{1}{2}\frac{A_s}{A_p}\left(1 + \frac{A_f}{A_s}\right) k_1$$

$$\bar{M} = \frac{M}{A\,\sigma_o\,d} \quad ; \quad \bar{N} = \frac{N}{A\,\sigma_o}$$

$$\bar{\sigma}_p = \frac{\sigma_p}{\sigma_o} \quad ; \quad \bar{\sigma}_f = \frac{\sigma_f}{\sigma_o}$$

$$\bar{\sigma}_h = \frac{\sigma_h}{\sigma_o} \quad ; \quad \bar{h} = \frac{h}{d}$$

$$\bar{\phi} = \frac{\phi}{\varepsilon_o/d} \quad ; \quad \bar{\varepsilon}_p = \frac{\varepsilon_p}{\varepsilon_o}$$

A_s = area of the stiffener

A = area of the longitudinal beam = $A_p + A_s$

$\left.\begin{aligned}\sigma_o &= \sigma_{cr}\\ \varepsilon_o &= \varepsilon_{cr}\end{aligned}\right\}$ if $\sigma_{cr} < \sigma_y$

$$\left.\begin{aligned}\sigma_o &= \sigma_{yp} \\ \varepsilon_o &= \varepsilon_{yp}\end{aligned}\right\} \text{if } \sigma_{cr} \geq \sigma_y$$

The establishment of the moment-curvature-axial force relationship would require determination of M and ϕ for a given value of N and some specified strain (e.g., plate edge strain). Since N, in general, varies along the length of the longitudinal beam, it would seem that an infinite number of moment-curvature-axial force relationships would be required. However, numerical results have indicated that the variation of N along the longitudinals is negligible.[40] Therefore, the moment-curvature relationship for N = P is used for the entire length of the beam with P being the externally applied axial load. A typical $\bar{M} - \bar{\phi}$ relationship for a constant P is shown in Fig. 10. Because of the eccentricity of the axial force N due to plate buckling, the curve does not pass through the origin of the coordinate axes.

2.2.4 Equilibrium Equations and Numerical Integration

A typical segment of infinitesimal length ds of the longitudinal beam of Fig. 5 is shown in Fig. 11a. The equilibrium equations for this segment are

$$dH = q\ b\ ds_p \sin\theta \tag{2.10}$$

$$dV = q\ b\ ds_p \cos\theta \tag{2.11}$$

$$dM = -H \sin\theta\ ds - V \cos\theta\ ds - \frac{1}{2} q\ b\ ds_p\ ds \tag{2.12}$$

where $ds_p = (1 - \phi\alpha d)\, ds$

$$\phi = \frac{d\theta}{ds}$$

$$\sin\theta = \frac{dy}{ds} \tag{2.13}$$

$$\cos\theta = \frac{dx}{ds} \tag{2.14}$$

After rearranging and nondimensionalizing, the equilibrium equations in the final form are

$$\frac{d\bar{H}}{d\bar{s}} = k_6 \left(1 - k_7 \frac{d\theta}{d\bar{s}}\right) \frac{d\bar{y}}{d\bar{s}} \tag{2.15}$$

$$\frac{d\bar{V}}{d\bar{s}} = k_6 \left(1 - k_7 \frac{d\theta}{d\bar{s}}\right) \frac{d\bar{x}}{d\bar{s}} \tag{2.16}$$

$$\frac{d\bar{M}}{d\bar{s}} = k_8 \left(\bar{H} \frac{d\bar{y}}{d\bar{s}} + \bar{V} \frac{d\bar{x}}{d\bar{s}}\right) \tag{2.17}$$

where $$\frac{d\theta}{d\bar{s}} = k_5 \bar{\phi} \tag{2.18}$$

and $k_5 = r\,\epsilon_o/d$; $k_6 = 0.001\bar{q} = q\,br/\sigma_o A$

$k_7 = \alpha d/r$; $k_8 = -r/d$

$\bar{H} = H/\sigma_o A$; $\bar{V} = V/\sigma_o A$

$\bar{x} = x/r$; $\bar{y} = y/r$

$\bar{s} = x/r$

r = radius of gyration of the cross section

$$= \frac{d}{1 + A_s/A_p} \quad \frac{A_s}{12\ A_p} \left[\left(4 + \frac{A_s}{A_p}\right) \left(1 + 2\ \frac{A_f}{A_s}\right) - 3 \left(\frac{A_s}{A_p}\right) \left(\frac{A_f}{A_s}\right)^2 \right]$$

and all other parameters are as defined earlier.

A typical longitudinal beam segment of finite length $\overline{\Delta s}$ located between points (i) and (i+1) is shown in Fig. 11b with all the forces and dimensions given in nondimensional form. Assuming a linear variation of curvature within the segment, the curvature at location $\bar{z}$ is

$$\bar{\phi}\ (\bar{z}) = \bar{\phi}_i + \frac{\bar{\phi}_{i+1} - \bar{\phi}_i}{\overline{\Delta s}}\ \bar{z} \tag{2.19}$$

Integration of Eq. 2.18, after expressing $\bar{\phi}$ according to Eq. 2.19, gives

$$\Delta\theta = \theta\ (\bar{z}) - \theta_i = k_s\ \bar{\theta}_i\ \bar{z} + \frac{1}{2}\ \frac{\bar{\phi}_{i+1} - \bar{\phi}_i}{\overline{\Delta s}}\ \overline{z^2} \tag{2.20}$$

Nondimensionalizing and rearranging Eq. 2.13 gives

$$\overline{\Delta y} = \bar{y}_{i+1} - \bar{y}_i = \int_{\bar{s}_i}^{\bar{s}_i + \overline{\Delta s}} \sin\theta\ (\bar{z})\ d\bar{z} \tag{2.21}$$

where $\sin\theta\ (\bar{z}) = \sin\ (\theta_i + \Delta\theta)$, and $\Delta\theta$ is given by Eq. 2.20.

By expanding $\sin\ (\theta_i + \Delta\theta)$ and noting that, for small $\Delta\theta$, $\cos\Delta\theta = 1.0$ and $\sin\Delta\theta = \Delta\theta$, the integration of Eq. 2.21 results in

$$\overline{\Delta y} = \bar{y}_{i+1} - \bar{y}_i = \overline{\Delta s}\ \sin\theta_i + k_5 \left(\frac{\bar{\phi}_i}{3} + \frac{\bar{\phi}_{i+1}}{6}\right) (\overline{\Delta s})^2\ \cos\theta_i \qquad (2.22)$$

Similarly, using Eq. 2.14 $\overline{\Delta x}$ is

$$\overline{\Delta x} = \bar{x}_{i+1} - \bar{x}_i = \overline{\Delta s}\ \cos\theta_i - k_5 \left(\frac{\bar{\phi}_i}{3} + \frac{\bar{\phi}_{i+1}}{6}\right) (\overline{\Delta s})^2\ \sin\theta_i \qquad (2.23)$$

By letting $z = \Delta s$, Eq. 2.20 gives

$$\theta_{i+1} = \theta_i + k_5 \left(\frac{\bar{\phi}_i + \bar{\phi}_{i+1}}{2}\right) \overline{\Delta s} \qquad (2.24)$$

From the equilibrium equations (Eqs. 2.15, 2.16, and 2.17), the forces at location $\bar{s}_{i+1}$ are

$$\bar{H}_{i+1} = \bar{H}_i + k_6 \left[\overline{\Delta y} + k_7\ (\cos\theta_{i+1} - \cos\theta_i)\right] \qquad (2.25)$$

$$\bar{V}_{i+1} = \bar{V}_i + k_6 \left[\overline{\Delta x} - k_7\ (\sin\theta_{i+1} - \sin\theta_i)\right] \qquad (2.26)$$

$$\bar{M}_{i+1} = \bar{M}_i + k_8 \left[(\bar{H}_i - k_6\, k_7\, \cos\theta_i)\ \overline{\Delta y} + (\bar{V}_i + k_6\, k_7\, \sin\theta_i)\ \overline{\Delta x} + \frac{1}{2} k\ (\overline{\Delta y}^2 + \overline{\Delta x}^2)\right] \qquad (2.27)$$

When point (i+1) coincides with the point of application of a concentrated redundant force $\bar{V}_r$ (such as $\bar{V}_{ij}$ of Fig. 5), then Eq. 2.26 must be replaced with

$$\bar{V}_{i+1} = \bar{V}_i + k_6 \left[\overline{\Delta x} - k_7\ (\sin\theta_{i+1} - \sin\theta_i)\right] - \bar{V}_r \qquad (2.28)$$

Knowing stress resultants $\bar{H}_i$ and $\bar{V}_i$ and the geometric parameters $\bar{\phi}_i$, θ_i, $\bar{x}_i$, and $\bar{y}_i$ at location $\bar{s}_i$, the above equations are used to determine these parameters at location $\bar{s}_{i+1}$. $\bar{\phi}_{i+1}$ is determined iteratively by first assigning to it an assumed value. Then, using Eqs. 2.22, 2.23, 2.24, 2.27, and the moment-curvature relationship, successively, a new $\bar{\phi}_{i+1}$ is computed and used as the assumed value for the next iteration cycle. This process is repeated until the two consecutive $\bar{\phi}_{i+1}$ are within a specified tolerance. With the $\bar{\phi}_{i+1}$ now known, Eqs. 2.22, 2.23, 2.24, 2.25, 2.26 (or 2.28), and 2.27 are used to calculate $\bar{y}_{i+1}$, $\bar{x}_{i+1}$, θ_{i+1}, $\bar{H}_{i+1}$, $\bar{V}_{i+1}$, and $\bar{M}_{i+1}$, respectively. In general, to start the integration, any arbitrary point can be selected as the starting point. Figure 13 shows the j^{th} longitudinal beam of the grillage of Fig. 12. Point Fj, with the known location $\bar{s}_{Fj}$, an arbitrary $\bar{y}_{Fj}$, the unknown slope θ_{Fj}, and the unknown stress resultants $\bar{H}_{Fj}$, $\bar{V}_{Fj}$, and $\bar{M}_{Fj}$ (or $\bar{\phi}_{Fj}$) is the starting point for the integration. Integration to the left and to the right of point Fj gives, after some manipulation:

$$\bar{M}_{oj} = M\,(\bar{H}_{Fj}, \bar{V}_{Fj}, \bar{\phi}_{Fj}, \theta_{Fj}, \bar{V}_{ij}) \qquad i = 1,\ell \qquad (2.29)$$

$$\theta_{oj} = \theta\,(\bar{H}_{Fj}, \bar{V}_{Fj}, \bar{\phi}_{Fj}, \theta_{Fj}, \bar{V}_{ij}) \qquad i = 1,n \qquad (2.30)$$

$$\bar{H}_{oj} = H\,(\bar{H}_{Fj}, \bar{V}_{Fj}, \bar{\phi}_{Fj}, \theta_{Fj}, \bar{V}_{ij}) \qquad i = 1,n \qquad (2.31)$$

$$\bar{y}_{kj} = y\,(\bar{H}_{Fj}, \bar{V}_{Fj}, \bar{\phi}_{Fj}, \theta_{Fj}, \bar{V}_{ij}) \qquad \begin{matrix} i = 1,\ell \\ k = o,\ell \end{matrix} \qquad (2.32)$$

$$\bar{M}_{(n+1),j} = M\,(\bar{H}_{Fj}, \bar{V}_{Fj}, \bar{\phi}_{Fj}, \theta_{Fj}, \bar{V}_{ij}) \qquad i = (\ell+1),n \qquad (2.33)$$

$$\theta_{(n+1),j} = \theta\ (\bar{H}_{Fj},\ \bar{V}_{Fj},\ \bar{\phi}_{Fj},\ \theta_{Fj},\ \bar{V}_{ij}) \qquad i = 1,n \qquad (2.34)$$

$$\bar{H}_{(n+1),j} = H\ (\bar{H}_{Fj},\ \bar{V}_{Fj},\ \bar{\phi}_{Fj},\ \theta_{Fj},\ \bar{V}_{ij}) \qquad i = 1,n \qquad (2.35)$$

$$\bar{y}_{kj} = y\ (\bar{H}_{Fj},\ \bar{V}_{Fj},\ \bar{\phi}_{Fj},\ \theta_{Fj},\ \bar{V}_{ij}) \qquad \begin{matrix} i = (\ell+1),n \\ k = (\ell+1),(n+1) \end{matrix} \qquad (2.36)$$

$$\bar{\Delta}_{kj} = \Delta\ (\bar{H}_{Fj},\ \bar{V}_{Fj},\ \bar{\phi}_{Fj},\ \theta_{Fj},\ \bar{V}_{Fj}) \qquad \begin{matrix} i = 1,n \\ k = 1,n \end{matrix} \qquad (2.37)$$

where subscripts are as shown in Figs. 12 and 13.

Similar relations are obtained for other longitudinal beams of Fig. 12 by varying j from 1 to m.

The values given by the functions of Eqs. 2.29 to 2.31, 2.33 to 2.35 and 2.37 are used for enforcement of the compatibility requirements and boundary conditions discussed later in Section 2.4.

2.3 TRANSVERSE BEAMS

The transverse beams of the analytical model (Section 2.1) are subjected only to concentrated redundants V_{ij} Fig. 4b). Because of the absence of axial loads, the second order effects in the transverse beam are negligible. Therefore, they can be analyzed according to the small deflection first order elasto-plastic beam theory. In general, the ends of the transverse beam can be subjected by the adjoining structural elements to restraints of unknown characteristics, but in this

presentation, only fixed ends are considered, a simply supported beam being a special case of the fixed ended beam.

Each transverse beam is assumed to contain not more than three plastic hinges before the ultimate capacity of the grillage is reached; numerical results shown in later chapters have confirmed this assumption.

A typical transverse beam (the i^{th} transverse of Fig. 12) is shown in Fig. 14a. In the elastic range, displacements $\{\bar{\Delta}_{ij}\}$ can be directly related to forces $\{\bar{V}_{ij}\}$ by

$$\{\bar{\Delta}_{ij}\} = [f_{k1}]_i \{\bar{V}_{ij}\} \qquad j = 1,m \qquad (2.38)$$

where $[f_{k1}]_i$ is the flexibility matrix of the transverse beam.

After the formation of the first plastic hinge (location C_i in Fig. 14b or s in Fig. 14c), the plastic hinge is replaced with a real hinge. Then, additional displacements $\delta_1 \{\bar{\Delta}_{ij}\}$ and forces $\delta_1 \{\bar{V}_{ij}\}$ can be related by

$$\delta_1 \{\bar{\Delta}_{ij}\} = [f'_{k1}]_i \delta_1 \{\bar{V}_{ij}\} \qquad j = 1,m \qquad (2.39)$$

where $[f'_{k1}]_i$ is the flexibility matrix of the transverse beam shown in Fig. 14b or 14c, whichever is the case.

After the formation of the second hinge, the transverse beam is replaced by the beam shown in Fig. 14d or 14e. Then the additional displacements $\delta_2 \{\bar{\Delta}_{ij}\}$ and forces $\delta_2 \{\bar{V}_{ij}\}$ can be related by

$$\delta_2 \{\bar{\Delta}_{ij}\} = [f''_{k1}]_i \, \delta_2 \{\bar{V}_{ij}\} \qquad j = 1,m \qquad (2.40)$$

where $[f''_{kj}]_i$ is the flexibility matrix of the transverse beam shown in Fig. 14d or 14e whichever is applicable.

When all three plastic hinges are formed, the transverse beam can be represented by the beam of Fig. 14f. In this case, the additional displacements of the beam are composed of a rigid body displacement and elastic deformations. By introducing an additional unknown displacement $\bar{\delta}_{is}$, the following relationships can be obtained

$$\delta_3 \{\bar{\Delta}_{ij}\} = [f'''_{k1} \vdots g_k]_i \left\{\begin{array}{c} \delta_3 \bar{V}_{ij} \\ \hdashline \bar{\delta}_{is} \end{array}\right\} \qquad j = 1,s \qquad (2.41)$$

$$\delta_3 \{\bar{\Delta}_{ij}\} = [f''''_{k1} \vdots g'_k]_i \left\{\begin{array}{c} \delta_3 \bar{V}_{ij} \\ \hdashline \bar{\delta}_{is} \end{array}\right\} \qquad j = (s+1),m \qquad (2.42)$$

where $[f'''_{k1}]_i$ and $[f''''_{k1}]_i$ are, respectively, the flexibility matrices of segments $C_i A_i$ and $A_i D_i$ with simply supported ends, and the elements of $\{g_k\}_i$ and $\{g'_k\}_i$ are given by

$$g_k = \frac{k}{s} \qquad k = 1,s \qquad (2.43)$$

$$g'_k = \frac{(m - s+1) - k}{(m - s+1)} \qquad k = 1,(m-s) \qquad (2.44)$$

The locations of plastic hinges considered above are those expected in grillages of usual proportions. If, in some unusual cases,

any other combinations of plastic hinges are possible (such as two or more plastic hinges forming within the span), the previous procedure can be readily extended.

Relations similar to Eqs. 2.38 through 2.44 are obtained for all other transverse beams of Fig. 12 by varying i from 1 to n.

For simply supported transverses, the beam of Fig. 14d should be used as the starting system and then replaced with the beam of Fig. 14f after the plastic hinge is formed within the span.

2.4 GRILLAGE--A COMBINATION OF LONGITUDINALS AND TRANSVERSES

Knowing the force-displacement functions for each longitudinal and transverse beam, the relationship between the external loads and the unknown parameters of the grillage can be expressed as a set of simultaneous nonlinear equations. These equations are then to be solved to obtain the grillage unknowns.

Before the formation of any plastic hinges in the transverse beams, each of the m longitudinals (e.g., the j^{th} one) contains (n+4) unknowns consisting of $\overline{H}_{Fj}$, $\overline{V}_{Fj}$, θ_{Fj}, $\overline{\phi}_{Fj}$, and n unknown redundants $\overline{V}_{ij}$ (i = 1,n). Therefore, a total of m (n+4) equations are required for determining these unknowns.

By satisfying the following compatibility conditions at the beam junctions, (mn) equations are obtained.

$$(\overline{\Delta}_{ij})_L - (\overline{\Delta}_{ij})_T = 0 \qquad \begin{cases} i = 1,n \\ j = 1,m \end{cases} \qquad (2.45)$$

where $(\bar{\Delta}_{ij})_L$ is given by Eq. 2.37 and $(\bar{\Delta}_{ij})_T$ by Eq. 2.38. The remaining (4m) equations are obtained by satisfying the following boundary conditions:

B.C.1

$$\theta_{oj} = 0 \text{ or } \bar{M}_{oj} = 0 \qquad j = 1,m \qquad (2.46)$$

B.C.2

$$\theta_{(n+1),j} = 0 \text{ or } \bar{M}_{(n+1),j} = 0 \qquad j = 1,m \qquad (2.47)$$

B.C.3

$$\bar{H}_{oj} - \bar{P} = 0 \qquad j = 1,m \qquad (2.48)$$

B.C.4

$$\bar{H}_{(n+1),j} - \bar{P} = 0 \qquad j = 1,m \qquad (2.49)$$

where $\bar{M}_{oj}$, θ_{oj}, $\bar{H}_{oj}$, $\bar{M}_{(n+1),j}$, $\theta_{(n+1),j}$, and $\bar{H}_{(n+1),j}$ are given, respectively, by Eqs. 2.29, 2.30, 2.31, 2.33, 2.34, and 2.35.

These m (n+4) equations are then solved for the unknown parameters $\bar{H}_{Fj}$, $\bar{V}_{Fj}$, θ_{Fj}, $\bar{\phi}_{Fj}$, and $\bar{V}_{ij}$ (i = 1,n and j = 1,m). Then, the deformations and stress resultants can be determined for any point in the grillage model.

As the loads increase, the deformations and stress resultants increase until either the ultimate capacity of the grillage is reached

or the first plastic hinge is formed in one of the transverses. In the latter case, the deformations and forces corresponding to this condition are denoted by subscript "1", e.g., $(\bar{\Delta}_{ij})_1$ and $(\bar{V}_{ij})_1$. By replacing the plastic hinge with a real hinge (see Fig. 14b and 14c), a modified grillage model is obtained. Then, a new system of m (n+4) nonlinear equations in terms of unknowns $\delta\bar{H}_{Fj}$, $\delta\bar{V}_{Fj}$, $\delta\theta_{Fj}$, $\delta\bar{\phi}_{Fj}$, and $\delta\bar{V}_{ij}$ is obtained. Here, δ refers to the changes beyond the formation of the first hinge. (mn) equations are obtained from the following compatibility conditions at the beam junctions:

$$\delta\ (\bar{\Delta}_{ij})_L - \delta\ (\bar{\Delta}_{ij})_T = 0 \qquad \begin{cases} i = 1,n \\ j = 1,m \end{cases} \tag{2.50}$$

where

$$\delta\ (\bar{\Delta}_{ij})_L = (\bar{\Delta}_{ij})_L - (\bar{\Delta}_{ij})_1 \tag{2.51}$$

$(\bar{\Delta}_{ij})_L$ is obtained from Eq. 2.37 and $\delta\ (\bar{\Delta}_{ij})_T$ is given by Eq. 2.39 for the transverse beam containing the hinge and by

$$\delta\ \{\bar{\Delta}_{ij}\}_T = [f_{k\ell}]_i\ \delta\ \{\bar{V}_{ij}\} \qquad j = 1,n \tag{2.52}$$

for transverse beams with no hinge; $[f_{k\ell}]_i$ is as defined in Eq. 2.38. The remaining (4m) equations are obtained from the boundary conditions, Eqs. 2.46 to 2.49. If the loads could be increased until the second hinge is formed in the transverse beams, yet before the ultimate capacity is reached, then the corresponding forces and deformations are obtained from

$$(\bar{V}_{ij})_2 = (\bar{V}_{ij})_1 + \delta\bar{V}_{ij} \qquad (2.53)$$

$$(\bar{\Delta}_{ij})_2 = (\bar{\Delta}_{ij})_1 + \delta\bar{\Delta}_{ij} \qquad (2.54)$$

In general, once the deformation and forces corresponding to r^{th} plastic hinge of transverse beams are known, the deformations and forces corresponding to plastic hinge (r+1) can be found as follows. The compatibility relations of Eq. 2.50 and boundary conditions of Eqs. 2.46 to 2.49 are used to obtain the m (n+4) equations; where δ, now, denotes the incremental changes beyond the r^{th} hinge, Eq. 2.51 becomes

$$\delta\ (\bar{\Delta}_{ij})_L = (\bar{\Delta}_{ij})_L - (\bar{\Delta}_{ij})_r \qquad (2.55)$$

and $\delta\ (\bar{\Delta}_{ij})_T$ is given by Eq. 2.39, 2.40, 2.41, and 2.42 or 2.52, whichever is applicable. Then, Eqs. 2.53 and 2.54 can be rewritten as

$$(\bar{V}_{ij})_{r+1} = (\bar{V}_{ij})_r + \delta\ \bar{V}_{ij} \qquad (2.56)$$

$$(\bar{\Delta}_{ij})_{r+1} = (\bar{\Delta}_{ij})_r + \delta\ \bar{\Delta}_{ij} \qquad (2.57)$$

Whenever Eqs. 2.41 and 2.42 are used for $\delta\ (\bar{\Delta}_{ij})_T$, additional unknowns $\bar{\delta}_{is}$ are introduced. Since, for each additional unknown an additional equation is needed, the moment equilibrium equations of the segments $C_i\ A_i$ of Fig. 14f are used.

$$\delta \bar{M}_{C_i} = \sum_{j=1}^{s-1} (j) \left(\frac{b}{r}\right) \delta \bar{V}_{ij} = 0 \qquad i = 1,n \qquad (2.58)$$

The number of additional unknowns (or equations) may vary from 1 to n (1 per transverse beam). Therefore, the total number of equations, n_t, to be solved may vary from m (n+4) to m (n+4) + n.

2.5 INCREMENTAL LOADING AND DETERMINATION OF THE ULTIMATE CAPACITY

As noted in Section 2.4, after the formation of each plastic hinge in the transverse beams, the model is modified and the increments of forces and deformations are related using the modified model. This process requires determination of the loading at which a new plastic hinge is formed and the corresponding deformations and internal forces. This is accomplished by applying the load incrementally. The numerical technique used for solving the nonlinear equations also requires increasing the loads in small increments for obtaining proper convergence, especially on approaching the ultimate capacity.

In general, the loads could be incremented in any desired proportion; here, the axial load is kept constant and the lateral load is increased in small increments.

Because of the lack of convergence in the neighborhood of the ultimate condition, the true ultimate strength could not be obtained; the flattening of the load versus deflection curve was used as the criterion for reaching the ultimate condition.

2.6 SOLUTION OF NONLINEAR EQUATIONS

Each time the lateral load is increased, a system of nonlinear simultaneous equations must be solved. These equations can be expressed as

$$f_i\ (x_j) = 0 \qquad \begin{cases} i = 1,n_t \\ j = 1,n_t \end{cases} \tag{2.59}$$

They are solved using the generalized Newton-Raphson method.[50] This method linearizes the system of equations through a series expansion of functions $f_i\ (x_j)$ about the solution vector $\{x_j^o\}$ and ignoring the higher order terms of the series

$$\{f_i\ (x_j^o + \delta x_j)\} = \{f_i\ (x_j^o)\} + \left[\frac{\partial f_i\ (x_j)}{\partial x_j}\right]_{x_j = x_j^o} \{\delta x_j\} \tag{2.60}$$

where $\{\delta x_j\}$ is the change in solution vector and $[\partial f_i\ (x_j)/\partial x_j]$ is the Jacobian matrix of the first derivatives; the derivatives are obtained numerically by a differencing technique.

Setting the left-hand side of Eq. 2.60 equal to zero, as required by Eq. 2.59, results in

$$\left[\frac{\partial f_i\ (x_j)}{\partial x_j}\right]_{x_j = x_j^o} \{\delta x_j\} = -\{f_i\ (x_j^o)\} \tag{2.61}$$

Equation 2.61 is a set of linear simultaneous equations which can be solved for the correction vector $\{\delta x_j\}$. The addition of x_j^o and δx_j will give a new solution vector which is used in the next iteration cycle.

$$\{x_j^o\}_{new} + \{x_j^o\}_{old} + \{\delta x_j\} \tag{2.62}$$

In general, the Newton-Raphson method does not guarantee convergence since the convergence behavior is highly problem dependent. For the problem at hand, the following was observed:

1. The convergence behavior was sensitive to the first load increment and the corresponding assumed initial values of $\overline{V}_{ij}$. It was found desirable to assign a small value to the first load increment to ensure elastic or nearly elastic behavior and select the initial values of $\overline{V}_{ij}$ equal to the tributary lateral load qab.

2. Allowance of the full correction to the solution vector according to Eq. 2.62 leads to divergence in some cases. A factored correction according to Eq. 2.63 proved to ensure proper convergence

$$\{x_j\}_{new} = \{x_j\}_{old} + c_k \{\delta x_j\} \tag{2.63}$$

where

$$c_k = c_{k-1} + 0.2 \leq 1.0 \qquad k = 2,3, \ldots$$

and (2.64)

$$c_1 = 0.1$$

3. For the second and subsequent load increments, prorating of the solution vector proportionally to the loading proved to improve convergence.

4. Smaller load increments had to be used on approaching the ultimate capacity.

5. The moment-curvature relationship with the definite limits as shown in Fig. 10 could not be utilized since the method required a value of moment for any given curvature. Therefore, the moment-curvature curve was extended at both ends indefinitely with a very small slope of $d\bar{M}/d\bar{\phi} = 0.00002$, thus, introducing an arbitrary strain-hardening effect.

2.7 MODES OF FAILURE

Depending on the geometrical and material properties and loading, grillages are subject to one of two different modes of failure. If the failure occurs in a portion of the grillage between two adjacent transverses, the grillage is said to fail by "panel" mode. This is essentially a local failure due to the instability of longitudinal beam(s) between two transverses. On the other hand, if the transverses are of such proportions as to, either, allow the longitudinals reach their capacity as long beam-columns (of length equal to the length of the whole grillage) without offering any significant resistance to an increase in loads or to form a three-hinge mechanism before the ultimate capacity of the whole grillage is reached, the grillage is said to fail by "grillage" mode.

Figure 15 shows a schematic axial versus lateral load interaction diagram for grillages in which the transition from panel mode to grillage mode has been caused by the formation of the three-hinge mechanisms in the transverses. The grillage mode range (Q_2-Q_3) is seen to be more sensitive to lateral load than the panel mode range (Q_1-Q_2). This is because after formation of mechanisms in the transverses, the longitudinals behave as long beam-columns, and thus, have little resistance to an increase in lateral loads. Failure modes are further discussed in the application of the method to some sample grillages in Chapter 3.

3. NUMERICAL SOLUTIONS AND COMPARISON WITH TEST RESULTS

A computer program was developed to check the feasibility of the proposed method. The program was applied to four sample grillages to establish the size of increments and the values of some parameters required by the numerical techniques employed, and to study the convergence behavior of the method. To confirm the accuracy of the analytical model in simulating the true behavior of grillages, the proposed method was compared with some available test results.

3.1 COMPUTER PROGRAM

The following assumptions were made to simplify programming:

1. The grillage is doubly symmetrical and, thus, only a quarter of the grillage has to be analyzed (Fig. 16).

2. There are an even number of longitudinals and transverses (no stiffener on either axis of symmetry).

3. All stiffeners are T-shaped; rectangular stiffeners are a special case of tee stiffeners with the flange area equal to zero.

4. Stiffeners for a particular direction have the same geometrical and material properties.

5. Transverses are simply supported, but the longitudinals may be simply supported or fixed.

Except for these simplifying assumptions, the program follows the general procedure explained in Chapter 2.

Since, because of symmetry, the slope θ_{Fj} and the shear force $\bar{V}_{Fj}$ at the mid-span points of the longitudinals, points Fj (j=1,m) of Fig. 16, are equal to zero, these points are used as the starting points for the stepwise integration. Also, since the variation of axial force N along the longitudinal beam is negligible, force $\bar{H}_{Fj}$ is assumed to be equal to the axial load $\bar{P}$. Thus, the only unknown at point Fj is curvature $\bar{\phi}_{Fj}$, and the relations of Eqs. 2.33 to 2.35 and 2.37 become

$$\bar{M}_{(n+1),j} = M\ (\bar{\phi}_{Fj}\ ,\ \bar{V}_{ij}) \qquad i = 1,n \qquad (3.1)$$

$$\theta_{(n+1),j} = \quad (\bar{\phi}_{Fj}\ ,\ \bar{V}_{ij}) \qquad i = 1,n \qquad (3.2)$$

$$\bar{H}_{(n+1),j} = H\ (\bar{\phi}_{Fj}\ ,\ \bar{V}_{ij}) \qquad i = 1,n \qquad (3.3)$$

$$\bar{\Delta}_{ij} \quad = \quad (\bar{\phi}_{Fj}\ ,\ \bar{V}_{ij}) \qquad i = 1,n \qquad (3.4)$$

where j varies from 1 to m with m and n now denoting the number of longitudinals and transverses in the quarter grillage. In this case, before any of the transverses develop a plastic hinge, the total number of unknowns is m (n+1). Therefore, besides the (mn) compatibility conditions at the beam junctions, only m boundary conditions given by Eq. 2.46 have to be satisfied since the other 3m boundary conditions given by Eqs. 2.48 and 2.49 are automatically met.

In the computer program, the transverses are treated according to the procedure described in Section 2.3. However, because of the symmetry, the mid-segment of the transverse beam (segment AB of Fig. 17) is subjected to a uniform moment and undergoes plastic flow once the magnitude of the moment reaches the plastic moment of the cross section, M_p. It is assumed that a plastic hinge is formed at point B and that the incremental displacement of segment BC is composed of a rigid body displacement and elastic deformations with the ends simply supported. Equations 2.42 and 2.44 become, respectively,

$$\delta_3 \{\bar{\Delta}_{ij}\} = [f'''_{k1} \vdots g_k]_i \left\{\begin{matrix} \delta_3 \bar{V}_{ij} \\ \hline \bar{\delta}_{is} \end{matrix}\right\} \qquad j = 1,m \qquad (3.5a)$$

$$g_k = \frac{m+1 - k}{m} \qquad k = 1,m \qquad (3.5b)$$

where $[f'''_{k1}]_i$ is now the flexibility matrix of portion BC.

A brief flow chart of the computer program is given in Fig. 18. The subroutines used in establishing the effective average stress-edge strain and the moment-curvature-axial load relationships are, except for some minor modifications, the same as those given in Ref. 51. The program commences the stepwise integration along the longitudinals after specifying the following stress resultants and geometric parameters at points Fj:

$$\bar{H}_{Fj} = \bar{P} \quad ; \quad \bar{V}_{Fj} = 0 \qquad (3.6a)$$

$$\theta_{Fj} = 0 \quad ; \quad \bar{y}_{Fj} = 0 \qquad (3.6b)$$

$$\bar{x}_{Fj} = 0 \qquad ; \qquad \bar{s}_{Fj} = 0 \tag{3.6c}$$

$\bar{\phi}_{Fj}$ is an unknown and is treated according to Section 2.6. The remainder of the program follows the analytical procedure of Chapter 2.

3.2 ANALYSIS OF SAMPLE GRILLAGES

Four grillages with extreme values of geometrical parameters were assumed as samples for developing and refining computational techniques. One of these, Sample Grillage 1 (SG-1), was analyzed much more extensively than the others (SG-2, SG-3, and SG-4) and therefore is used here to indicate general trends. The other sample grillages are brought out later in Chapter 4 in connection with the effect of some of the grillage parameters on the ultimate strength.

Sample Grillage 1 is shown in Fig. 19 and its geometrical and material properties are listed in Table 1. It consists of a plate with slenderness ratio of b/t = 76.2 and aspect ratio of a/b = 2.0, four T-shaped transverse stiffeners spaced at 48 in., and four T-shaped longitudinals spaced at 24 in. The yield stress is assumed to be equal to 37.0 ksi for all grillage components. All four edges of the grillage are assumed to be simply supported.

3.2.1 Behavior of Sample Grillages

The plots of deflection are shown versus an increasing lateral load in Fig. 20 for six different values of axial load. The curves for the lower three values (p/σ_{yp} = 0.10, 0.45, and 0.60) are drawn for the mid-point deflection of the inner longitudinal. The other three

(p/σ_{yp} = 0.66, 0.68, and 0.70) are for the deflection of the same longitudinal at a point 22.6 in. from the loaded edge. The solid dots indicate the computed points and the circles denote the formation of plastic hinges in the transverses. The figure shows that under the first three axial loads (p/σ_{yp} = 0.10, 0.45, and 0.60), the grillage reaches its ultimate capacity after both transverses form plastic hinges. Thus, it exhibits the grillage failure mode. However, under the higher three axial loads (p/σ_{yp} = 0.66, 0.68, and 0.70), the grillage reaches its ultimate capacity before the formation of any plastic hinges in the transverses and the failure is in the end panels, that is, the grillage exhibits the panel failure mode.

The axial versus lateral load interaction diagram is given in Fig. 21 where the solid dots are the computed points. The interaction between the axial and the lateral load in the panel mode range Q_1-Q_2 appears to be linear. This is to be expected since the linear load interaction is typical for beam-columns of small slenderness ratios such as a/r = 20.5 for this sample grillage.[52]

In the grillage failure range Q_2-Q_3 of Fig. 21, the computed points show a slight deviation from the linear relationship. This is because after the formation of plastic hinges in the transverses, the longitudinals behave similarly to long beam-columns of a length equal to the length of the whole grillage ($2L_L/r$ = 102.3). Thus, the grillage has a nonlinear load interaction which is typical for beam-columns of large slenderness ratio. For this grillage, however, since the deviation

from a straight line is rather negligible, a linear interaction is assumed in later discussion.

The deformation pattern of a grillage undergoing the grillage mode of failure is illustrated in Fig. 22 by SG-1 subjected to an axial load of $p/\sigma_{yp} = 0.45$ and lateral load of $\bar{q} = 4.45$.

The moment diagrams of the inner longitudinal under an axial compression $p/\sigma_{yp} = 0.45$ and three lateral loads ($\bar{q} = 4.45$, 4.90, and 4.97) are given in Fig. 23. Respectively, these diagrams correspond to the moment distributions at the following three stages: 1) formation of a plastic hinge in the inner transverse beam (first hinge), 2) formation of a plastic hinge in the outer transverse beam (second hinge), and 3) the ultimate load (see also Fig. 20). The figure shows the redistribution of the moment toward the outer transverse after the formation of the plastic hinge in the inner transverse. The figure also shows that after both transverses have formed plastic hinges, some additional load is carried by the longitudinal acting as a long beam-column of length $2L_L$. When the ultimate capacity is reached, the midpoint moment is about 78% of the moment capacity of the cross section $\bar{M}_{pc}$ and the longitudinal fails by instability.

The moment diagrams for the inner transverse beam of SG-1 at the formation of the plastic hinge (solid line) and at the ultimate condition (dotted line) are shown in Fig. 24. The change in moments is seen to be negligible. This supports the assumption made in the method

that not more than one plastic hinge need be formed in a simply supported transverse beam before the ultimate capacity is reached.

3.2.2 Convergence Behavior of the Method

The convergence behavior of the method was found to be satisfactorily rapid. This is illustrated in Figs. 25 to 28 for the first (solid line) and last (dotted line) increments of load of SG-1 subjected to the axial compression of $p/\sigma_{yp} = 0.45$ (see also Fig. 20).

Figure 25 shows how the end moment of the inner longitudinal, $\bar{M}_{(n+1)}$, converges to zero (as it should for a simply supported end) against the number of iterations. Figure 26 shows similar plots for the compatibility requirement at the stiffener junction (1,1). $[(\bar{\Delta}_{11})_L - (\bar{\Delta}_{11})_T]$ is seen to converge to zero (as is required by Eq. 2.45) against the number of iterations. Figures 27 and 28 give the plots of redundant $\bar{V}_{11}$ and curvature $\bar{\phi}_{F_1}$ versus the number of iterations; the flattening of the curves indicates convergence to the correct value.

The convergence is seen to be satisfactory even on approaching the ultimate condition. Six and five iterations for the first and last load increments were sufficient. It should be noted, however, that the last load increment is much smaller than the first load increment.

3.3 COMPARISON WITH TEST RESULTS

An intensive search of literature has revealed an acute scarcity of test results on grillages. Besides a few grillages tested

under concentrated lateral loads,[12,21] only two specimens tested under uniform lateral pressure alone have been reported.[53] Unfortunately, there was not enough information given to analyze them.

The only test results that could be found for comparison with the proposed method are those informally provided by the Naval Construction Research Establishment on seven test specimens.[54] The specimens were of the type shown in Fig. 29 with four longitudinal and four transverse T-stiffeners and the longitudinal edges simply supported. The axial loads were applied through the plates welded at the two ends. The test specimen parameters are given in columns 3 to 10 of Table 2 and the experimental ultimate loads in columns 11 and 12. The first three test grillages (TG-1a, 1b, and 1c) were identical and had a plate slenderness ratio $b/t = 76.2$ and an aspect ratio of $a/b = 2.0$. TG-1a was tested under axial load alone, while TG-1b and TG-1c were subjected to combined loads. TG-2a and TG-2b were also identical, having a plate slenderness ratio of 47.7 and an aspect ratio of 5.0 and were, respectively, tested under combined loads and axial load alone. TG-3 and TG-4 had, respectively, plate slenderness ratios of 95.0 and 96.4 and aspect ratios of 2.5 and 2.0. All seven specimens failed by the panel failure mode.

Since additional data was needed in order to be able to use the computer program, the following assumptions were made: 1) the loaded edges were assumed to be fixed; 2) since no information on residual stresses was available, some residual stresses typical for plates with these dimensions were assumed as shown in column 13 of Table 2; and

3) the effective plate width for the transverses a_e was assumed to be equal to 30t for all specimens*.

Comparison of the method with the test results is shown in Figs. 30 to 33. In each figure, the test results (indicated by triangles) and a portion of the axial versus lateral load interaction diagrams for $\sigma_{rc} = 0$ (solid line) and for the assumed σ_{rc} (dotted line) are shown. The computed points are indicated by solid dots. A summary of the comparisons in terms of the ratio of the radial distances R_{th}/R_{ex} is given in the last two columns of Table 2. The meaning of R_{th} and R_{ex} is illustrated in Fig. 30.

Figure 30 gives the comparison of the method with the test results of specimens TG-1a, 1b, and 1c. The deviations are +2%, +5%, and 0% for $\sigma_{rc} = 0$ and -6%, -1%, and -6% for $\sigma_{rc}/\sigma_{yp} = 0.082$. Figure 31 compares the method with the test results of specimens TG-2a and 2b. The method correlates extremely well with the test result of TG-2a (deviations are +3% for $\sigma_{rc} = 0$ and -2% for $\sigma_{rc}/\sigma_{yp} = 0.2$), but gives a poor correlation for TG-2b with deviations of +43% and +36%. However, since TG-2b with zero lateral load exhibited a 14% lower compressive strength than TG-2a even though TG-2a was subjected to a lateral load of $\bar{q} = 0.235$, it is believed that this deviation could have been due to a premature failure of some grillage components or due to unusually large residual stresses, possibly in combination with large initial imperfections.

*The effect of a_e on the ultimate strength of grillages is discussed in Chapter 4.

The method is compared with the experimental results of TG-3 and TG-4 in Figs. 32 and 33. The deviations are -8% (for $\sigma_{rc} = 0$) and 14% (for $\sigma_{rc}/\sigma_{yp} = 0.1$) for TG-3 and +11% (for $\sigma_{rc} = 0$) and 0% (for $\sigma_{rc}/\sigma_{yp} = 0.1$) for TG-4.

A point which should be considered in judging the above comparisons is that residual stresses have a significant effect on the ultimate strength of grillages, especially of those having plates with large b/t, yet, in this case they had to be assumed. In general, for a more accurate comparison, the intensity of residual stresses in the specimens must be measured.

3.4 CONCLUDING REMARKS

In previous sections, the feasibility, efficiency, and the accuracy of the proposed method was checked and proved satisfactory. Thus, the method can be accepted as a working tool for studying the behavior of grillages with various combinations of geometries, material properties, and loads. Also, it can be used for evaluating the effect of some numerical assumptions which have to be made in the analysis, such as, the effective width of the plate for the transverses and the intensity of residual stresses. This is done for the sample grillages in Chapter 4.

4. EFFECT OF SOME GRILLAGE PARAMETERS ON THE ULTIMATE STRENGTH

With the computer program operational, the effect of the following parameters on the ultimate strength of the sample grillages was studied: the assumed effective plate width for transverse beams, the boundary conditions for the loaded ends, initial lateral deflections, and residual stresses.

4.1 EFFECT OF THE EFFECTIVE WIDTH OF PLATE FOR TRANSVERSES

As noted in Section 2.1, a constant effective width of the plate, a_e, was assumed to work as the top flange of the transverse beams (Fig. 4b). To investigate the effect of this essentially arbitrary assumption, two comparative interaction diagrams were computed for SG-1 using two extreme values of a_e, 30t and 150t.

Figure 34 shows that the change of a_e from 30t to 150t increases the ultimate strength of SG-1 only negligibly when the grillage fails by the panel mode, range Q_1-Q_2. On the other hand, when the grillage fails in the grillage mode, range Q_2-Q_3, the strength is affected significantly. This effect was to be expected since for SG-1, $a_e t$ (with a_e = 30t) represents 41.5% of the area of the transverse stiffener A_{st} thus making the plastic moment M_p of the transverse beam very dependent on a_e.

The change in a_e of SG-1 also changes the mode of failure for the combinations of axial and lateral loads falling in the shaded area of Fig. 34.

It should also be pointed out that, since in the panel failure range a_e affects the analysis only through the flexibility coefficients of the transverse beams, it is expected that the size of the transverse stiffeners would affect the ultimate strength in the same manner as a_e. To investigate this, sample grillages SG-2 and SG-3, given in Fig. 35 and Table 1, were analyzed. SG-2 and SG-3 are identical except for the size of the transverse stiffeners (A_{st} = 0.96 in.^{2} for SG-2 and A_{st} = 0.65 in.^{2} for SG-3). Each grillage consists of a plate with slenderness ratio b/t = 65.3 and aspect ratio a/b = 2.4, six rectangular longitudinals, and two T-shaped transverse stiffeners. a_e of 50t is assumed for both grillages. The axial versus lateral load interaction diagrams of both grillages are shown in Fig. 36. The change of the strength in the panel mode range is rather negligible, but it is quite significant in the grillage mode range.

The above results seem to indicate that, when grillages fail in the panel mode, the ultimate strength is not sensitive to the elastic flexibility of the transverse beams. Since a_e affects only the flexibility of the transverses, it may be concluded that a_e has a negligible effect on the ultimate strength.

When a grillage fails in the grillage mode as a result of the formation of plastic hinges in the transverse beams, the grillage strength is very dependent on the plastic moment capacity of the transverse beams M_p. This means that the effect of a_e on the strength should be less significant as the effect of a_e on M_p becomes less pronounced. Thus, for grillages with $a_e t > A_{st}$, the effect of a_e on the strength

should be expected to be negligible. No generally conclusive statement can be made at this point, however.

Experimental as well as theoretical work is needed for arriving at a more suitable value of the effective width. Temporarily, an effective width of $a_e = 30t$ is suggested and is felt to be on the conservative side. This has been used by other investigators in the elastic analysis[53] and in the ultimate strength analysis[55] of grillages under lateral loading alone. Also, some sample computations for shear lag have indicated that $a_e = 30t$ is on the conservative side.

4.2 EFFECT OF BOUNDARY CONDITIONS FOR LONGITUDINALS

4.2.1 Restraint Against Rotation

As stated in Chapter 3, the computer program considers simply supported transverses and simply supported or fixed longitudinals. The effect of the two end conditions for the longitudinals on the ultimate strength of SG-1 (Fig. 19) is shown in Fig. 37. As expected, the restraint against rotation increases the strength in both the panel and grillage modes of failure.

To study this effect further, another grillage, SG-4 of Fig. 38 and Table 1, was analyzed. The proportions were selected so that a grillage failure mode would be expected for the most of the interaction range. This grillage consists of a plate with slenderness ratio $b/t = 110$ and an aspect ratio $a/b = 1.33$, six longitudinal and two transverse tee stiffeners. An effective width of $a_e = a/2$, that

is a_e = 73t, was used in the analysis. The axial versus lateral load interaction diagram for this grillage with simply supported longitudinals and two computed values for the grillage with fixed ended longitudinals are shown in Fig. 39. It is seen that the effect of the restraint against rotation on the strength is much more pronounced for this grillage than for SG-1. The reason for this difference is as follows.

The transverse beams of SG-1 are quite stiff and, thus, would force the longitudinals to behave as short beam-columns (a/r = 20.50) spanning between adjacent transverses. On the other hand, the transverse beams of SG-4 are very flexible and allow the longitudinals to behave as long beam-columns of the length equal to the grillage length ($2L_L/r$ = 58.0). Since the restraint against rotation is known to have greater effect on the behavior of longer beam-columns, the greater increase in strength of SG-4 due to end fixity should be expected.

4.2.2 Straight Loaded Edge (Non-Uniform Axial Compression)

It was assumed in the method described in Chapter 2 that the grillage is subjected to uniformly distributed axial compression and that no restraint is imposed against the in-plane movement of the loaded edges. These conditions adequately simulate the test conditions of the specimens discussed in Chapter 3. However, in a real ship structure, the edges are restrained from the in-plane movement by the adjoining grillages and other structural elements. To evaluate the effect of such a restraint on the ultimate strength, the computer program was modified to enforce the loaded edge to remain straight. Under this condition, the

axial edge compression is no longer constant as was assumed previously. However, the total applied force P_t (or the average axial compression p_{ave}) is kept constant.

$$P_t = \sum_{j=1}^{m} P_j \tag{4.1}$$

where P_j is the axial force applied to the j^{th} longitudinal beam.

After establishing the equilibrium position under lateral loading q and axial forces P_j (j = 1,m), the total shortening of the j^{th} longitudinal beam is determined from

$$(u_t)_j = (u_a)_j + (u_c)_j \tag{4.2}$$

where $(u_a)_j$ and $(u_c)_j$ are the in-plane displacements of the end due to the axial strains and curvature, respectively, they are given by

$$u_a = \sum_i (\epsilon_c)_i \cdot (\Delta x)_i \tag{4.3}$$

$$u_c = L_L - \sum_i (\Delta x)_i \tag{4.4}$$

where the summation is over the half length of the longitudinal, ϵ_c is the strain of the centroidal fiber, L_L is as defined in Fig. 16, and Δx and Δs are as defined in Chapter 2. A schematic distribution of u_a, u_c, and u_t is shown in Fig. 40.

The values of P_j are adjusted by an iterative process until the edge displacements u_t's of all the longitudinals are practically the

same. Having the current point ℓ and the previous point (ℓ-1) of the P_j versus $(u_t)_j$ relationship as shown in Fig. 41 the tangent axial stiffness k_j is estimated by

$$k_j = \frac{\delta P_j}{(\delta u_t)_j} \qquad (j = 1,m) \qquad (4.5)$$

Designating the total end displacement for the straight edge by u_{st} (Fig. 40), the change in P_j for the next iteration cycle can be expressed by

$$\delta P_j = k_j \left[u_{st} - (u_t)_j\right] \qquad (j = 1,m) \qquad (4.6)$$

The imposition of Eq. 4.1 requires that the sum of all the changes of axial forces P_j (j = 1,m) be equal to zero, that is,

$$\sum_{j=1}^{m} \delta P_j = \sum_{j=1}^{m} k_j \left[u_{st} - (u_t)_j\right] = 0 \qquad (4.7)$$

Equation 4.7 can then be solved for u_{st} to give

$$u_{st} = \frac{\sum_{j=1}^{m} k_j (u_t)_j}{\sum_{j=1}^{m} k_j} \qquad (4.8)$$

With u_{st} now known, the corresponding changes for the axial loads are found from Eq. 4.6.

After modifying the axial forces, a new equilibrium position is found and the process of modifying is repeated until the following tolerance condition is met:

$$\frac{u_{st} - (u_t)_j}{u_{st}} \leq 0.01 \qquad j = 1,m \qquad (4.9)$$

This concludes the solution for the given intensity of lateral loading q. Then, q is incremented and the process is repeated.

It was observed that to obtain the same degree of accuracy, the increments of lateral load on approaching the ultimate condition had to be much smaller than the corresponding increments for the case of free end movement. This is because after the lateral load is incremented and before the corresponding adjustments are made in axial forces P_j (j = 1,m), the grillage may experience a premature instability, which means the instability of some longitudinal beam due to a too large axial force, although after proper adjustment of the axial forces, the grillage may still be stable. Selection of a smaller lateral load increment ensures that such premature instability would occur closer to the ultimate condition.

The effect of enforcing a straight edge boundary on the behavior of grillages was studied for SG-1 and SG-4. The behavior of SG-1 (Fig. 19) is shown in Fig. 42a. The solid curves are the plots of the lateral load versus the deflection of an inner and an outer longitudinal beam for the case of free edge movement; because of symmetry the behavior of the other two longitudinals is, respectively,

the same. The dotted curves are similar plots for the case of a straight edge. In both cases, the average axial compression is $p_{ave} = 0.66\ \sigma_{yp}$. The figure indicates by the end slopes of the curves that when the edge is free to move, the ultimate strength of the grillage is reached when the inner longitudinal attains its ultimate capacity (at $\bar{q} = 4.00$) while the outer longitudinal still has the capacity to carry some more load. When the edge is to remain straight, failure of the grillage is caused by the simultaneous failure of both longitudinals (at $\bar{q} = 4.34$) and, as a consequence, the grillage is capable of a higher carrying capacity than when the edge is free to move. However, the gain in strength for proportional loading is quite negligible as can be seen from the two axial versus lateral load interaction diagrams of Fig. 42b.

A plot similar to that of Fig. 42a is shown in Fig. 43 for SG-4 (Fig. 38) where the lateral load is plotted versus the mid-point deflections of the longitudinals for $p_{ave} = 0.245\ \sigma_{yp}$. Again, because of symmetry, the behavior of only three longitudinals is given. Here, in contrast to SG-1, when the edge is free to move (solid line), the ultimate strength of the grillage is attained when the two inner longitudinals reach their ultimate capacity (at $\bar{q} = 3.89$) with little reserve capacity left in the outer one. When the edge is to remain straight (dotted curves), a substantial increase in bending stiffness is indicated for all longitudinals and the failure of the grillage is caused by the simultaneous failure of the two inner longitudinals. As illustrated in Fig. 44, a gain of about 10% in the proportional strength is obtained by enforcing the straight edge condition for this specimen.

The difference in behavior of SG-1 and SG-4 is due to the difference in the stiffness of their transverse beams. SG-1, having strong transverses, undergoes an almost uniform edge displacement in the free edge case, and thus, the change in behavior due to the enforcement of a straight edge is negligible. In SG-4, however, because of the very flexible transverses, the inner longitudinals undergo much larger deflections than the outer ones and, thus, cause a noticeable variation of the end displacements along the edge. As a consequence, the enforcement of the straight edge condition significantly reduces the forces in the inner longitudinals and increases those in the outer longitudinals. The effect of the redistribution of the axial forces in this grillage is so pronounced that even the sign of redundant V_{11} is changed. This means that the two inner most longitudinals help the transverse beams in supporting the other longitudinals. This is the reason for the increase in the bending stiffness indicated in Fig. 43.

It should be pointed out that SG-4, having very weak transverses, represents a type of grillage seldom encountered in practice, especially in ship structures. Grillages, more commonly used in ships, are of the type similar to SG-1. Therefore, it may be concluded that the proposed method with the assumption of a free edge movement can be used with confidence for analyzing grillages commonly encountered in ship structures.

4.3 CONSIDERATION OF INITIAL LATERAL DEFLECTIONS

Since the differential equations of the longitudinals are integrated numerically along the length, any form of initial lateral

deflections, expressed as a function or as a set of values specified for points along the longitudinals, can be incorporated in the method.

To show the capability of the method, Sample Grillage 1 (SG-1) was analyzed for an initial deflection in the form of a product of trigonometric functions.

$$w_o = C \sin \frac{\pi z}{2L_T} \sin \left(\frac{\pi}{2} - \frac{\pi x}{2L_L}\right) \tag{4.10}$$

Where coordinates x and z and parameters L_L and L_T are as defined in Fig. 16, and C is the amplitude of the deflected shape.

The effect of initial deflection was incorporated into the analysis simply by adding, respectively, the first and second derivatives of the initial deflection function (Eq. 4.10) to the slope θ and curvature $\overline{\phi}$ in Eqs. 2.22, 2.23, and 2.25 to 2.28, and accounting for the initial deflections in imposing the compatibility requirements.

The effect of the initial deflections on the deflection behavior and the ultimate strength of SG-1 is shown in Fig. 45. Although the final deflection is seen to be directly influenced by the initial deflections, the strength is reduced only negligibly (a reduction of 0.002 in p/σ_{yp} due to C/t = 3.2). The reason for such small reduction appears to be the fact that the ultimate strength of this grillage was controlled by the failure of the end panel in all cases. Thus, the longitudinals behaved as a series of short beam-columns (a/r = 20.5) for which the effect of initial deflections is usually rather small.

It can be readily expected that initial deflections will have much more significant influence on the ultimate strength of grillages with transverses relatively weaker than in SG-1. Although no such grillages were analyzed in this study, no difficulties are expected in the application of the method.

4.4 EFFECT OF WELDING RESIDUAL STRESSES

Consideration of residual stresses and their influence on the effective average stress-edge strain relationship were explained in Chapter 2. Also, their significant influence on the ultimate strength of the test specimens, in the panel failure mode, was discussed in Section 3.3.

To explore the effect of residual stresses on the grillage failure mode, complete interaction diagrams for SG-1, based on $\sigma_{rc}/\sigma_{yp} = 0$ and on $\sigma_{rc}/\sigma_{yp} = 0.082$, were computed as shown in Fig. 46. The reduction of the strength in the grillage failure mode is smaller, about 2%, than in the panel failure mode, about 9.5%.

5. SUMMARY, CONCLUSIONS AND RECOMMENDATIONS

5.1 SUMMARY

A survey of the methods for analyzing grillages revealed that none is presently available which is capable of determining the ultimate strength of plate grillages subjected to combined loads. To fill this need, a method was developed and it is presented in Chapter 2. Analytically, the grillage is simulated by a grid model in which the post-buckling behavior of the plate and the large deflection elasto-plastic behavior of the longitudinal stiffeners are considered. The transverse stiffeners, together with an assumed effective width of the plate, are treated according to the small deflection elasto-plastic beam theory.

A computer program was developed to illustrate the feasibility of the method. It was applied to some sample grillages in order to establish the size of geometrical and load increments and the values of some parameters required by the numerical technique employed, as well as to study the convergence behavior of the method and to evaluate the effect of some of the grillage parameters on the ultimate strength. The accuracy of the analytical model in simulating the true behavior of grillages was confirmed by a comparison with some available test results.

5.2 CONCLUSIONS

Based on the results obtained from the application of the proposed method to four sample grillages, the following conclusions were drawn:

1. The method is acceptably accurate and efficient for use. (Excluding TG-2b, the average deviation from the test results was 5%.)

2. The flexibility of the transverses has a negligible effect on the ultimate capacity of grillages when they fail in the panel mode.

3. As a consequence of conclusion 2, the effective width of the plate for the transverses has a negligible effect on the ultimate capacity of grillages when they fail in the panel mode. However, when the grillage mode is to be expected, this effect may be significant for grillages with $a_e t < A_{st}$.

4. The design nomographs of Ref. 49, which are based on the assumption of infinite bending rigidity of the transverses, can be used for design of grillages failing in the panel mode.

5. Residual stresses have a significant effect on the ultimate strength of grillages and their intensity in test specimens should be measured for an accurate comparison with theoretical solutions. For practical use, levels of residual stresses typical for actual structures should be statistically established from field measurements and theoretical solutions.

6. Imposition of a constant in-plane displacement along the loaded edge (edge remains straight) seems to have a negligible effect on the strength of grillages commonly used in ship building practice.

5.3 RECOMMENDATIONS FOR FUTURE WORK

The following recommendations can be made for future work:

1. More experimental information (on models and full scale specimens) should be obtained to further check the accuracy of the method especially in grillage mode failure range for which no test results are available.

2. Experimental and theoretical work should be undertaken to establish a reasonable effective plate width for the transverses, to be used for grillages failing in the grillage mode.

3. A design procedure (nomographs, tables, and/or formulas) should be developed based on the proposed method. This may be accomplished by curve fits using the numerical results of the computer outputs. Similar work has been successfully done in developing the design nomographs for longitudinally stiffened panels.[49]

4. Effect of initial deflections on the ultimate strength should be studied and appropriate recommendations for design be made.

6. NOMENCLATURE*

A	total cross sectional area of a longitudinal beam
A_f	flange area of the longitudinal stiffener
A_p	plate area, $A_p = bt$
A_s	area of the longitudinal stiffener
A_{st}	area of the transverse stiffener
C	amplitude of the initial lateral deflection
E_t	tangent modulus of elasticity
H	horizontal stress resultant, nondimensionally $\bar{H} = H/A\sigma_o$
$\bar{H}_{Fj}$	nondimensional horizontal stress resultant at the starting point for stepwise integration along the j^{th} longitudinal beam
K	plate buckling coefficient
L_L	half length of the grillage
L_T	half width of the grillage
M	moment, nondimensionally $\bar{M} = M/dA\sigma_o$
M_p	plastic moment capacity of the cross section of a transverse beam
M_{pc}	reduced plastic moment capacity of the cross section of a longitudinal beam when subjected to an axial force, nondimensionally $\bar{M}_{pc} = M_{pc}/dA\sigma_o$
N	axial force, nondimensionally $\bar{N} = N/A\sigma_o$
P	axial load applied at the ends of the longitudinal beam, nondimensionally $\bar{P} = P/A\sigma_o$

*In nondimensionalizing the parameters, the units are to be consistent.

V vertical stress resultant, nondimensionally $\bar{V} = V/A\sigma_o$

$\bar{V}_{Fj}$ nondimensional vertical stress resultant at the starting point for the stepwise integration along the longitudinal beam

V_{ij} redundant force at the junction of i^{th} transverse and j^{th} longitudinal beams, nondimensionally $\bar{V}_{ij} = V_{ij}/A\sigma_o$

a spacing of the transverse beams

b spacing of the longitudinal beams

c width of the tensile residual stress zone

d distance from the mid-plane of the longitudinal stiffener flange to the mid-plane of the plate

$f_{k1}, f'_{k1}, f''_{k1}, f'''_{k1}, f''''_{k1}$ flexibility coefficients

h distance from a point in the cross section of a longitudinal stiffener to the plate, nondimensionally $\bar{h} = h/r$

k_j axial tangent stiffness of the j^{th} longitudinal beam

m number of longitudinal beams

n number of transverse beams

n_t total number of nonlinear equations

p axial compression per unit area (stress dimension)

p_{ave} average axial compression per unit area (stress dimension)

p_u ultimate axial compression of a grillage when $q = 0$

p_{ult} ultimate axial compression of a grillage when $q \neq 0$

q uniformly distributed lateral loading, nondimensionally $\bar{q} = \frac{qbr}{\sigma_o A} \times 10^3$

q_u ultimate lateral load when $p = 0$

r	radius of gyration of the longitudinal beam
s	distance along the centroidal axis of the longitudinal beam, nondimensionally $\bar{s} = s/r$
t	plate thickness
t_w	web thickness of the longitudinal stiffener
u_a	displacement of the end of the longitudinal beam due to axial strains
u_c	displacement of the end of the longitudinal beam due to curvature
u_t	$u_a + u_c$
w_o	initial lateral deflection
x	horizontal coordinate axis and distance, nondimensionally $\bar{x} = x/r$
$\{x_j\}$	solution vector for the nonlinear equations
y	vertical coordinate axis and distance, nondimensionally $\bar{y} = y/r$
$\bar{y}_{Fj}$	vertical coordinate of the starting point for the stepwise integration along the j^{th} longitudinal beam
α	nondimensional distance from the plate to the centroidal axis of the longitudinal beam
$\bar{\delta}_{is}$	nondimensional rigid body displacement
$\bar{\Delta}_{ij}$	nondimensional deflection of the junction of a longitudinal and a transverse beam
Δs	segment length, nondimensionally $\overline{\Delta s} = \Delta s/r$
Δy	change in y in segment length Δs, nondimensionally $\overline{\Delta y} = \Delta y/r$
Δx	change in x in segment length Δs, nondimensionally $\overline{\Delta x} = \Delta x/r$

ϵ_{cr} plate buckling strain

ϵ_f strain in the flange of the longitudinal, nondimensionally $\bar{\epsilon}_f = \epsilon_f/\epsilon_o$

ϵ_p edge strain in plate, nondimensionally $\bar{\epsilon}_p = \epsilon_p/\epsilon_o$

ϵ_o nondimensionalizing parameter, either ϵ_y or ϵ_{cr}

ϵ_{yp} yield strain for plate material

ϕ curvature, nondimensionally $\bar{\phi} = \phi d/\epsilon_o$

$\bar{\phi}_{Fj}$ nondimensional curvature at the starting point for the stepwise integration along the j^{th} longitudinal beam

ν Poisson's ratio

σ_{cr} plate buckling stress

σ_f stress in the flange of a longitudinal stiffener, nondimensionally $\bar{\sigma}_f = \sigma_f/\sigma_o$

σ_h stress in the cross section of a longitudinal stiffener at distance h from the mid-plane of the plate, nondimensionally $\bar{\sigma}_h = \sigma_h/\sigma_o$

σ_o nondimensionalizing parameter, either σ_y or σ_{cr}

σ_p effective average stress in the plate, corresponding to ϵ_p

$(\sigma_p)_u$ ultimate effective average stress in the plate

σ_{yp} yield stress for plate material

θ slope

θ_{Fj} slope at the starting point for the stepwise integration along the j^{th} longitudinal beam

7. TABLES

TABLE 1 Geometrical and Material Properties of Sample Grillages

Designation	t (in.)	$\frac{b}{t}$	$\frac{a}{b}$	d (in.)	m	n	σ_{yp} (ksi)	a_e	Longitudinal Stiffener (Stress in ksi)	Transverse Stiffener (Stress in ksi)	$\frac{\sigma_{rc}}{\sigma_{yp}}$
SG-1	0.315	76.2	2.0	6.00	4	4	37.0	30t and 150t	Flange=3.00"x0.56" Web=5.88"x0.28" Yield Stress=37.0	Flange=5.00"x0.72" Web=9.80"x0.36" Yield Stress=37.0	0.082 and 0.00
SG-2	0.125	65.3	2.4	1.31	6	2	36.0	50t	Plate=1.25"x0.25" Yield Stress=36.0	Flange=2.28"x0.19" Web=3.97"x0.13" Yield Stress=36.0	0.00
SG-3	0.125	65.3	2.4	1.31	6	2	36.0	50t	Plate=1.25"x0.25" Yield Stress=36.0	Flange=1.84"x0.17" Web=2.98"x0.11" Yield Stress=36.0	0.00
SG-4	0.327	110.1	1.33	6.00	6	2	47.0	73t	Flange=4.53"x0.75" Web=5.82"x0.39" Yield Stress=47.0	Flange=4.53"x0.75" Web=5.82"x0.39" Yield Stress=47.0	0.15

TABLE 2 Summary of Test Specimen Parameters and Comparison of the Method with Test Results

Specimen		$\frac{b}{t}$	$\frac{a}{b}$	Longitudinals			Transverses			$\left(\frac{P_{ex}}{\sigma_{yp}}\right)_u$	$\left(\frac{q_{ex}}{\sigma_{yp}}\right)_u \times 10^3$	$\frac{\sigma^{**}_{rc}}{\sigma_{yp}}$	Rth/Rex*	
				$\frac{A_s}{bt}$	$\frac{A_f}{bt}$	$\frac{d}{b}$	$\frac{A_s}{bt}$	$\frac{A_f}{bt}$	$\frac{d}{b}$				No σ_{rc}	With σ_{rc}
TG-1	a	76.2	2.0	0.444	0.222	0.250	0.954	0.477	0.416	0.792	0.000	0.082	1.02	0.94
	b									0.760	0.915		1.05	0.99
	c									0.714	0.915		1.0	0.94
TG-2	a	47.7	5.0	0.256	0.083	0.250	1.900	1.190	0.500	0.732	0.182	0.20	1.03	0.98
	b									0.642	0.000		1.43	1.36
TG-3		95.0	2.5	0.256	0.108	0.188	0.950	0.592	0.250	0.700	0.000	0.10	0.92	0.86
TG-4		96.4	2.0	0.130	0.042	0.125	0.874	0.601	0.188	0.477	0.000	0.10	1.11	1.00

*R is the radial distance in p-q interaction diagram.

**Values of the residual stresses were assumed.

8. FIGURES

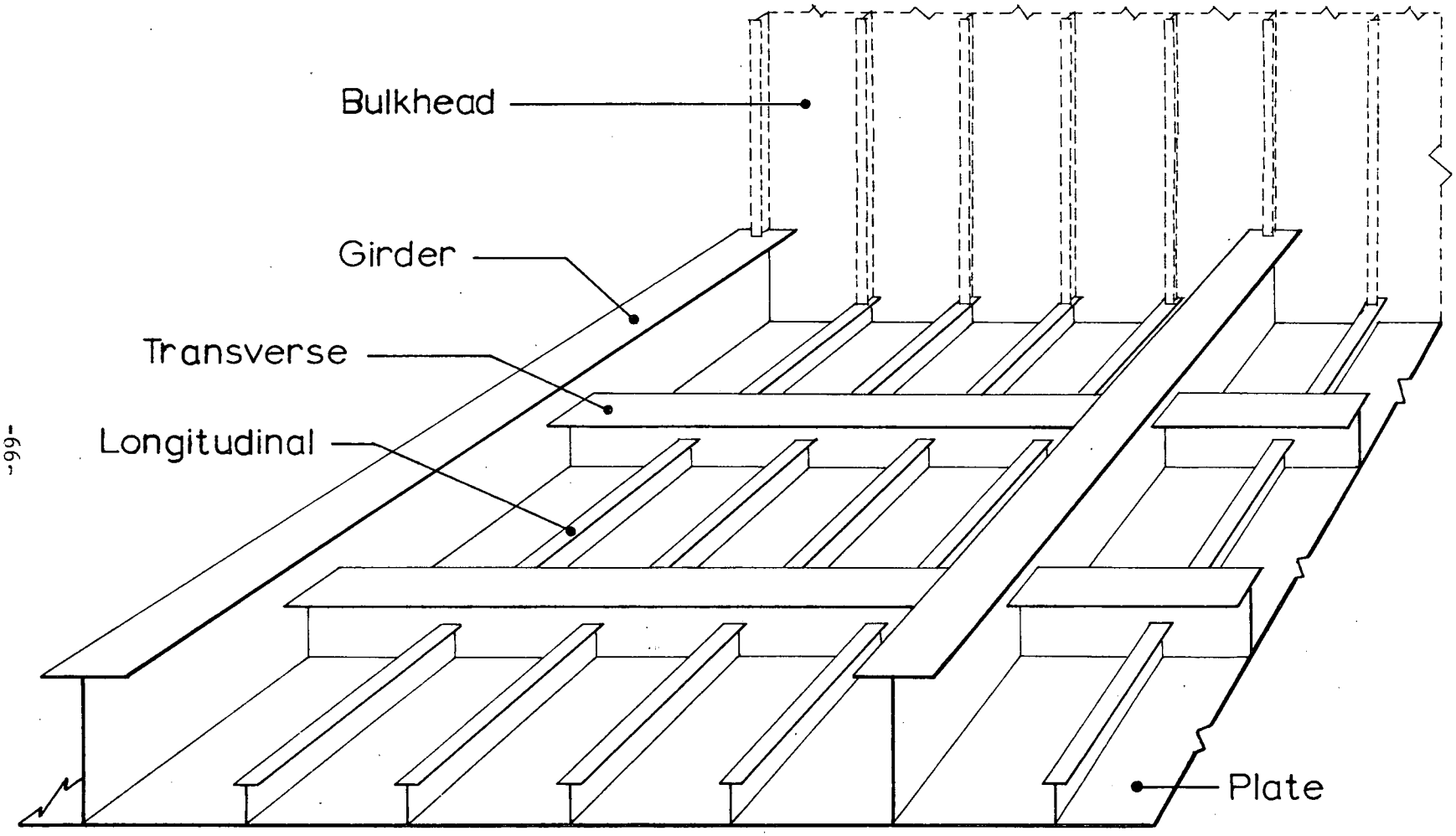

Fig. 1 PORTION OF SHIP BOTTOM STRUCTURE

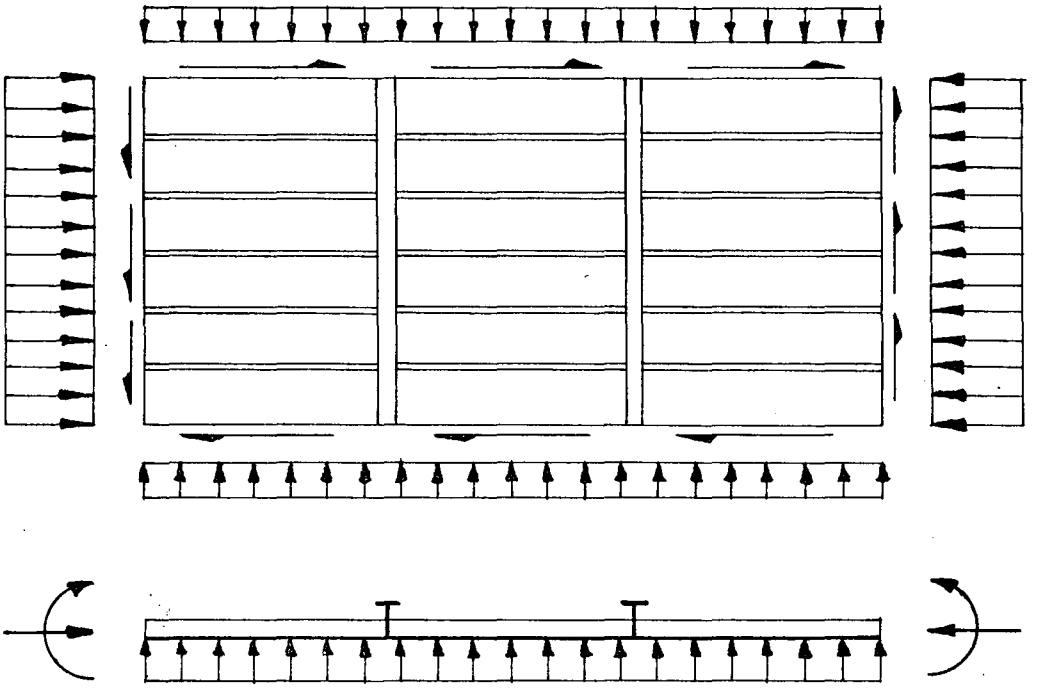

Fig. 2 LOADS ON SHIP GRILLAGE

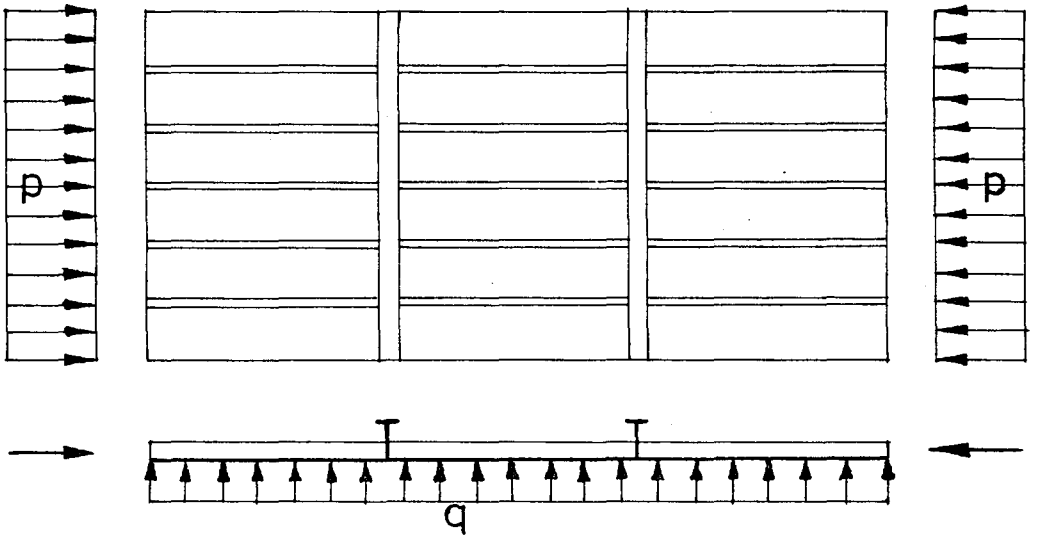

Fig. 3 ASSUMED LOADING CONDITION

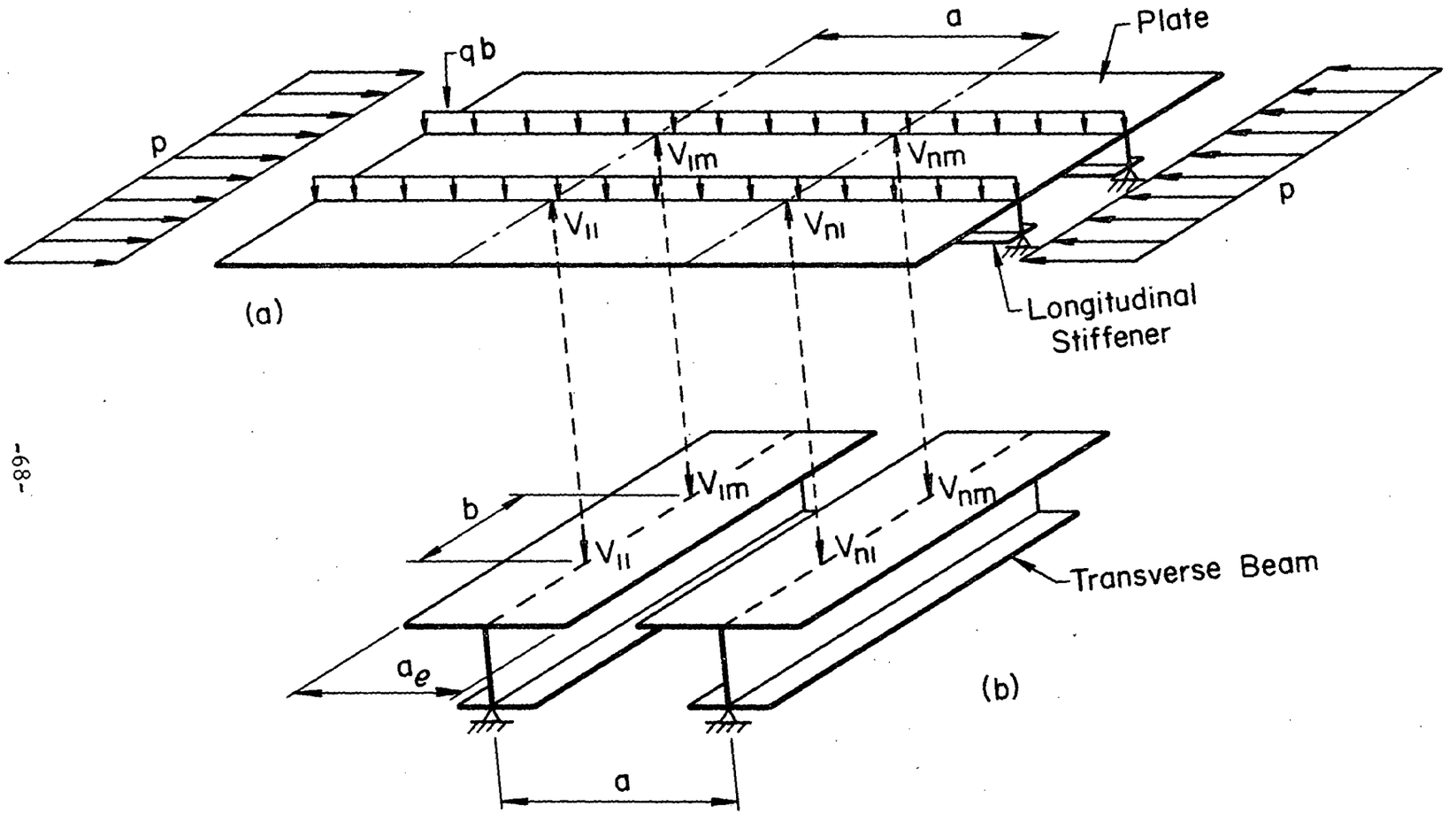

Fig. 4 COMPONENTS OF GRILLAGE MODEL

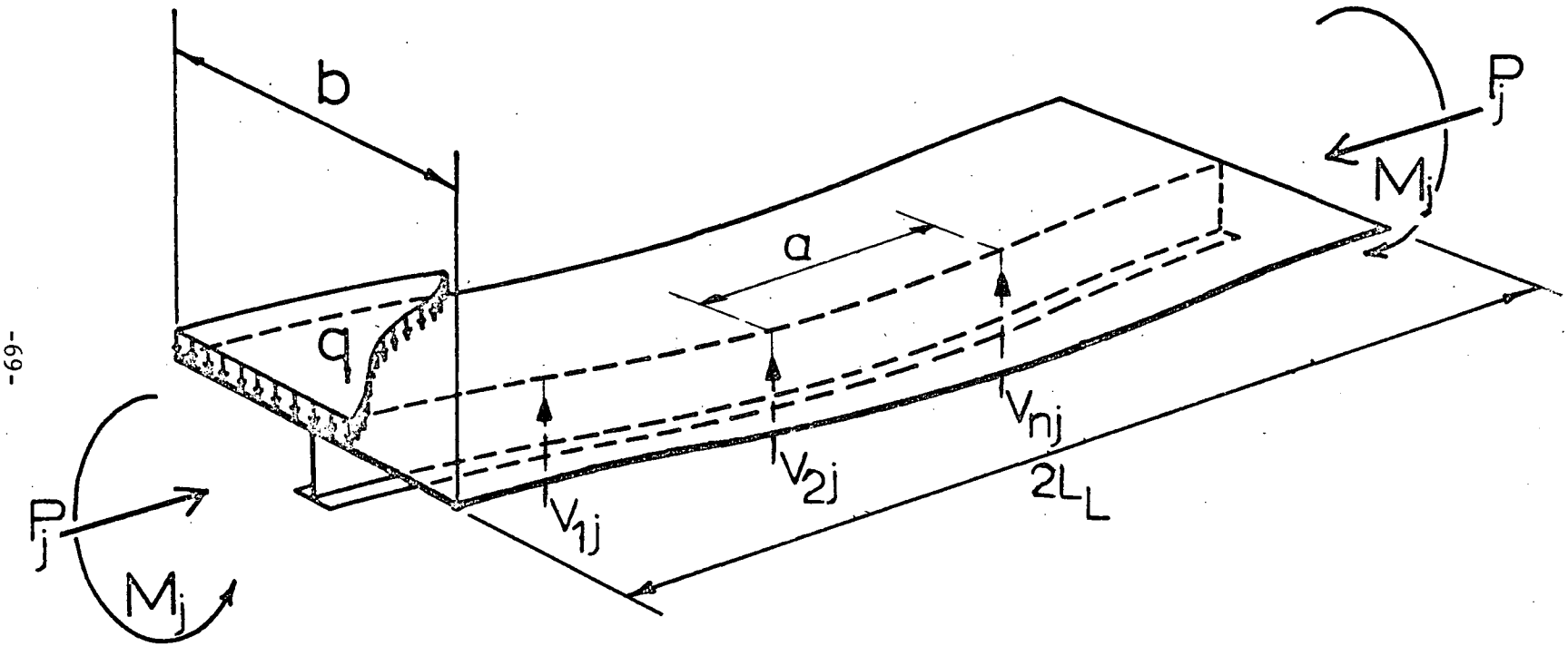

Fig. 5 LONGITUDINAL BEAM

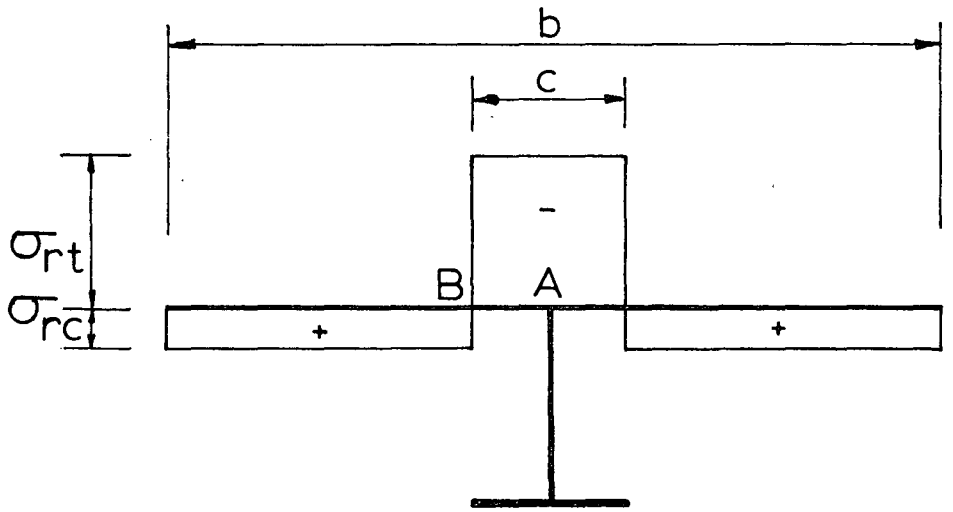

Fig. 6 RESIDUAL STRESS PATTERN

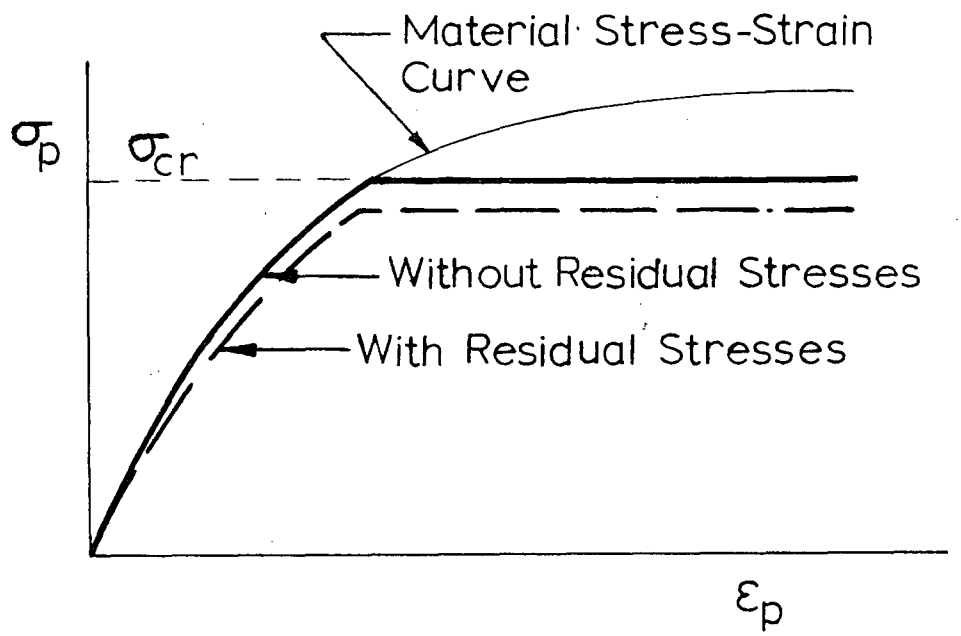

Fig. 7 COMPRESSION BRANCH OF EFFECTIVE AVERAGE EDGE STRAIN CURVE FOR PLATE WITH SMALL b/t

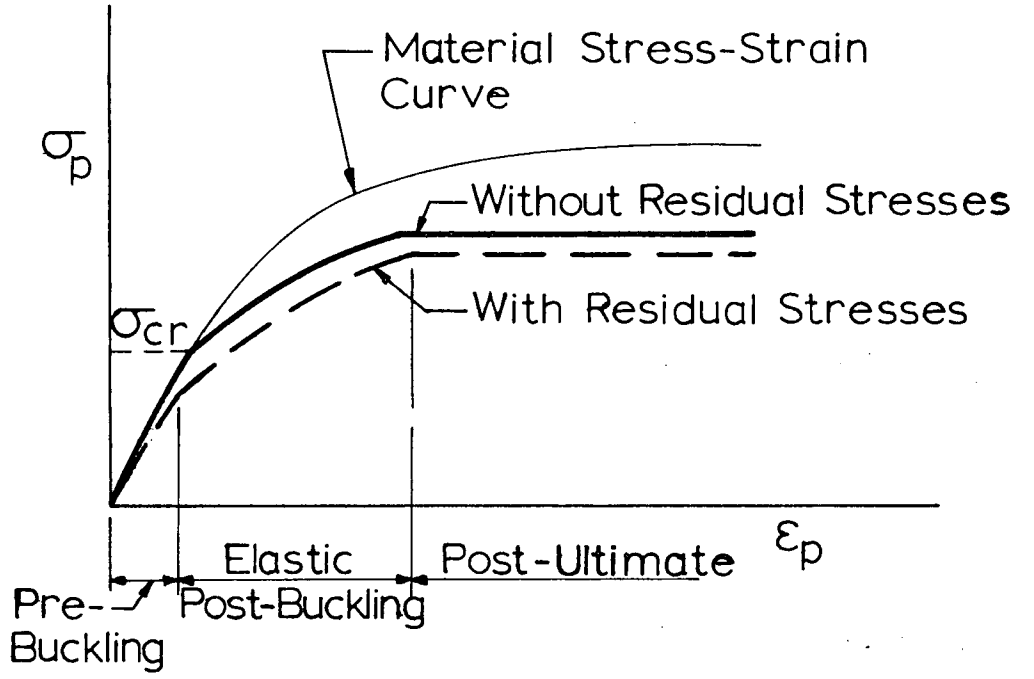

Fig. 8 COMPRESSION BRANCH OF EFFECTIVE AVERAGE STRESS-EDGE STRAIN CURVE FOR PLATE WITH LARGE b/t

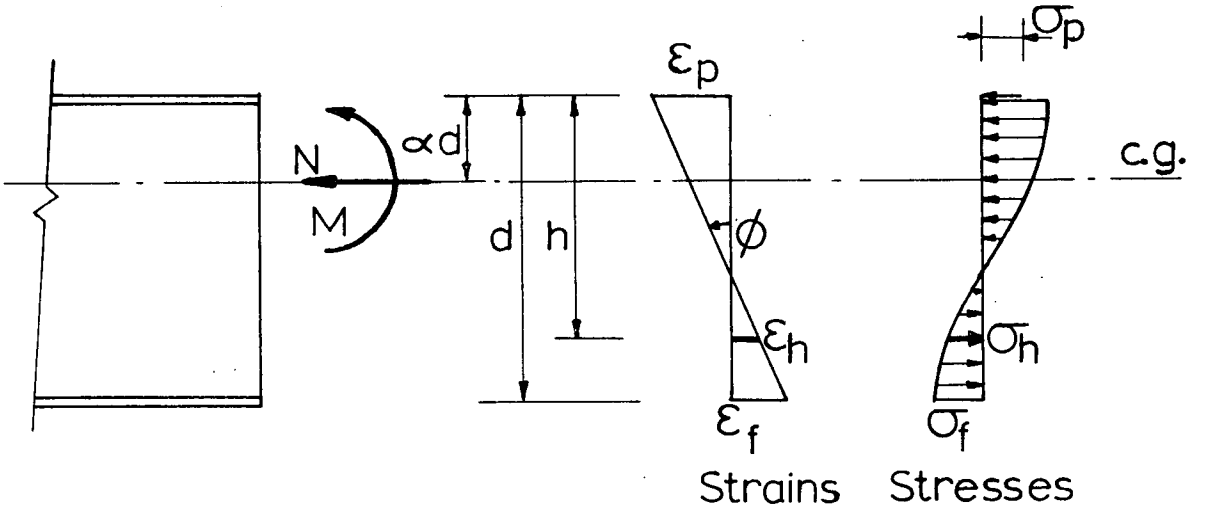

Fig. 9 DISTRIBUTION OF STRESSES AND STRAINS IN THE CROSS SECTION DUE TO LOADING

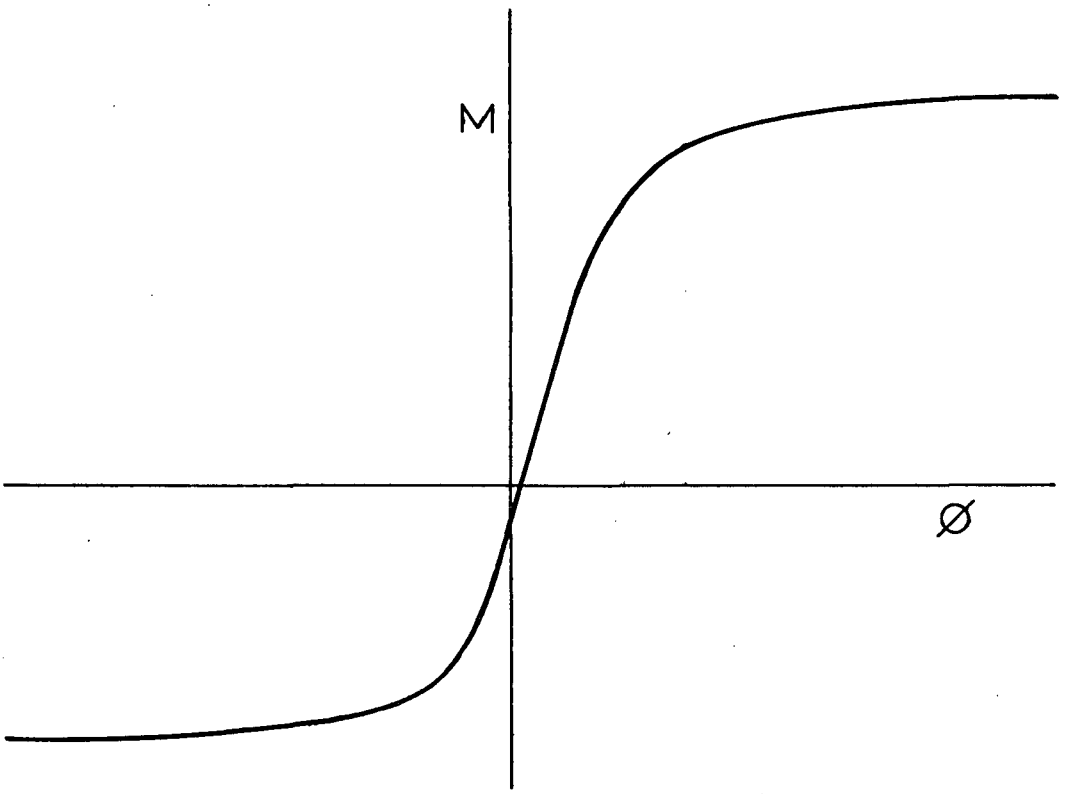

Fig. 10 MOMENT-CURVATURE RELATIONSHIP

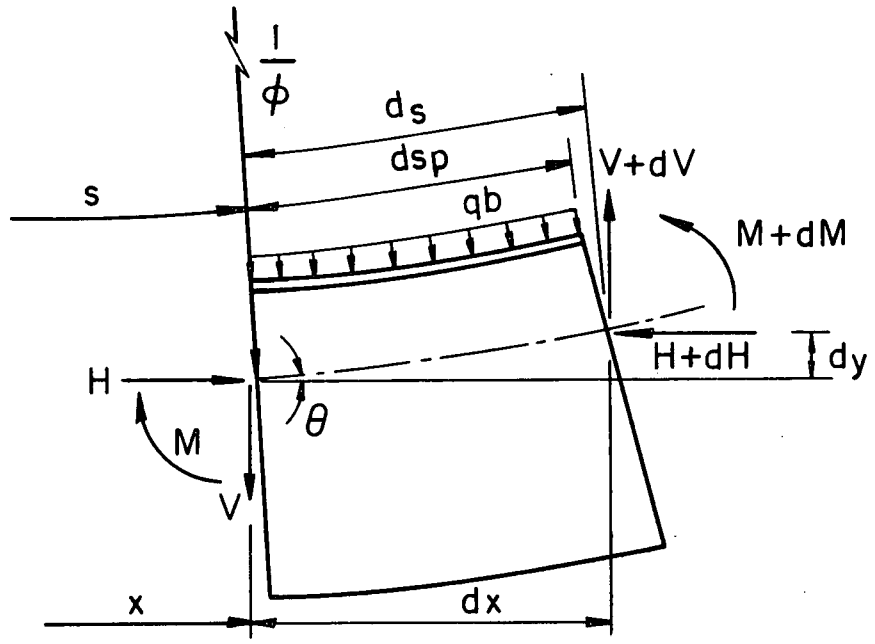

(a)

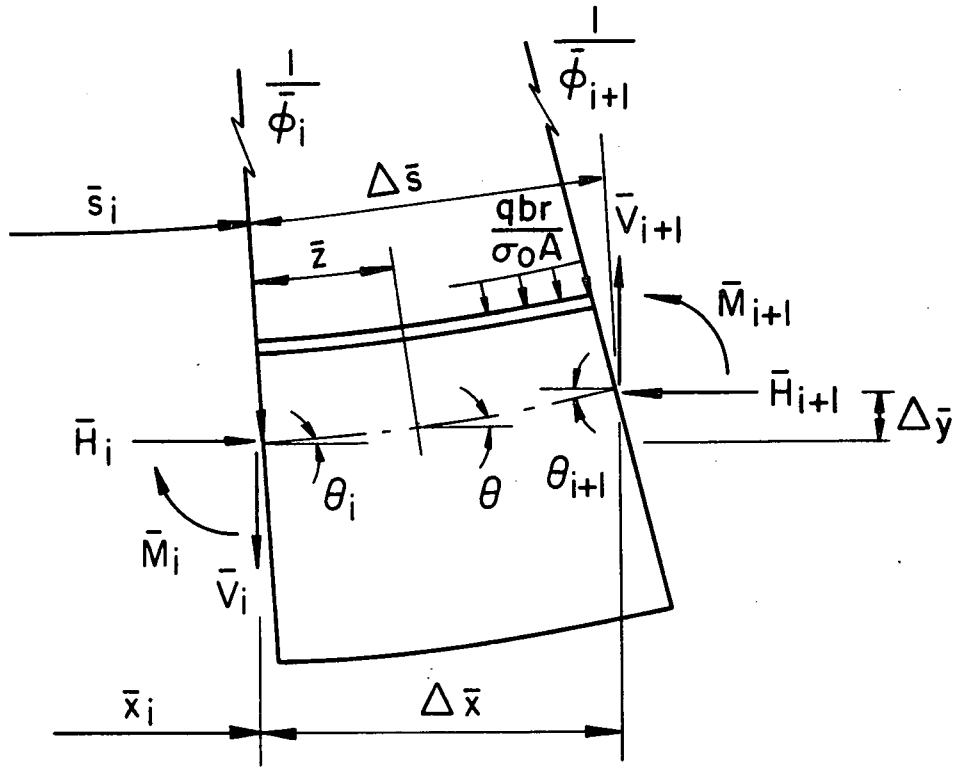

(b)

Fig. 11 BEAM SEGMENT OF LENGTH Δs (TAKEN FROM REF. 43)

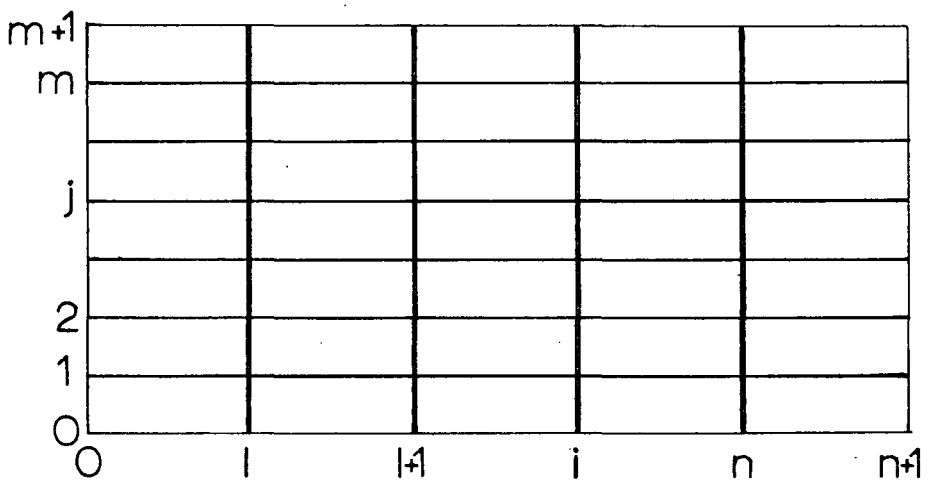

Fig. 12 GRILLAGE MODEL WITH m LONGITUDINAL AND n TRANSVERSE BEAMS

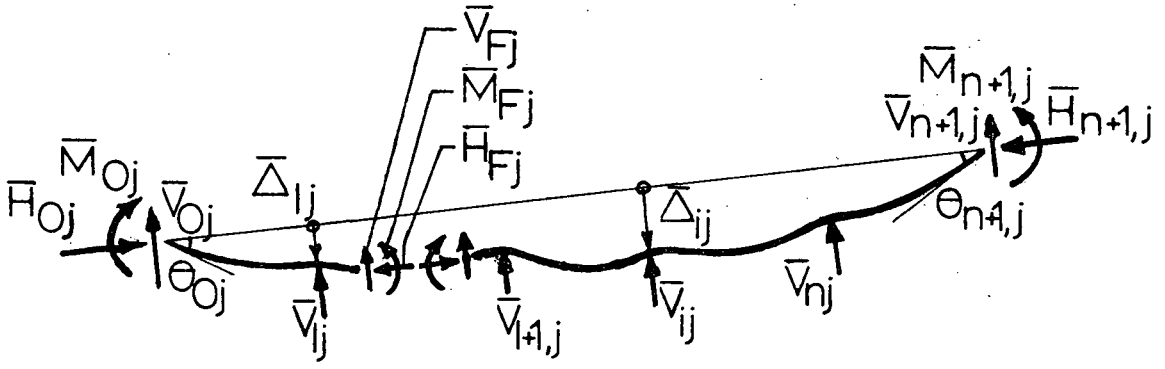

Fig. 13 j^{th} LONGITUDINAL BEAM

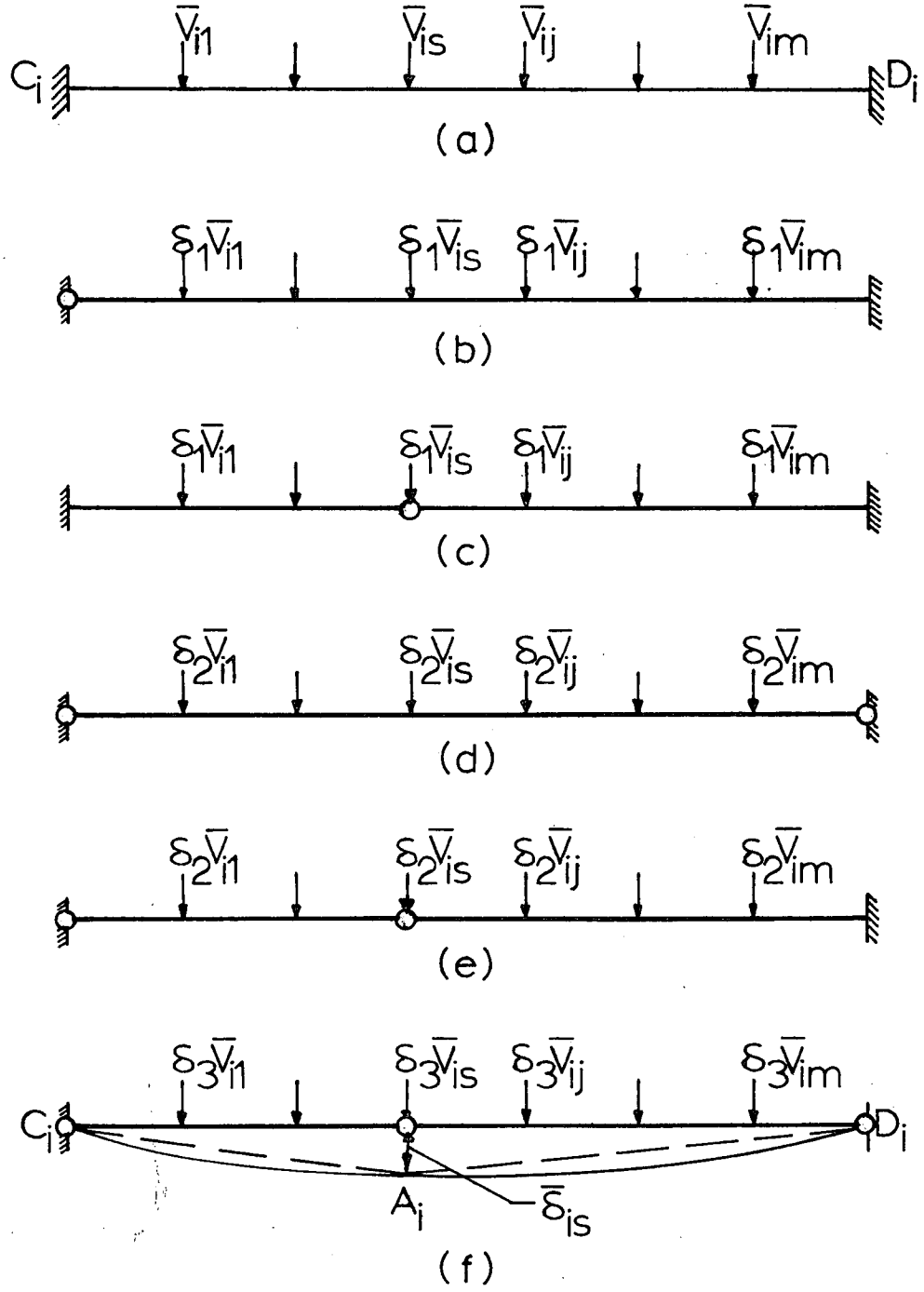

Fig. 14 i^{th} TRANSVERSE BEAM

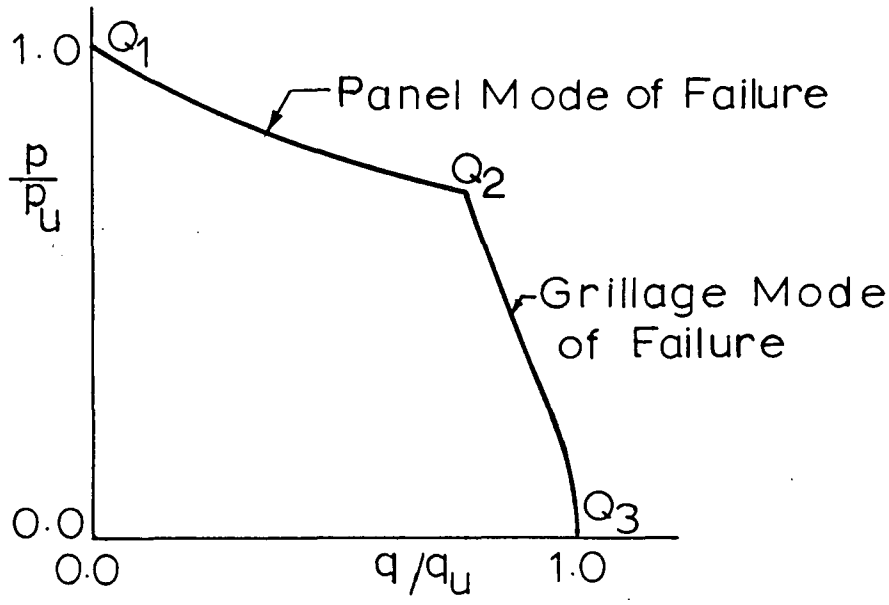

Fig. 15 SCHEMATIC AXIAL vs. LATERAL LOAD INTERACTION DIAGRAM

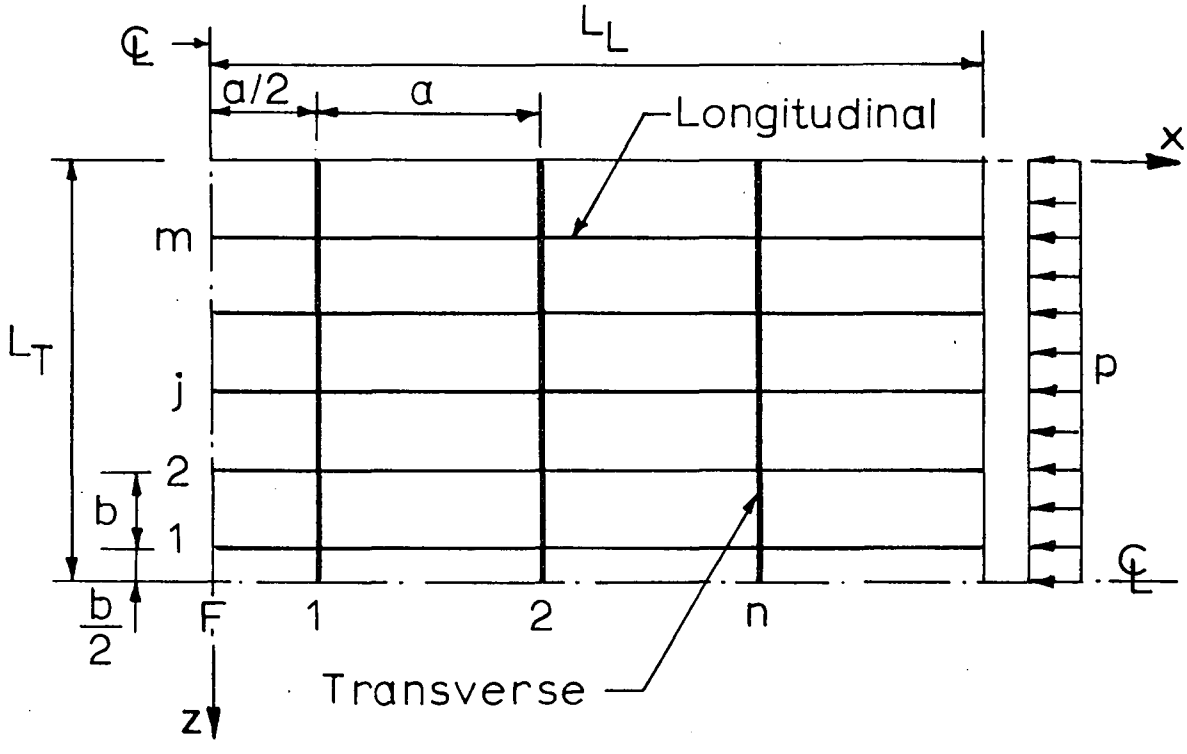

Fig. 16 TYPICAL QUARTER GRILLAGE USED IN ANALYSIS

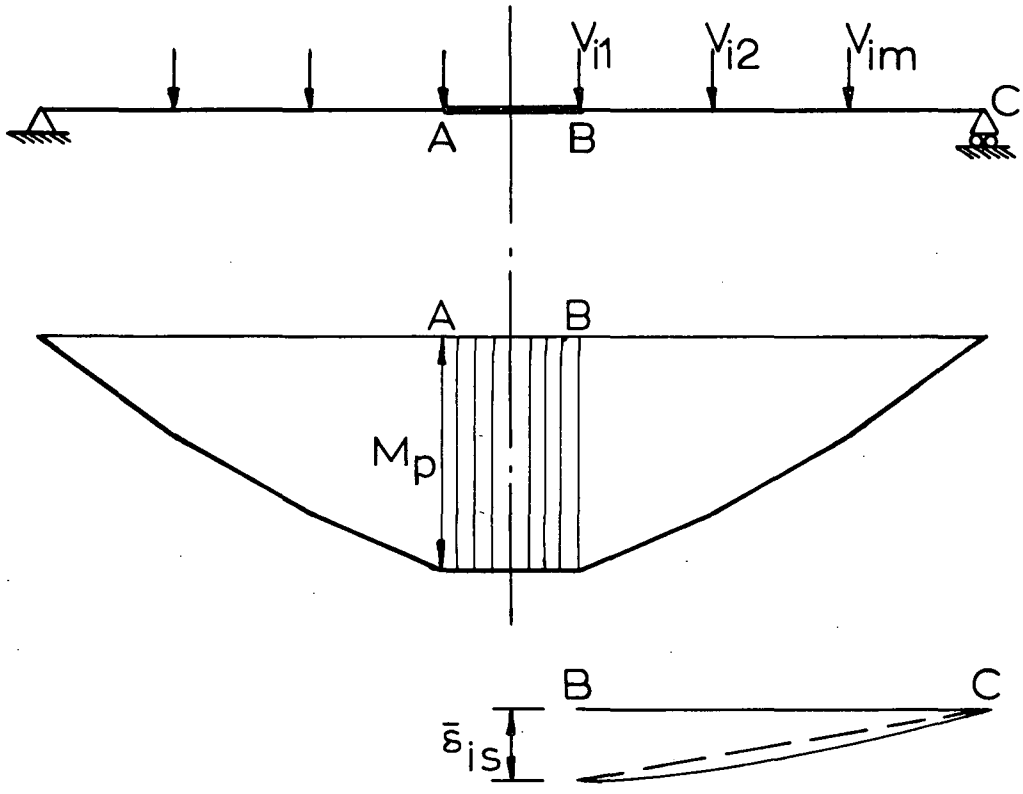

Fig. 17 SIMPLY SUPPORTED TRANSVERSE BEAM

Fig. 18 BRIEF FLOW CHART OF COMPUTER PROGRAM

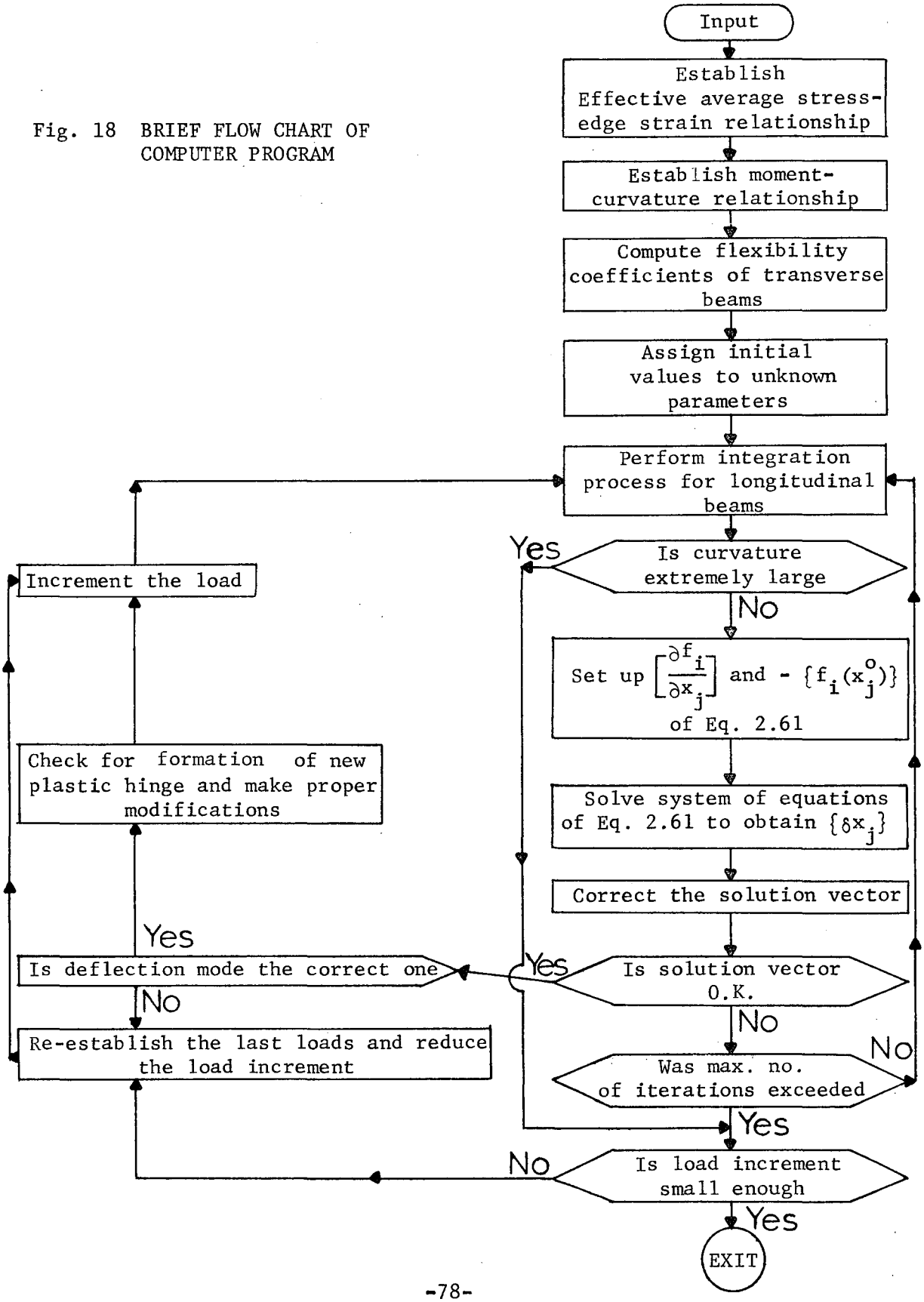

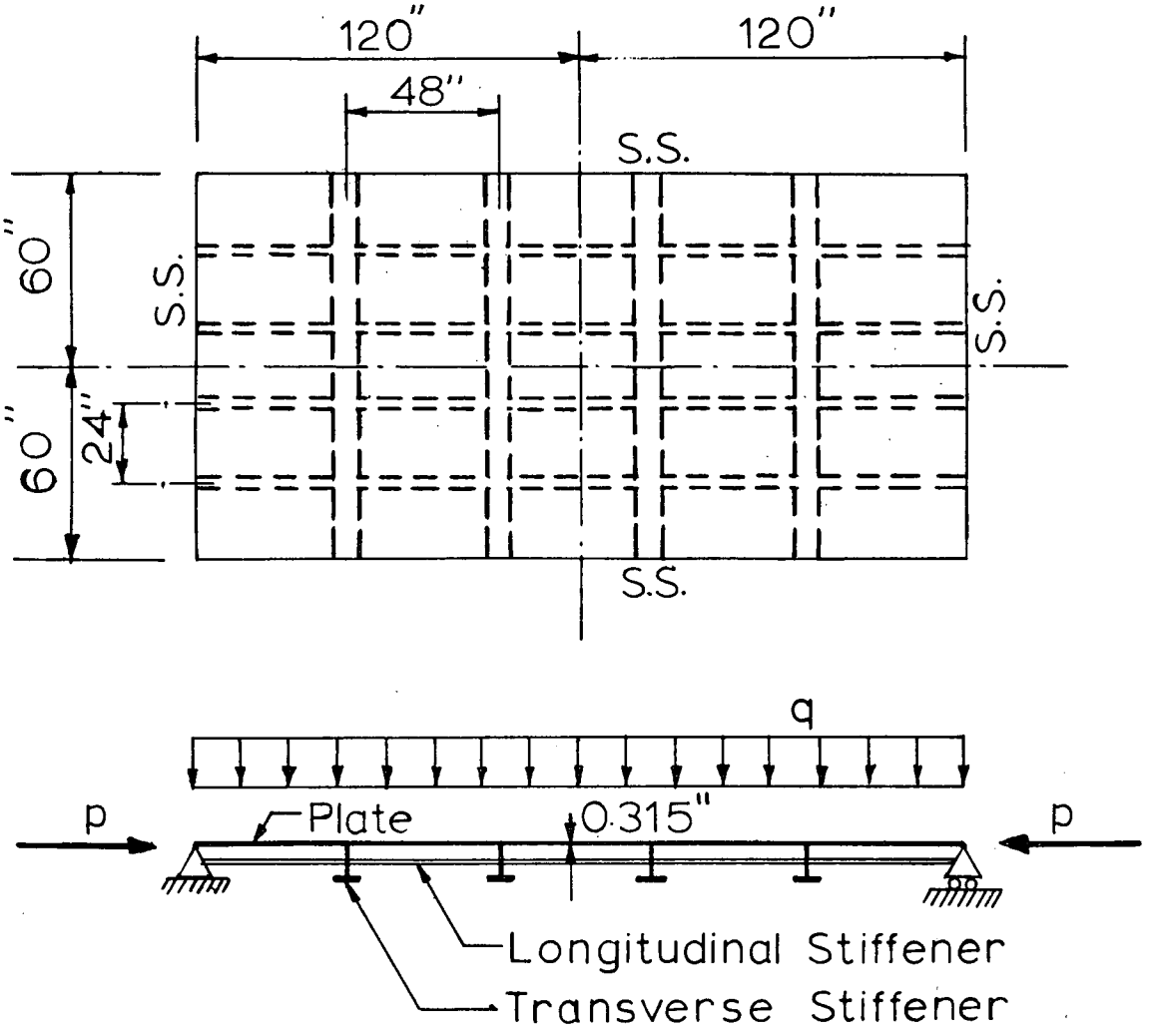

Fig. 19 SAMPLE GRILLAGE 1

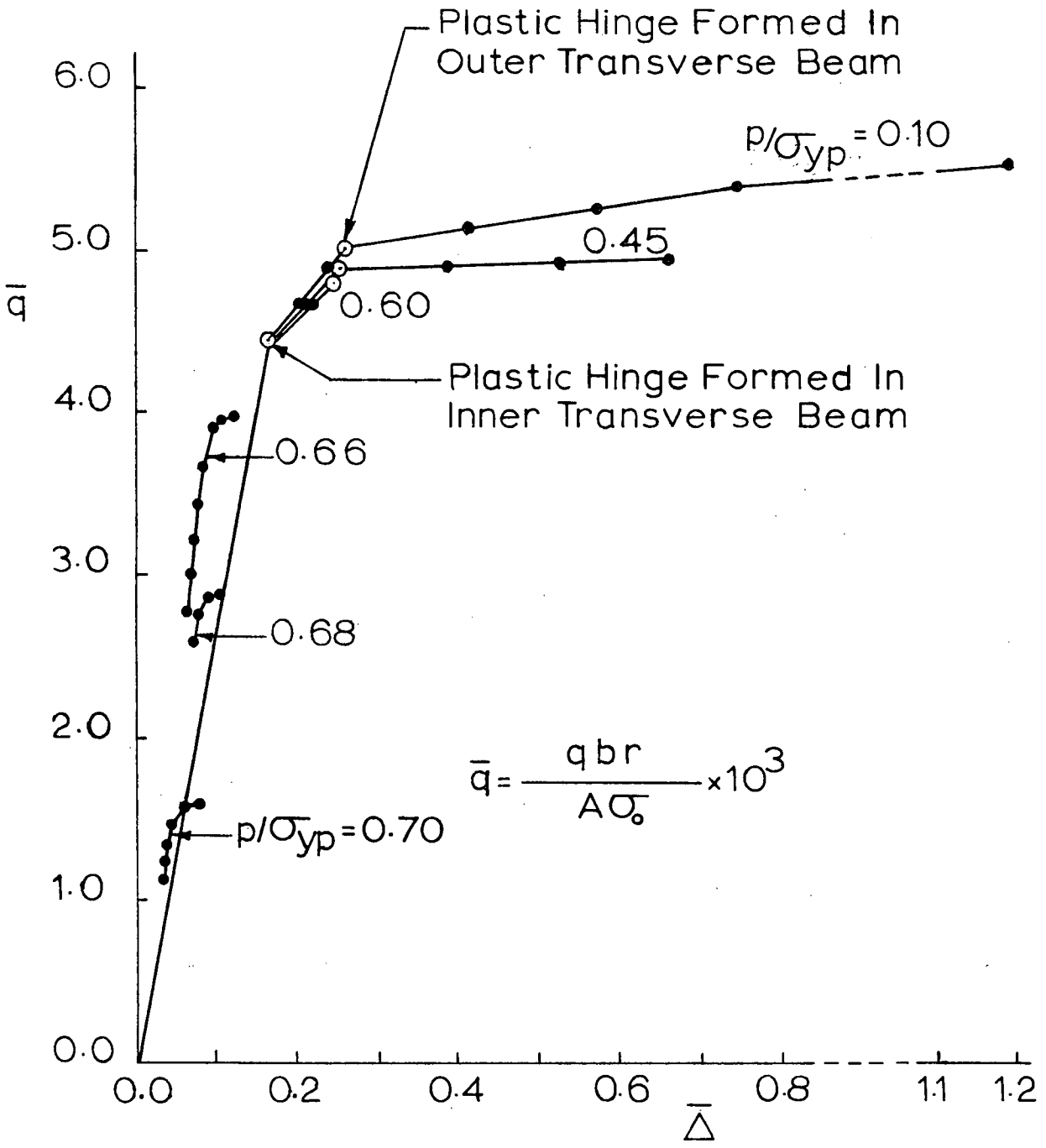

Fig. 20 LATERAL LOAD **vs.** DEFLECTION PLOTS FOR SAMPLE GRILLAGE 1 UNDER VARIOUS VALUES OF AXIAL COMPRESSION p/σ_{yp}

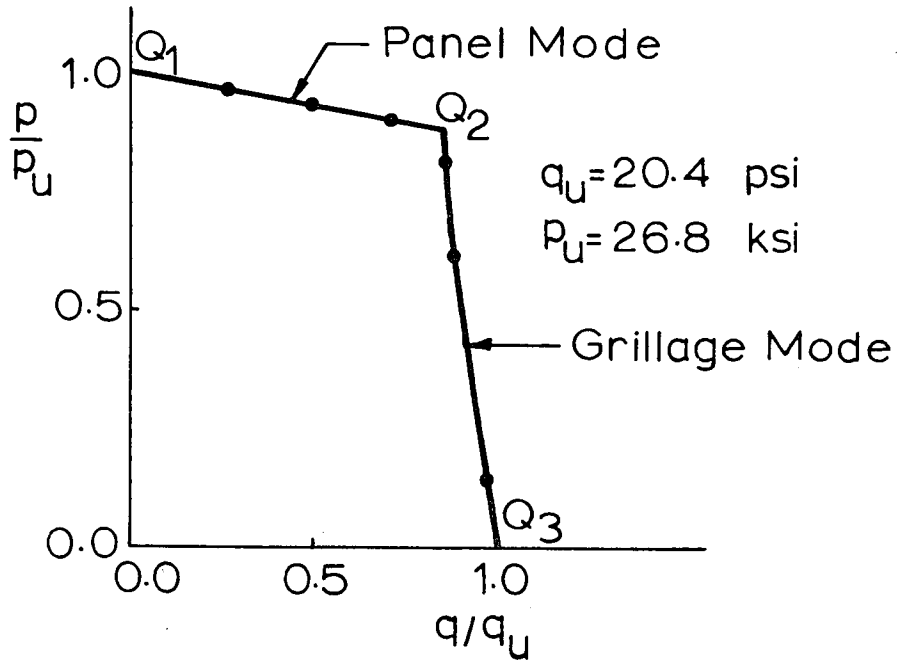

Fig. 21 AXIAL vs. LATERAL LOAD INTERACTION DIAGRAM FOR SAMPLE GRILLAGE 1

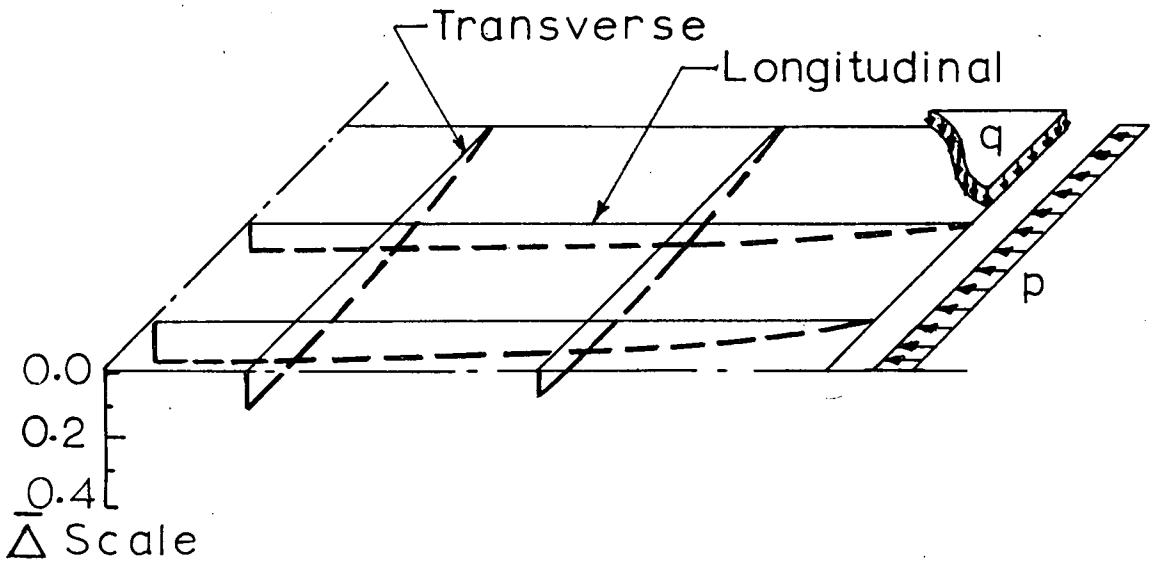

Fig. 22 DEFLECTION PATTERN OF SAMPLE GRILLAGE 1 UNDER p/σ_{yp} = 0.45 AND $\bar{q}$ = 4.45

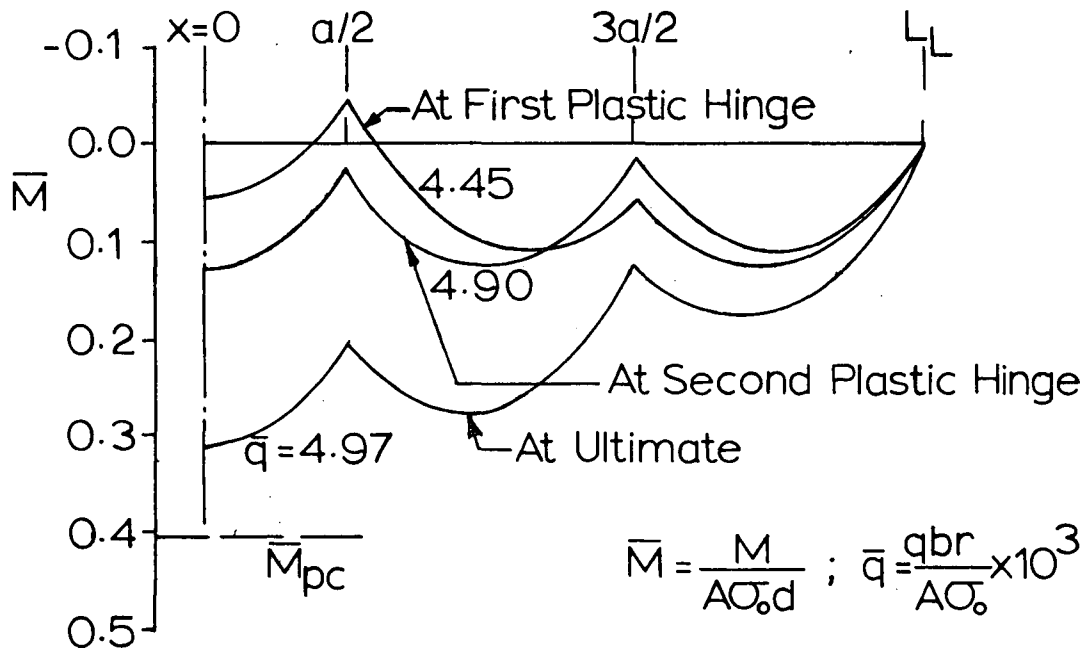

Fig. 23 MOMENT DIAGRAMS OF INNER LONGITUDINAL OF SAMPLE GRILLAGE 1 UNDER p/σ_{yp} = 0.45 AND THREE DIFFERENT VALUES OF $\bar{q}$

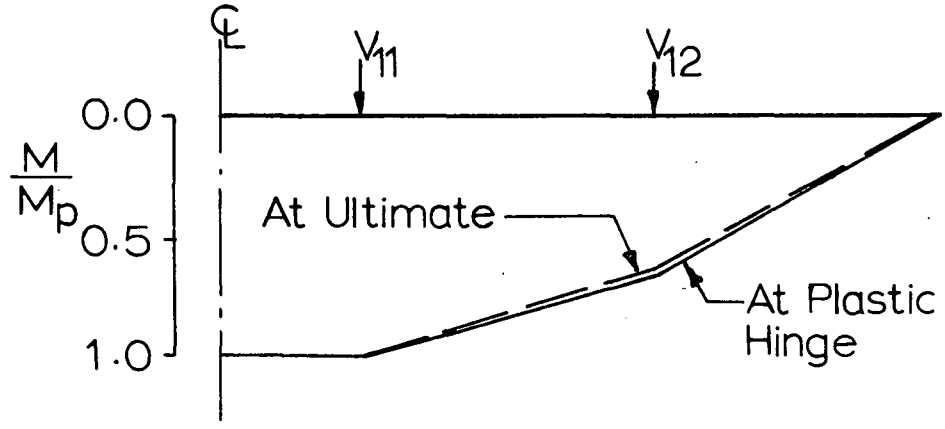

Fig. 24 MOMENT DIAGRAM FOR INNER TRANSVERSE BEAM OF SAMPLE GRILLAGE 1

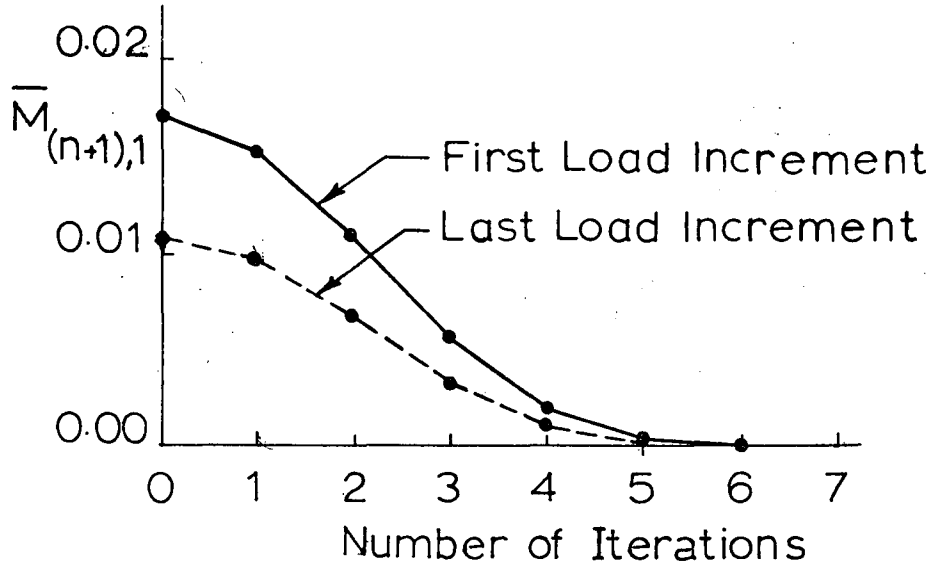

Fig. 25 CONVERGENCE BEHAVIOR OF THE END MOMENT OF INNER LONGITUDINAL BEAM

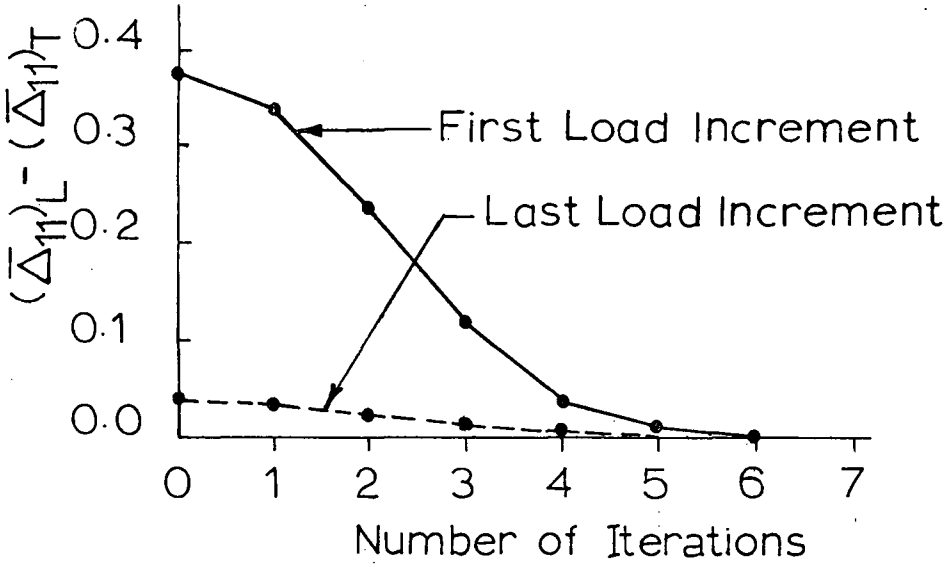

Fig. 26 CONVERGENCE BEHAVIOR OF COMPATIBILITY REQUIREMENT AT INNER BEAM JUNCTION

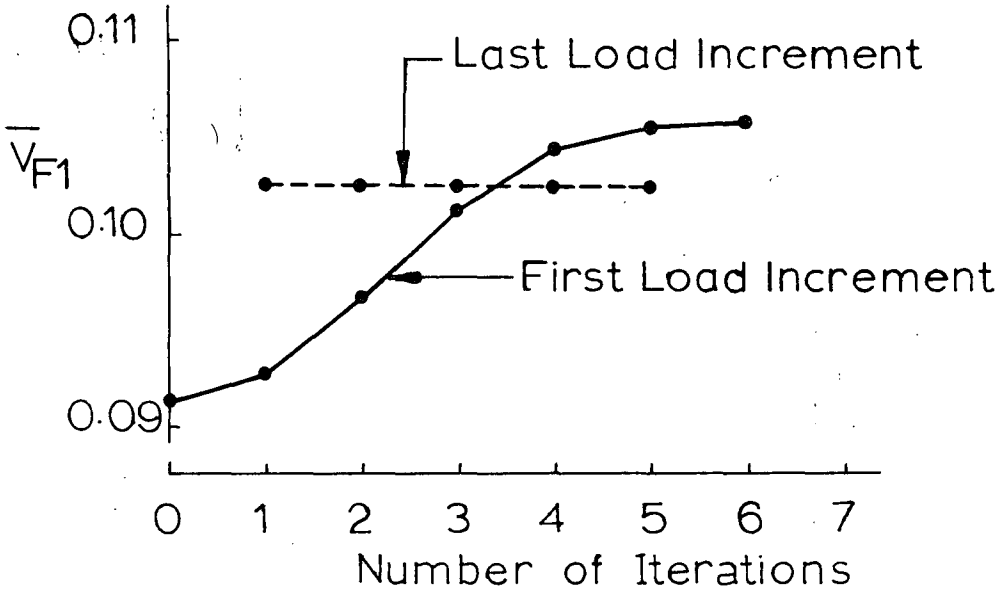

Fig. 27 CONVERGENCE BEHAVIOR OF REDUNDANT FORCE AT INNER BEAM JUNCTION

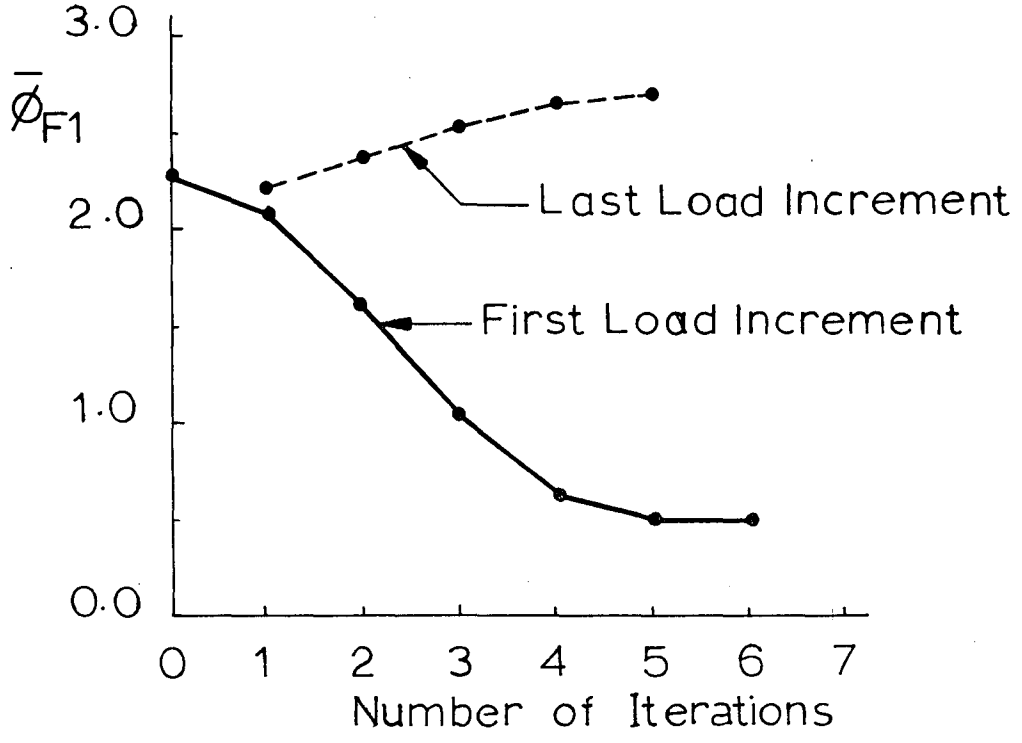

Fig. 28 CONVERGENCE BEHAVIOR OF CURVATURE AT MID-POINT OF INNER LONGITUDINAL BEAM

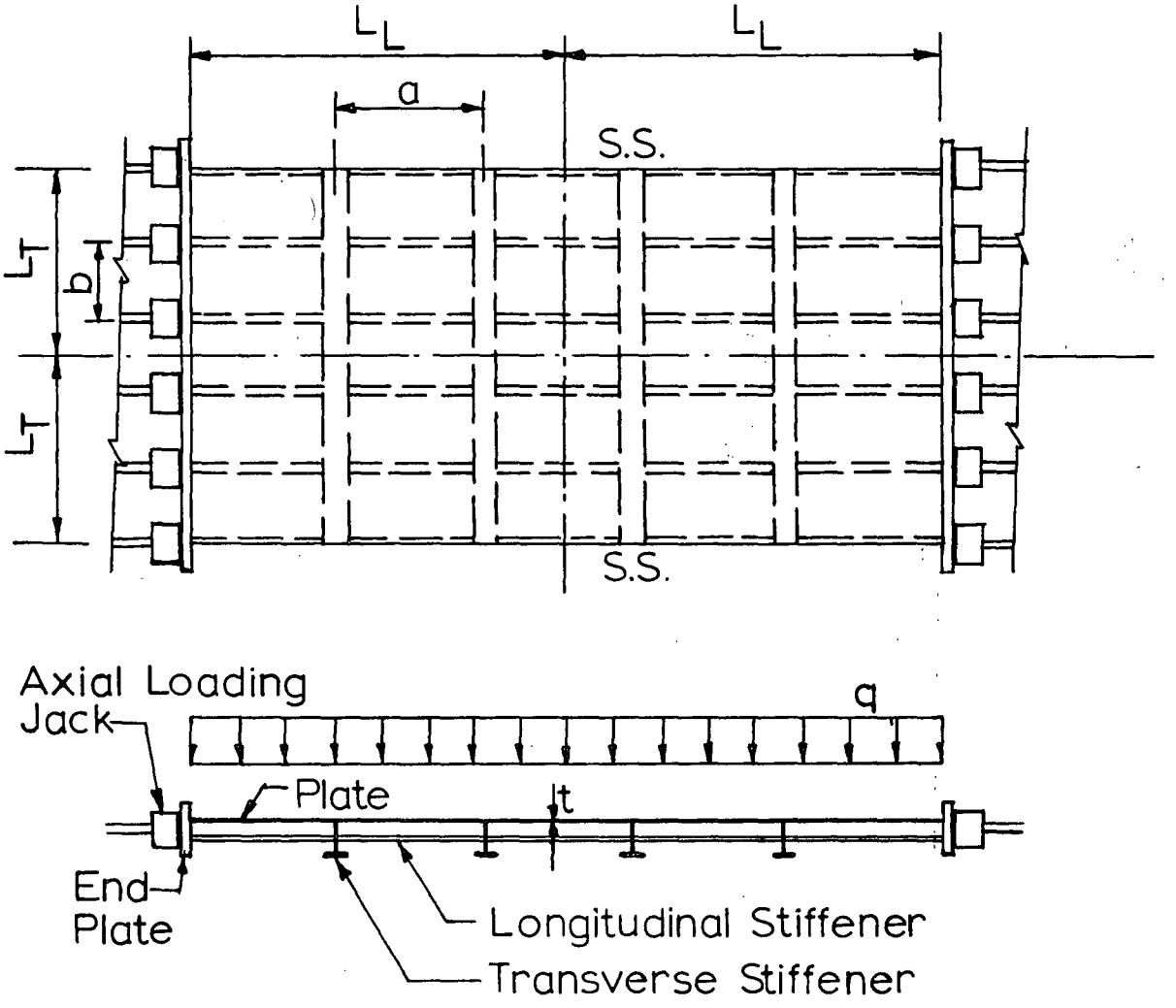

Fig. 29 CONFIGURATION OF TEST SPECIMEN

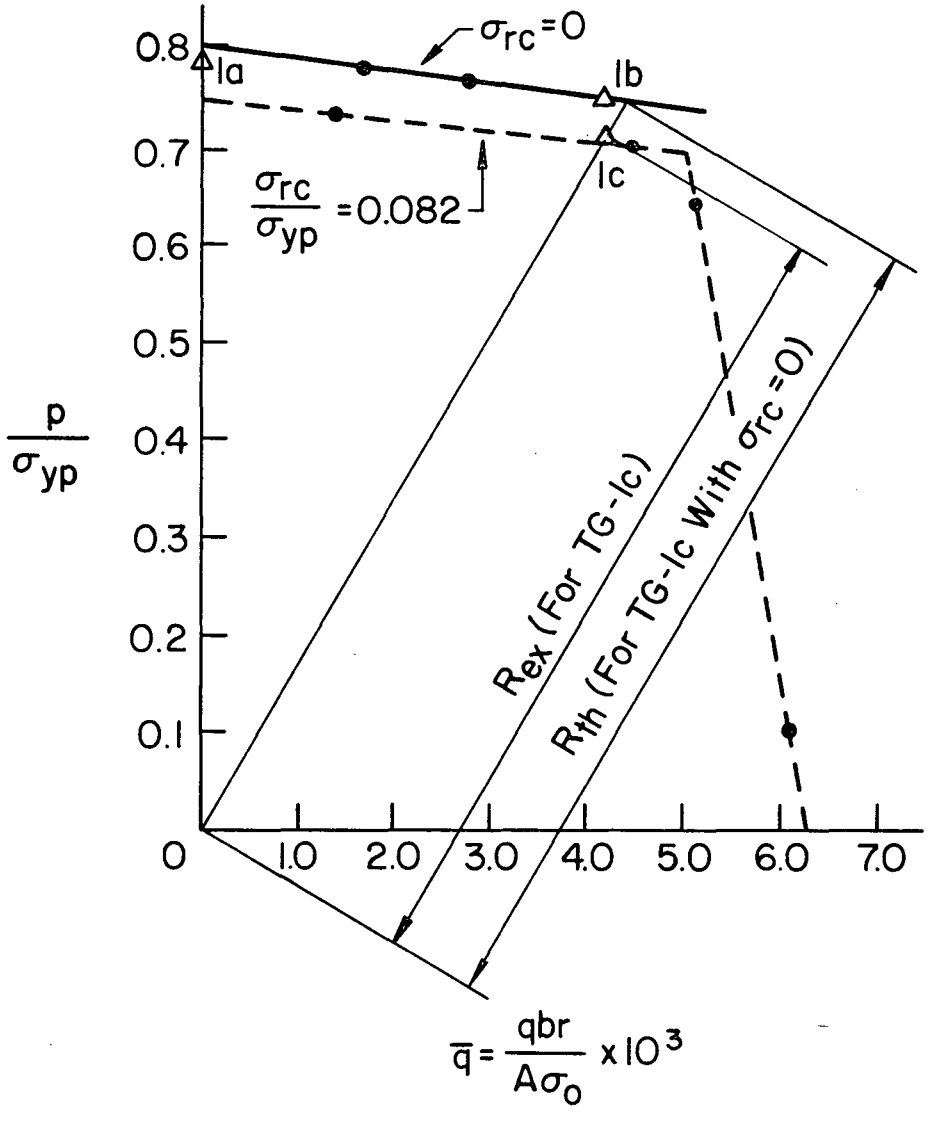

Fig. 30 COMPARISON OF THE METHOD WITH TEST RESULTS OF SPECIMENS TG-1a, 1b, AND 1c

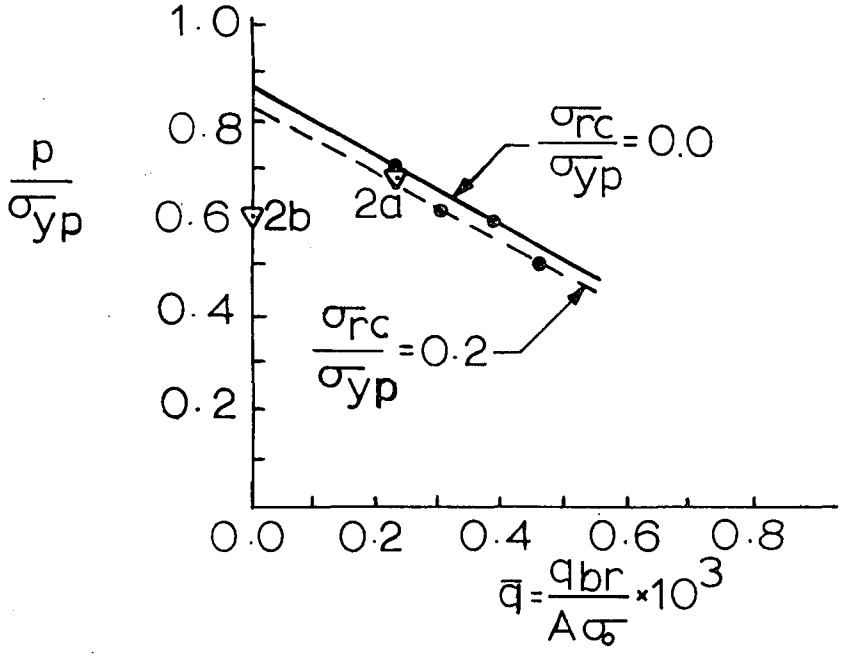

Fig. 31 COMPARISON OF THE METHOD WITH TEST RESULTS OF SPECIMENS TG-2a AND 2b

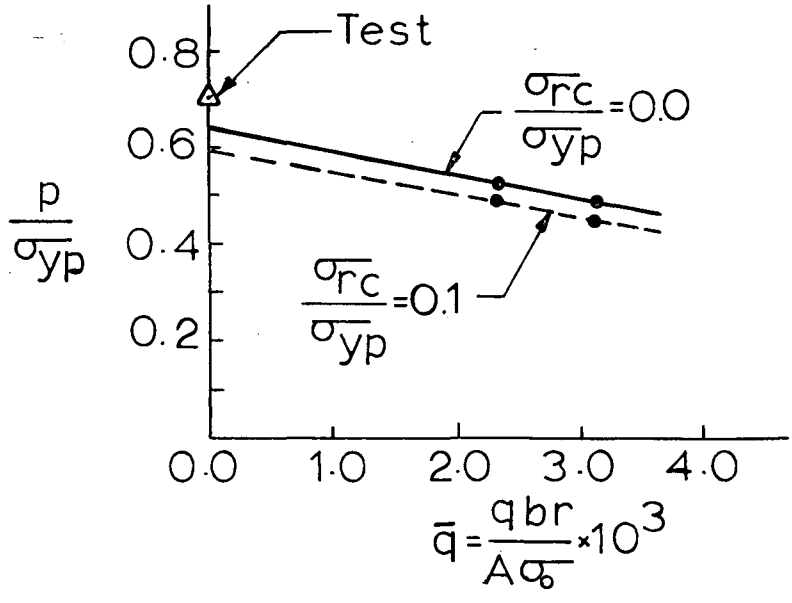

Fig. 32 COMPARISON OF THE METHOD WITH TEST RESULT OF SPECIMEN TG-3

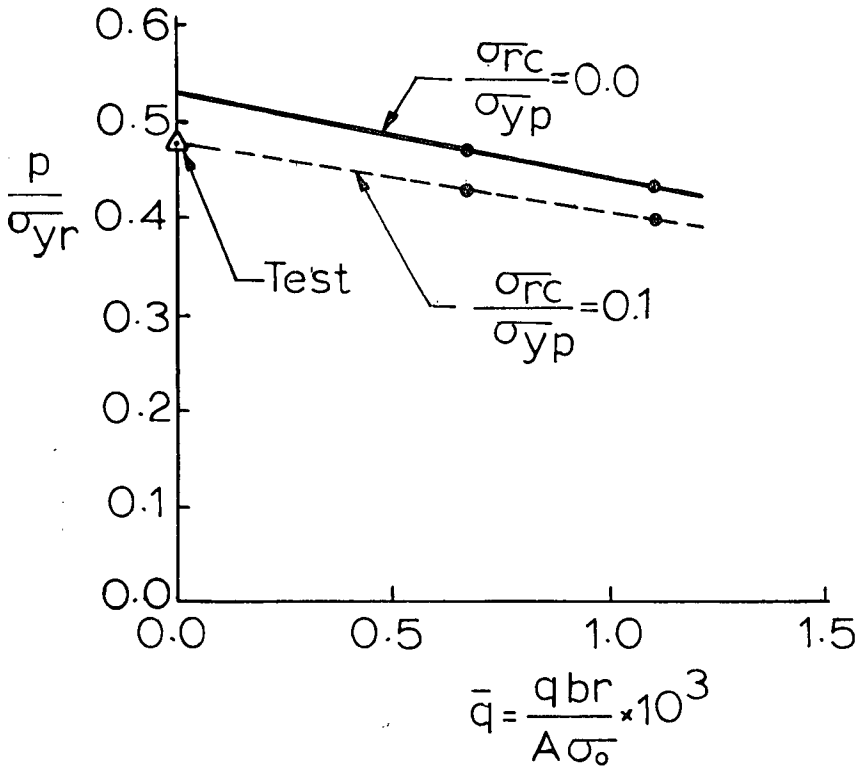

Fig. 33 COMPARISON OF THE METHOD WITH TEST RESULT OF SPECIMEN TG-4

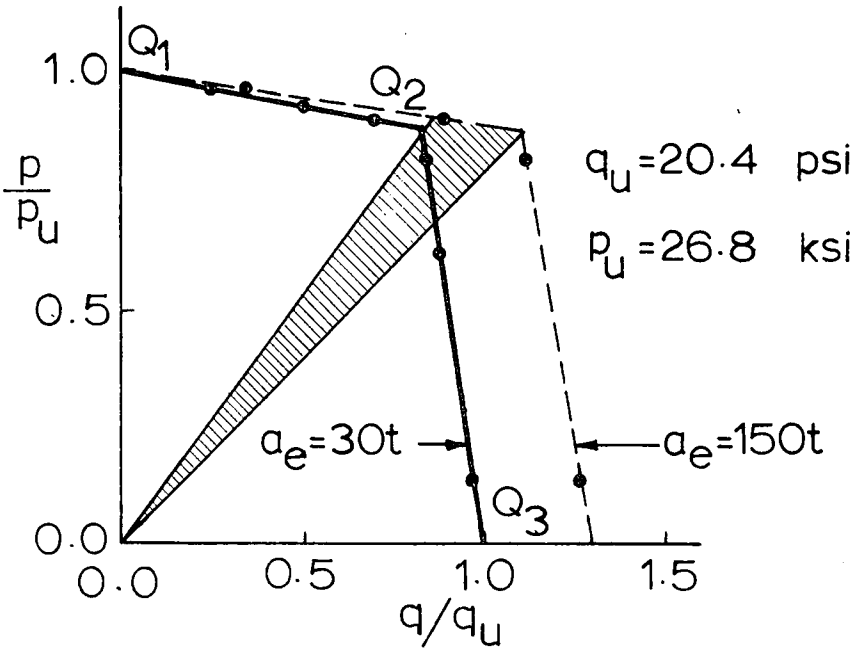

Fig 34 EFFECT OF THE EFFECTIVE PLATE WIDTH FOR TRANSVERSE STIFFENER ON THE ULTIMATE STRENGTH OF SG-1

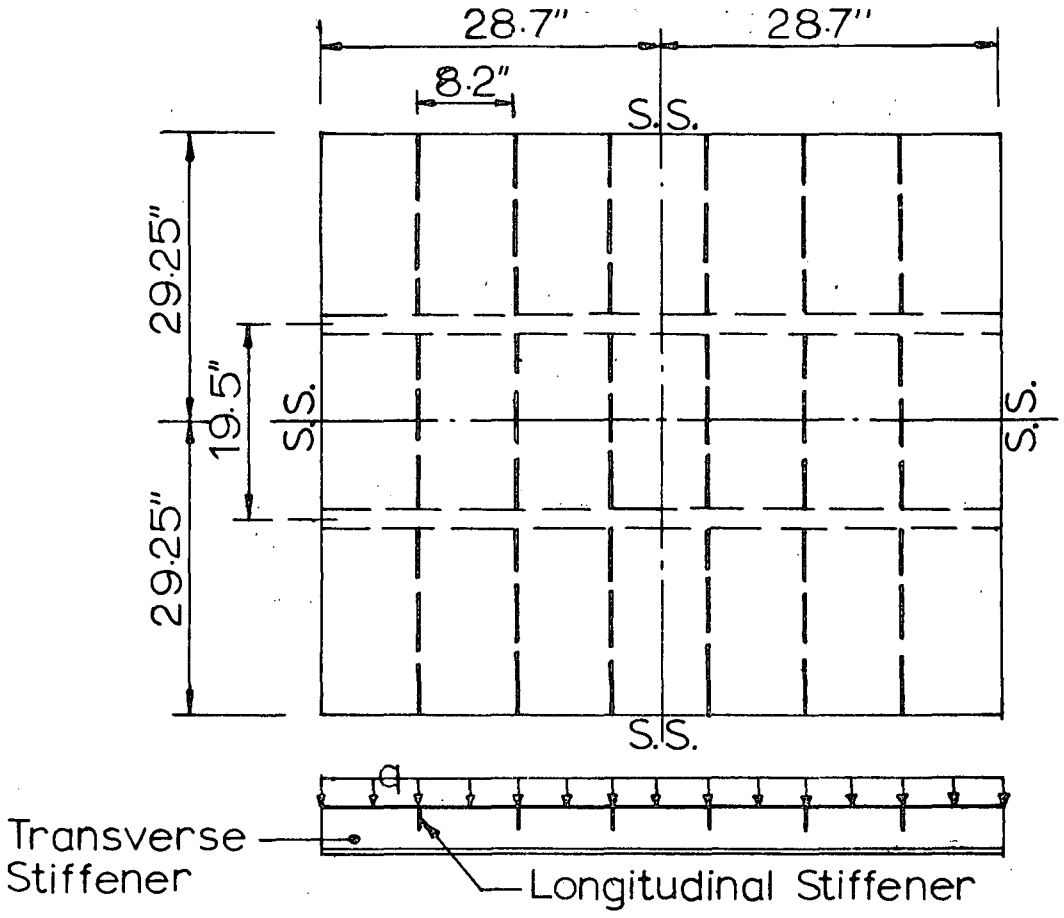

Fig. 35 SAMPLE GRILLAGES 2 AND 3

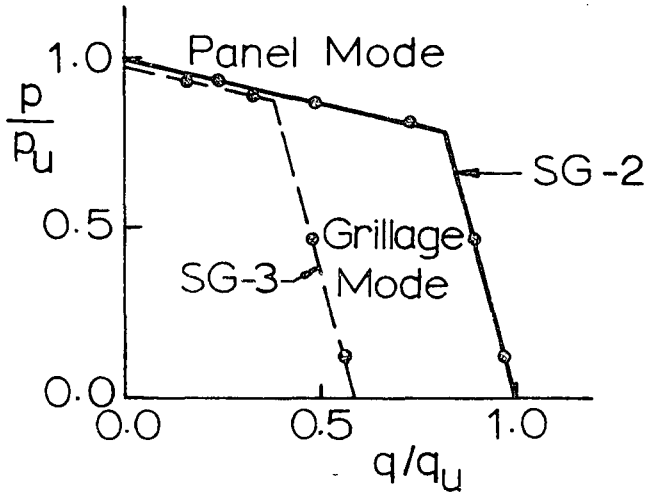

Fig. 36 EFFECT OF THE FLEXIBILITY OF TRANSVERSE BEAMS ON THE ULTIMATE STRENGTH OF SG-2 AND 3

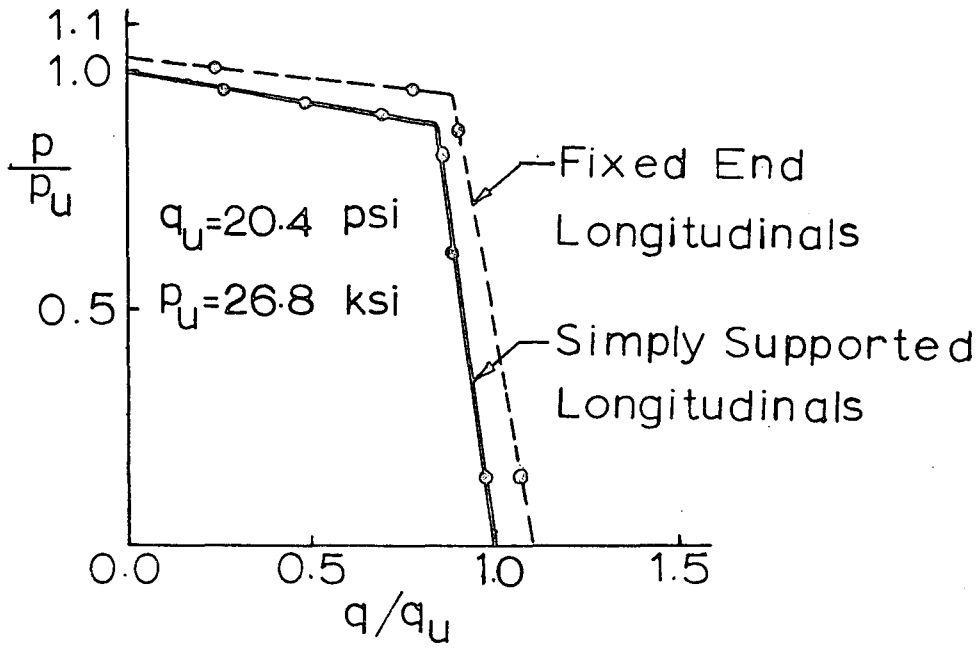

Fig. 37 EFFECT OF FIXED ENDS FOR THE LONGITUDINALS ON THE ULTIMATE STRENGTH OF SG-1

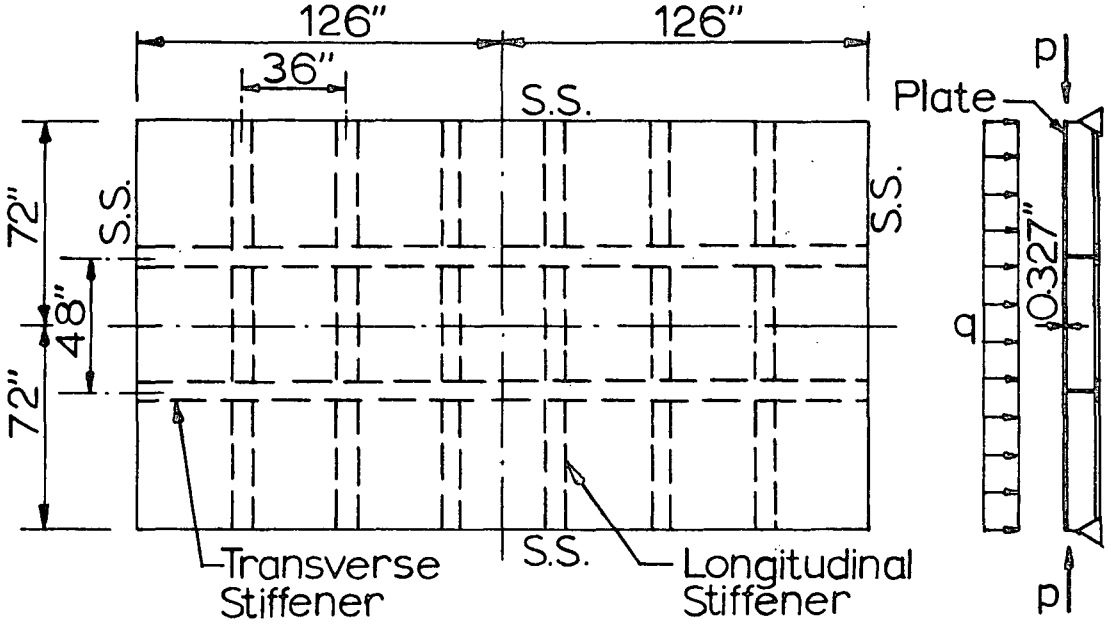

Fig. 38 SAMPLE GRILLAGE 4

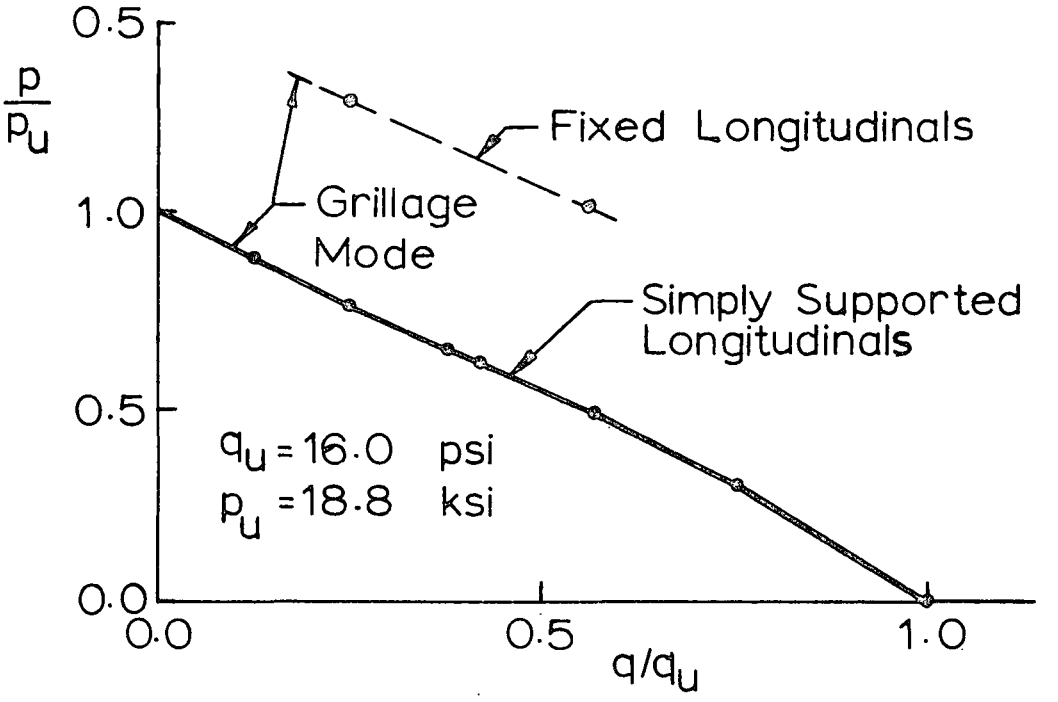

Fig. 39 EFFECT OF FIXED ENDS FOR THE LONGITUDINAL BEAMS ON THE ULTIMATE STRENGTH OF SG-4

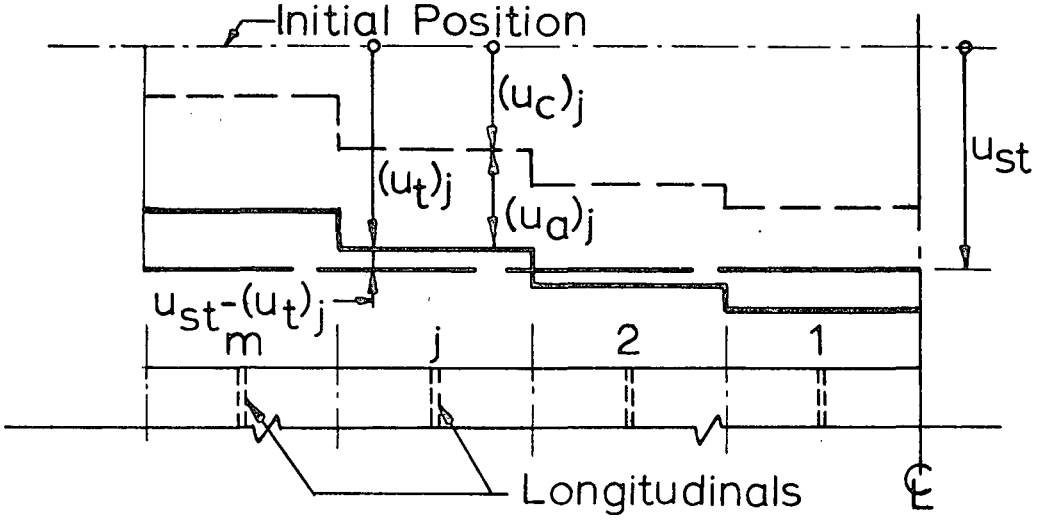

Fig. 40 IN-PLANE END DISPLACEMENTS

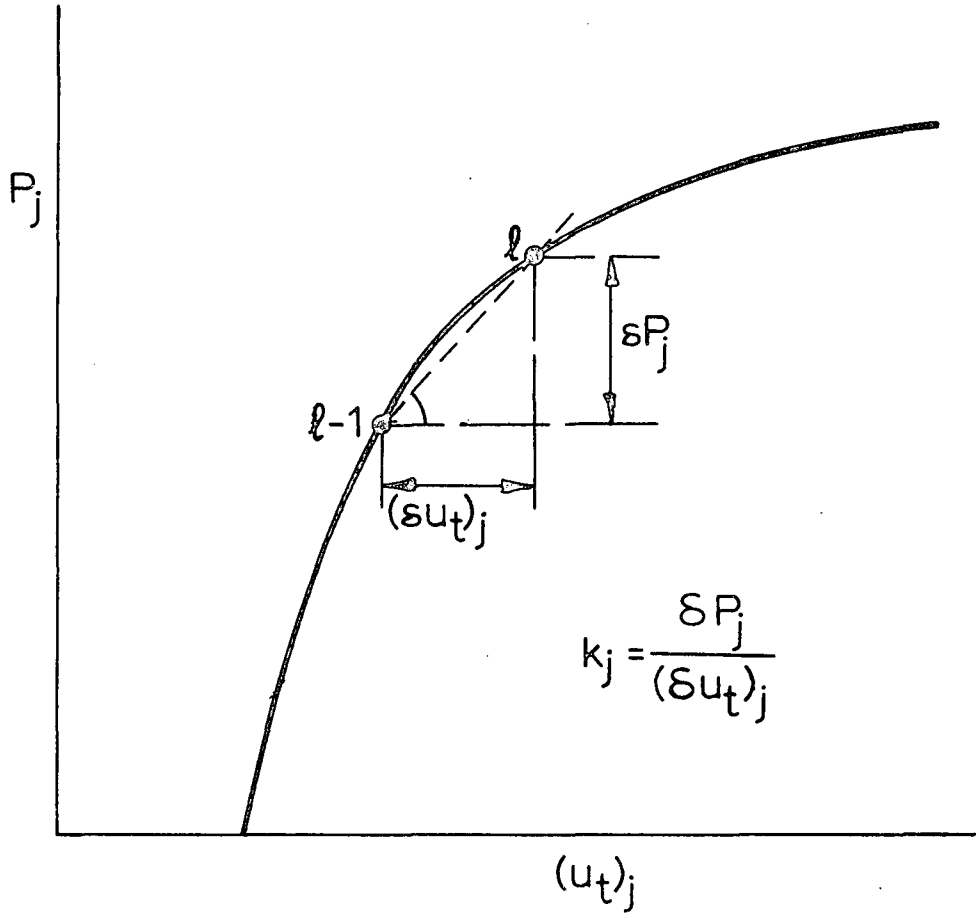

Fig. 41 AXIAL FORCE vs. TOTAL END DISPLACEMENT FOR j^{th}-LONGITUDINAL BEAM

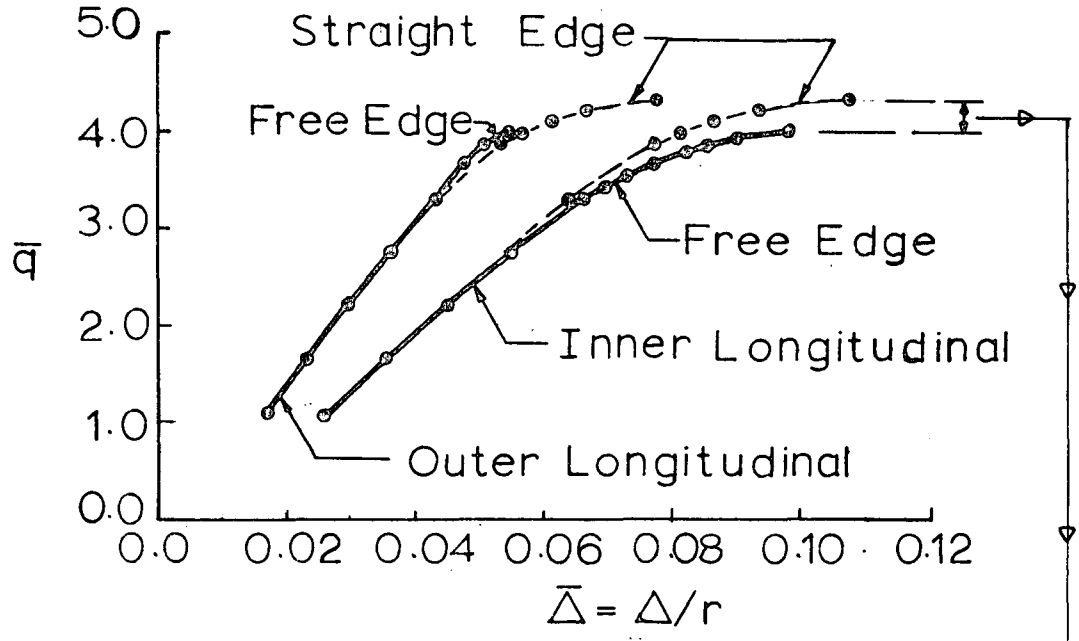

(a) LATERAL LOAD vs. DEFLECTION CURVES FOR SG-1 UNDER $p_{ave}/\sigma_{yp} = 0.66$

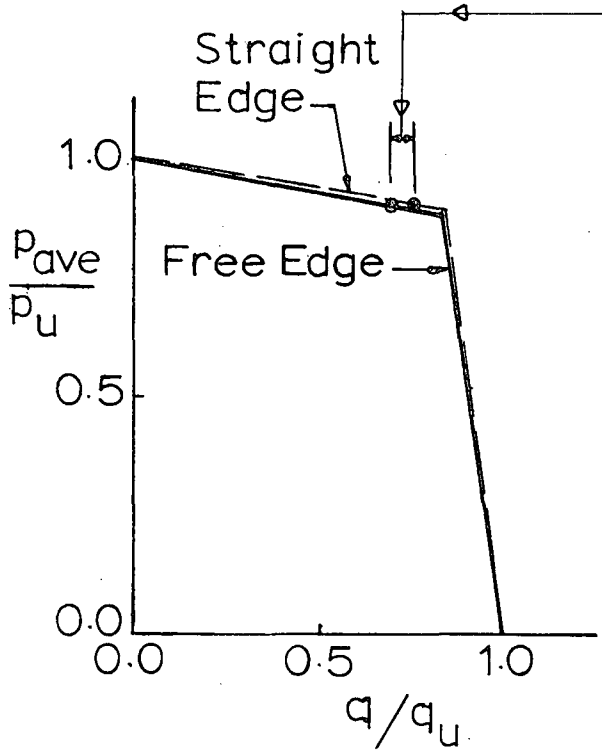

(b) INTERACTION DIAGRAMS FOR STRAIGHT AND FREE EDGES

Fig. 42 EFFECTS OF CONSTANT EDGE DISPLACEMENT ON THE ULTIMATE STRENGTH

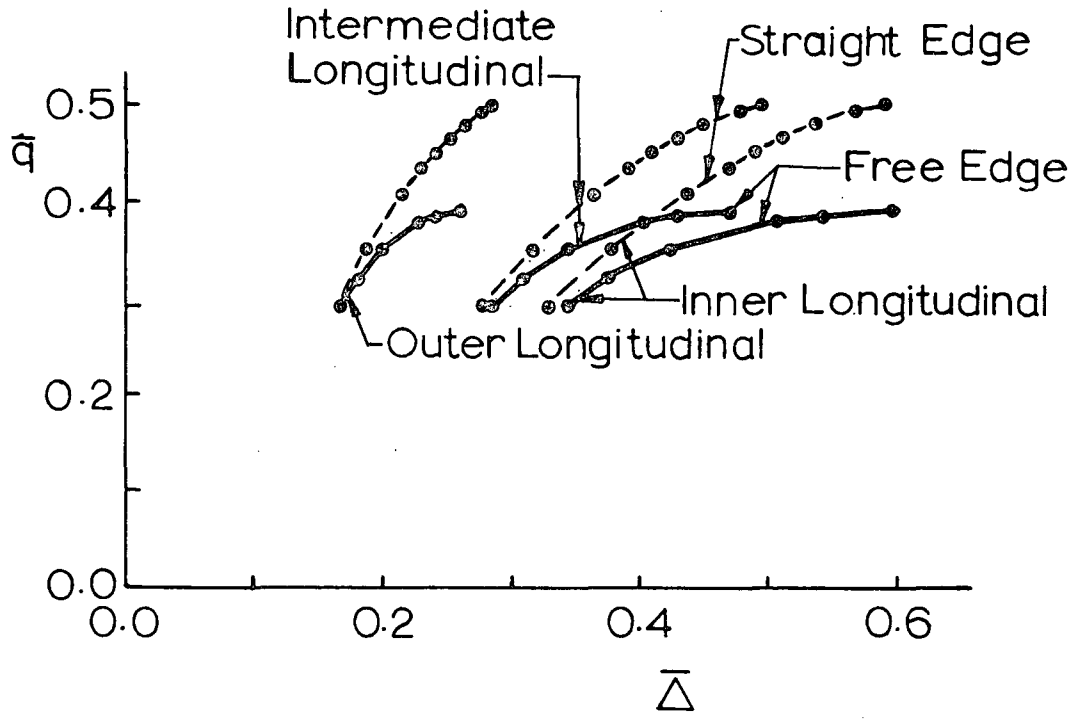

Fig. 43 LATERAL LOAD vs. DEFLECTION CURVES FOR SG-4 UNDER $p_{ave}/\sigma_{yp} = 0.225$

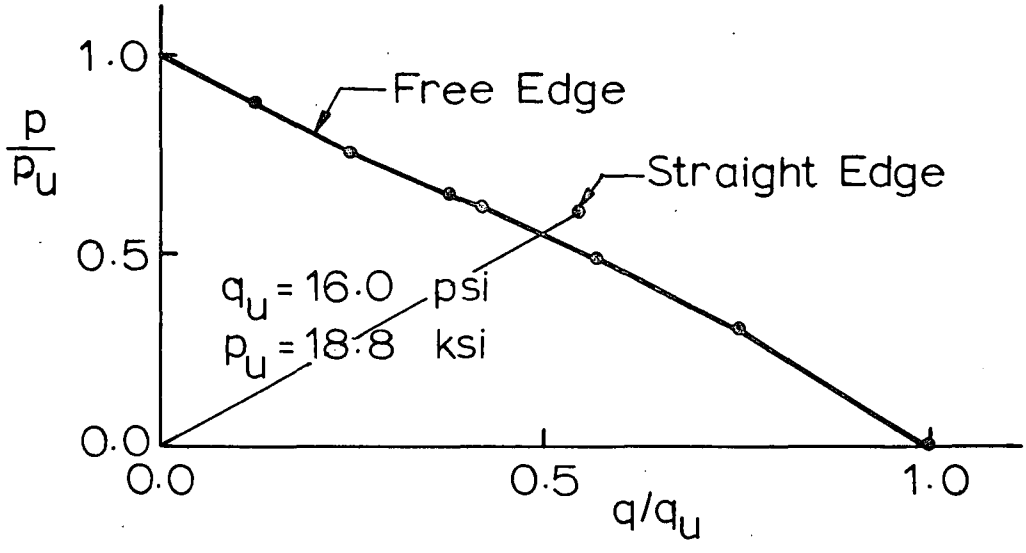

Fig. 44 EFFECT OF CONSTANT EDGE DISPLACEMENT ON THE ULTIMATE STRENGTH OF SG-4

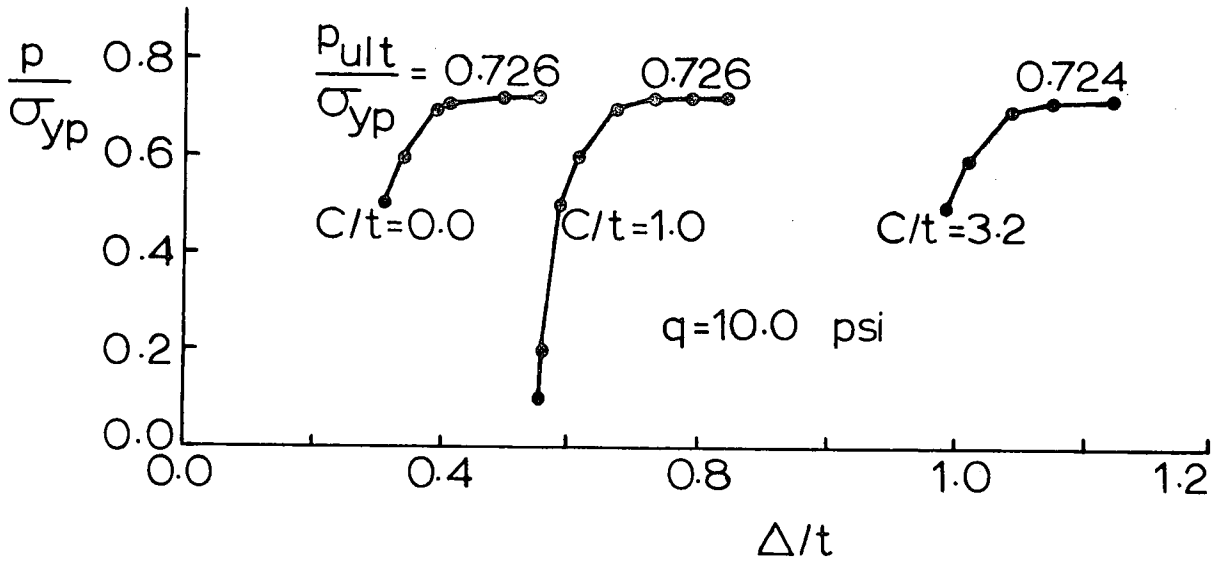

(Δ AT 22.6 IN. FROM THE LOADED EDGE)

Fig. 45 EFFECT OF INITIAL DEFLECTIONS ON THE ULTIMATE STRENGTH OF SG-1

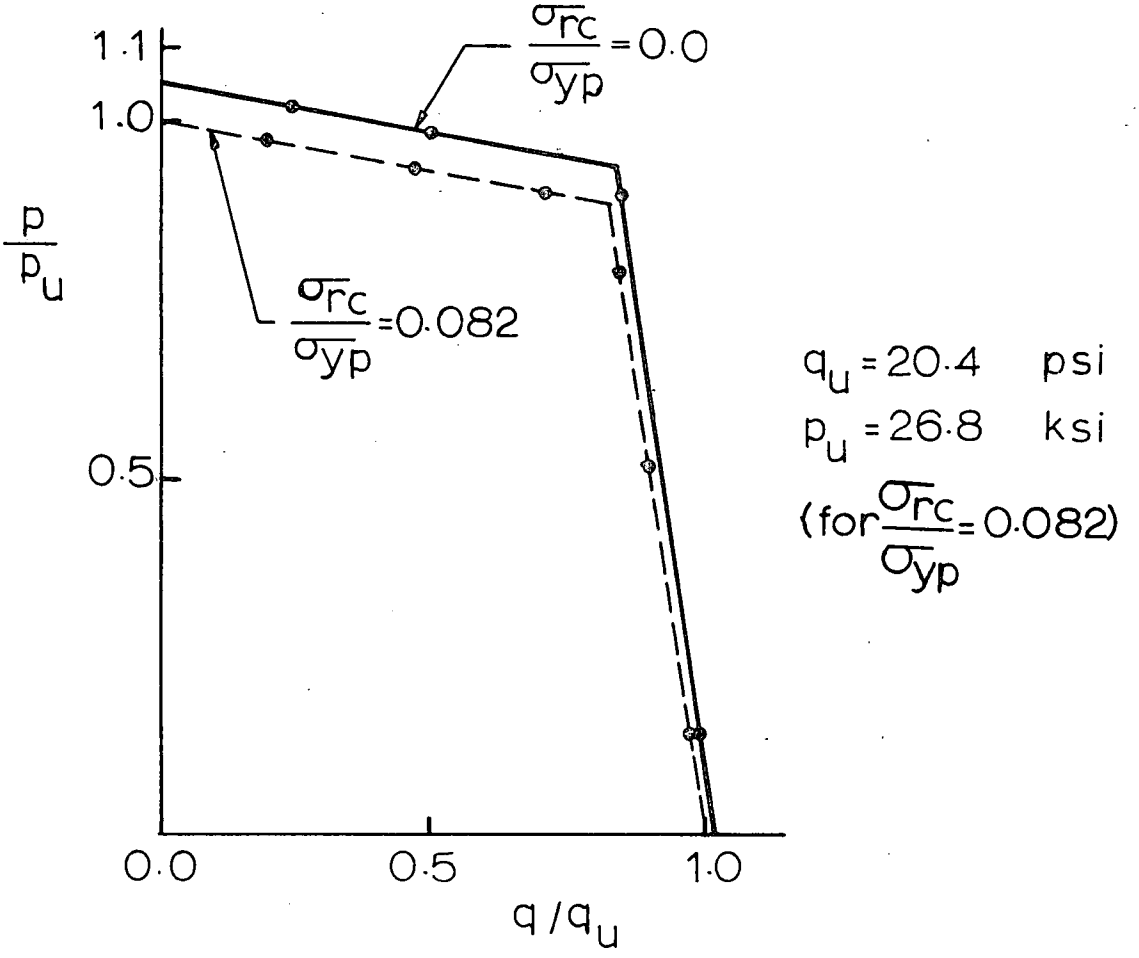

Fig. 46 EFFECT OF RESIDUAL STRESSES ON THE ULTIMATE STRENGTH OF SG-1

9. REFERENCES

1. Clarkson, J.
THE ELASTIC ANALYSIS OF FLAT GRILLAGES, Cambridge University Press, 1965

2. Holman, D. F.
A FINITE SERIES SOLUTION FOR GRILLAGES UNDER NORMAL LOADING, Aeronautical Quarterly, Vol. 8, Feb. 1957, pp.49-57

3. Hendry, A. W., and Jaeger, L. G.
THE ANALYSIS OF GRID FRAMEWORKS AND RELATED STRUCTURES, Chatto and Windus, London, 1958

4. Lightfoot, E., and Sawko, F.
GRID FRAMEWORKS RESOLVED BY GENERALIZED SLOPE-DEFLECTION, Engineering, Vol. 187, No. 1, p. 1920, 1959

5. Suhara, Jiro
THREE-DIMENSIONAL THEORY OF THE STRENGTH OF SHIP HULLS, Memoirs of the Faculty of Engineering Kyushu University, Vol. 19, No. 4, Fukuoka, Japan, 1960

6. Smith, C. S.
ANALYSIS OF GRILLAGE STRUCTURES BY THE FORCE METHOD, Trans, R. I. N. A., Vol. 106, 1964, p. 183-95

7. Wah, Thein
ANALYSIS OF LATERALLY LOADED GRIDWORKS. Proc. ASCE, Vol. 90, No. EM2, April 1964, p. 83-106

8. Nielsen, R., Jr.
ANALYSIS OF PLANE AND SPACE GRILLAGES UNDER ARBITRARY LOADING BY USE OF THE LAPLACE TRANSFORMATION, Report No. DSF-12, Danish ship Research Institute (Dansk Skibsteknisk Forshningsinstitut) Jan. 1965

9. Smith, C. S.
ELASTIC BUCKLING AND BEAM-COLUMN BEHAVIOR OF SHIP GRILLAGES, Report No. R528, Naval Construction Research Establishment, St. Leonard's Hill, Dunfermline, Fife, April 1967

10. Wah, Thein
THE BUCKLING OF GRIDWORKS, Journal of the Mechanics and Physics of Solids, Vol. 13, No. 1, Feb. 1965, p. 1

11. Heyman, J.
THE PLASTIC DESIGN OF GRILLAGES, Engineering, Vol. 176. p. 804-807, 1953

12. Clarkson, J., and Wilson, L. B.
TESTS ON THREE FLAT PLATED GRILLAGES: PART IV PLASTIC COLLAPSE, Naval Construction Research Establishment Report No. N.C.R.E./R.390D, Dunfermline, Dec. 1957

13. Hodge, P. G.
PLASTIC ANALYSIS OF STRUCTURES, McGraw-Hill Book Co., Inc., New York, 1959

14. Wolchuk, R.
DESIGN MANUAL FOR ORTHOTROPIC STEEL PLATE DECK BRIDGES, AISC, New York, 1963

15. Troitsky, M. S.
ORTHOTROPIC BRIDGES THEORY AND DESIGN, The James F. Lincoln Arc Welding Foundation, Cleveland, August 1967

16. Dow, N. F., Libove, C., and Hubka, R. E.
FORMULAS FOR THE ELASTIC CONSTANTS OF PLATES WITH INTEGRAL WAFFLE-LIKE STIFFENING, NACA Report 1195, 1954

17. Crawford, R. F., and Libove, C.
SHEARING EFFECTIVENESS OF INTEGRAL STIFFENING, NACA, Tech. Note 3443, June 1955

18. Crawford, R. F.
A THEORY FOR THE ELASTIC DEFLECTIONS OF PLATES INTEGRALLY STIFFENED ON ONE SIDE, NACA, Tech. Note 3646, April 1956

19. Richmond, B.
APPROXIMATE BUCKLING CRITERIA FOR MULTI-STIFFENED RECTANGULAR PLATES UNDER BENDING AND COMPRESSION, Proc. Institution of Civil Engrs., Vol. 20, Sept. 1961, p. 141-150

20. Gerard, G.
INTRODUCTION TO STRUCTURAL STABILITY THEORY, McGraw-Hill, New York, 1952

21. Kagan, H. A., and Kubo, G. M.
ELASTO-PLASTIC ANALYSIS OF REINFORCED PLATES, Proc. ASCE, Vol. 94, No. ST4, April 1968, p. 943-956

22. Scordelis, A. C.
ANALYSIS OF SIMPLY SUPPORTED BOX GIRDER BRIDGES, College of Engineering Office of Research Services Report No. SESM-66-17, University of California, Berkeley, Oct. 1966

23. Goldberg, J. E., and Leve, H. L.
THEORY OF PRISMATIC FOLDED PLATE STRUCTURES, International Association of Bridge and Structural Engineers, No. 87, 1957, pp. 59-86

24. Kerfoot, R. P., and Ostapenko, A.
A METHOD FOR LARGE DEFLECTION INELASTIC ANALYSIS OF PLATE GRILLAGES UNDER NORMAL AND AXIAL LOADS, Fritz Laboratory Report No. 323.5, Lehigh University, July 1971

25. Bergan, P. G., Clough, R. W., and Mojtahedi, S.
ANALYSIS OF STIFFENED PLATES USING THE FINITE ELEMENT METHOD, Report No. UC SESM 70-1, University of California, Berkeley, January 1970

26. Kavlie, D., and Clough, R. W.
A COMPUTER PROGRAM FOR ANALYSIS OF STIFFENED PLATES UNDER COMBINED INPLANE AND LATERAL LOADS, Report No. UC SESM 71-4, University of California, Berkeley, March 1971

27. Armen, H., Pifko, A., and Levine, H. S.
FINITE ELEMENT ANALYSIS OF STRUCTURES IN THE PLASTIC RANGE, N71-19276, Grumman Aerospacee Corp. Bethpage, N.Y., Feb. 1971

28. Brebbia, C., and Connor, J.
GEOMETRICALLY NONLINEAR FINITE ELEMENT ANALYSIS, Journal of the Engineering Mechanics Div., ASCE Vol. 95, No. EM2, April 1969.

29. Bonger, F. K.
FINITE DEFLECTION DISCRETE ELEMENT ANALYSIS OF SHELLS, Ph.D. Dissertation, Case Western Reserve University, Cleveland, 1967

30. Harris, H. G., and Pifko, A. B.
ELASTIC-PLASTIC BUCKLING OF STIFFENED RECTANGULAR PLATES, Proceedings of the Symposium on Application of Finite Element Methods in Civil Engineering, Nashville, Nov. 1969

31. Gallagher, R. H., Gellatly, R. A., Padlog, J., and Mallett, R. H.
A DISCRETE ELEMENT PROCEDURE FOR THIN SHELL INSTABILITY ANALYSIS, AIAA Journal, Vol. 5, No.1, Jan. 1967

32. Marcal, P. V.
FINITE ELEMENT ANALYSIS WITH MATERIAL NONLINEARITIES-THEORY AND PRACTICE, Proceedings of Seminar on Recent Advances in Matrix Methods of Strcutural Analysis and Design, Tokyo, Japan, 1969, University of Alabama Press, 1971

33. Zienkiewicz, O. C., Valliappan, S., and Ding, I. P.
ELASTIC-PLASTIC SOLUTIONS OF ENGINEERING PROBLEMS-INITIAL STRESS FINITE ELEMENT APPROACH, International Journal for Numerical Methods in Engineering, Vol., 1969

34. Kawai, T., and Yoshimura, N.
ANALYSIS OF LARGE DEFLECTION OF PLATES BY THE FINITE ELEMENT METHOD, International Journal for Numerical Methods in Engineering, Vol. 1, 1969

35. Mallet, R., and Marcal, P.
FINITE ELEMENT ANALYSIS OF NON-LINEAR STRUCTURES, Proceedings of ASCE, Vol. 94, No. ST9, Sept. 1968

36. Murray, W. D., and Wilson, E. L.
FINITE ELEMENT LARGE DEFLECTION ANALYSIS OF PLATES, Proceedings of ASCE, Vol. 95, No. ME1, Feb. 1969

37. Stricklin, J. A., and Haisler, W. E.
GEOMETRICALLY NONLINEAR STRUCTURAL ANALYSIS BY DIRECT STIFFNESS METHOD, Proceedings of ASCE, Vol. 97, No. ST9, Sept. 1971

38. Richards, R. M., and Blacklock, J. R.
FINITE ELEMENT ANALYSIS OF INELASTIC STRUCTURES, American Institute of Aeronautics and Astonautics, Journal, Vol. 7, No. 3, March 1969

39. Bergan, P. G.
NON-LINEAR ANALYSIS OF PLATES CONSIDERING GEOMETRIC AND MATERIAL EFFECTS, Report No. UC SESM 71-7, University of California, April 1971

40. Kondo, J.
ULTIMATE STRENGTH OF LONGITUDINALLY STIFFENED PLATE PANELS SUBJECTED TO COMBINED AXIAL AND LATERAL LOADING, Fritz Laboratory Report No. 248.13, Lehigh University, August 1965

41. Tsuiji, T.
STRENGTH OF LONGITUDINALLY STIFFENED PLATE PANELS, WITH LARGE b/t, Fritz Laboratory Report No. 248.14, Lehigh University, June 1965

42. Vojta, J. F., and Ostapenko, A.
ULTIMATE STRENGTH DESIGN OF LONGITUDINALLY STIFFENED PLATE PANELS WITH LARGE b/t, Fritz Laboratory Report No. 248.18, Lehigh University, August 1967

43. Rutledge, D. R., and Ostapenko, A.
ULTIMATE STRENGTH OF LONGITUDINALLY STIFFENED PLATE PANELS (LARGE AND SMALL b/t, GENERAL MATERIAL PROPERTIES), Fritz Engineering Laboratory Report No. 248.24, Lehigh University, Sept. 1968

44. Davidson, H. L.
POST-BUCKLING BEHAVIOR OF LONG RECTANGULAR PLATES, Fritz Laboratory Report No. 248.15, Lehigh University, June 1965

45. Besseling, J.F.
THE EXPERIMENTAL DETERMINATION OF THE EFFECTIVE WIDTH OF FLAT PLATES IN THE ELASTIC AND PLASTIC RANGE, Nationaal Luchtvaartlaboratorium(Netherlands), Rep. S414, 1953, (In Dutch)

46. Botman, M.
THE EXPERIMENTAL DETERMINATION OF THE EFFECTIVE WIDTH OF FLAT PLATES IN THE ELASTIC AND PLASTIC RANGE (PART 11), Nationaal Luchvaartlaboratorium (Netherlands), Rep. S438, 1954, (In Dutch)

47. Ojalvo, M., and Hull, F. H.
EFFECTIVE WIDTH OF THIN RECTANGULAR PLATES, Proc.ASCE, Vol. 84(EM-3) Paper 1718, July 1958

48. Koiter, W. T.
THE EFFECTIVE WIDTH OF FLAT PLATES FOR VARIOUS LONGITUDINAL EDGE CONDITIONS AT LOADS FAR BEYOND BUCKLING LOAD, Nationaal Luchtvaartlaboratorium (Netherlands), Rep. S287, 1943, (In Dutch)

49. Vojta, J. F., and Ostapenko, A.
ULTIMATE STRENGTH DESIGN CURVES FOR LONGITUDINALLY STIFFENED PLATE PANELS WITH LARGE b/t, Fritz Laboratory Report No. 248.19, Lehigh University, August 1967

50. McCracken, D. D., and Dorn, W. S.
NUMERICAL METHODS AND FORTRAN PROGRAMING, John Wiley and Sons, Inc., 1964

51. Rutledge D. R.
COMPUTER PROGRAM FOR ULTIMATE STRENGTH OF LONGITUDINALLY STIFFENED PANELS (LARGE AND SMALL b/t, GENERAL MATERIAL PROPERTIES), Fritz Laboratory Report No. 248.23, Lehigh University, July 1968

52. Atsuta, T.
ANALYSIS OF INELASTIC BEAM-COLUMNS,Ph.D. Dissertation, Lehigh University, 1972

53. Clarkson, J.
THE ELASTIC ANALYSIS OF GRILLAGES WITH PARTICULAR REFERENCE TO SHIP STRUCTURES, Cambridge University Press, London, 1965

54. Correspondence of A. Ostapenko with Dr. C. A. Smith (June 1966) and Cdr. D. Faulkner (July 1971), both of the Naval Construction Research Establishment

55. Kendrick, S.
A REVIEW OF RESEARCH CARRIED OUT AT THE NAVAL CONSTRUCTION RESEARCH ESTABLISHMENT INTO STRUCTURAL BEHAVIOR BEYOND THE ELASTIC LIMIT, Proceedings of the Second Symposium on Naval Structural Mechanics, Brown University, Rhode Island, April 5-7, 1960, Edited by E. H. Lee and P. S. Symonds, Pergamon Press, New York, 1960

10. ACKNOWLEDGMENTS

This study was conducted in the Department of Civil Engineering at Fritz Engineering Laboratory, Lehigh University, Bethlehem, Pennsylvania. Dr. D. A. VanHorn is Chairman of the Department and Dr. L. S. Beedle is Director of the Laboratory.

This work is an outgrowth of a research project on the ultimate strength of grillages which was supported by the Naval Ship Engineering Center of the United States Navy. Support for that project is gratefully acknowledged.

The authors are grateful to Lehigh University for providing computer time.

Special thanks are due to Mrs. S. Parsanejad, Mrs. J. Lenner, and Miss S. Matlock for typing the manuscript, and to Messrs. T. Shoraka and O. S. Okten for their help in preparation of the drawings.